

論文 / 著書情報
Article / Book Information

Title	Swi5-Sfr1 stimulates Rad51 recombinase filament assembly by modulating Rad51 dissociation
Authors	Hsin-Yi Yeh, Guan-Chin Su, Kentaro Ito, Yumiko Kurokawa, Hiroshi Iwasaki, Hung-Wen Li, Chih-Hao Lu, Hsin-Yi Yeh, Guan-Chin Su
Citation	Proceedings of the National Academy of Sciences of the United States of America, Vol. 115, No. 43, pp. E10059-E10068
Pub. date	2018, 10
DOI	https://doi.org/10.1073/pnas.1812753115
Note	This file is author (final) version.

1 **Swi5-Sfr1 Stimulates Rad51 Recombinase Filament Assembly by**
2 **Modulating Rad51 Dissociation**

3 Chih-Hao Lu¹, Hsin-Yi Yeh², Guan-Chin Su², Kentaro Ito³, Yumiko Kurokawa^{3,¶},
4 Hiroshi Iwasaki^{3,*}, Peter Chi^{2,4,*} and Hung-Wen Li^{1,*}

5 ¹ Department of Chemistry, National Taiwan University, Taiwan

6 ² Institute of Biochemical Sciences, National Taiwan University, Taiwan

7 ³ Institute of Innovative Research, Tokyo Institute of Technology, Japan

8 ⁴ Institute of Biological Chemistry, Academia Sinica, Taiwan

9

10

11 * To whom correspondence should be addressed:

12 Hiroshi Iwasaki, E-mail: hiwasaki@bio.titech.ac.jp

13 Peter Chi, E-mail: peterhchi@ntu.edu.tw

14 Hung-Wen Li, E-mail: hwli@ntu.edu.tw

15 ¶ current address: Center for Frontier Research, National Institute of Genetics, Japan

16

17

18 **Author contributions:** C.H.L., H.I., P.C. and H.W.L. designed research; C.H.L.
19 performed all single-molecule experiments and analyzed data; H.Y.Y, G.C.S., K.I.
20 and Y.K. purified proteins used in this article; C.H.L. H.I., P.C. and H.W.L. wrote the
21 paper.

22

23 **Key words:**

24 homologous recombination/ single-molecule microscopy/ Rad51/ Swi5-Sfr1

25

26

27 **ABSTRACT**

28 Eukaryotic Rad51 protein is essential for homologous recombination repair of
29 DNA double-strand breaks. Rad51 recombinases first assemble onto single-stranded
30 DNA to form a nucleoprotein filament, required for function in homology pairing and
31 strand exchange. This filament assembly is the first regulation step in homologous
32 recombination. Rad51 nucleation is kinetically slow, and several accessory factors
33 have been identified to regulate this step. Swi5-Sfr1 (S5S1) stimulates
34 Rad51-mediated homologous recombination by stabilizing Rad51 nucleoprotein
35 filaments, but the mechanism of stabilization is unclear. We used single-molecule
36 tethered particle motion (TPM) experiments to show that mouse S5S1 (mS5S1)
37 efficiently stimulates mouse RAD51 (mRAD51) nucleus formation, and inhibits
38 mRAD51 dissociation from filaments. We also used single-molecule fluorescence
39 resonance energy transfer (smFRET) experiments to show that mS5S1 promotes
40 stable nucleus formation by specifically preventing mRAD51 dissociation. This leads
41 to a reduction of nucleation size from three mRAD51 to two mRAD51 molecules in
42 the presence of mS5S1. Compared to mRAD51, fission yeast Rad51 (SpRad51)
43 exhibits fast nucleation but quickly dissociates from the filament. SpS5S1 specifically
44 reduces SpRad51 disassembly to maintain a stable filament. These results clearly
45 demonstrate the conserved function of S5S1 by primarily stabilizing Rad51 on DNA,
46 allowing both the formation of the stable nucleus and the maintenance of filament
47 length.

48

49 **SIGNIFICANCE STATEMENT**

50 In DNA homologous recombination, the recombinase-coated single-stranded
51 DNA filament formation is the first committed step and is subject to tight regulation.
52 Stabilization of nucleoprotein filament by accessory proteins can be achieved by
53 enhancing filament formation, reducing filament disassembly or both. However, the
54 mechanism of regulation is not understood by conventional biochemical methods.
55 This is the first study of the mechanism of how accessory proteins stimulate filament
56 assembly by applying single-molecule methods that allow us to monitor the binding
57 of Rad51 on DNA in mouse and fission yeast. Our results show that Swi5-Sfr1
58 complex demonstrates the evolutionarily-conserved stimulation on Rad51 filament
59 assembly by stabilizing Rad51 on DNA, allowing both the formation of the stable
60 nucleus and the reduction of Rad51 dissociation.

61

62

63 \body

64

65 **INTRODUCTION**

66 Rad51 recombinases are essential for eukaryotic homologous recombination
67 DNA repair(1, 2). As a replication fork encounters a lesion, collapsed forks lead to
68 DNA double-strand breaks (DSBs). Homologous recombination is the major pathway
69 to restart replication(3). To carry out homologous recombination repair, the broken
70 end of DNA is resected to reveal a 3' protruded single-stranded DNA (ssDNA), which
71 Rad51 binds to form a nucleoprotein filament(1, 2, 4-7). The resultant helical
72 nucleoprotein filament is the active component responsible for homology searching
73 and strand exchange and is essential for DSB repair and genomic maintenance.

74 Among the cascade of steps required for DSB repair, Rad51 nucleoprotein
75 filament assembly is the committed step and is subject to tight regulation(1, 2, 8-10).
76 Maintaining a stable but dynamic nucleoprotein filament is critical for recombinase
77 function, as this filament is essential for both the homology search and strand
78 exchange required for heteroduplex DNA formation. Filament assembly includes a
79 rate-determining nucleation step, where several Rad51 molecules bind ssDNA to form
80 a stable nucleus, followed by a faster extension step(11-14). The filament assembly
81 involves monomer addition occurring both at 3'- and 5'- ends of the recombinase
82 filament but with different rates, leading to the overall end preference. During strand
83 exchange, this filament likely maintains a certain length through dissociating and
84 rebinding of Rad51. Thus, the filament overall moves dynamically with polarity
85 (15-18). Several proteins stimulate and regulate Rad51 filament assembly(19-26).
86 Swi5 and Sfr1 were identified by genetic studies in the fission yeast
87 *Schizosaccharomyces pombe* (*S. pombe*)(27, 28). Mutations in fission yeast *swi5* and
88 *sfr1* decrease recombination rates and increase sensitivity to ionizing radiation and
89 DNA damaging chemicals(27, 28). *In vitro* biochemical and biophysical studies
90 showed that both fission yeast and mouse Swi5 and Sfr1 proteins form a
91 heterodimeric complex that physically interacts with Rad51 to facilitate
92 Rad51-mediated recombination(25, 26, 29-31). Both fission yeast and mouse
93 Swi5-Sfr1 (S5S1) complexes stabilize the Rad51 presynaptic filament and increase
94 the ssDNA-dependent ATPase activity of Rad51. Moreover, mouse S5S1 (mS5S1)
95 has been reported to enhance the release of ADP from the mRAD51 presynaptic
96 filaments(32).

97 How Rad51 nucleoprotein filaments are stabilized by these accessory factors is
98 not clear. Stabilization could be achieved by increasing the Rad51 on-rate or
99 decreasing the off-rate, or both. Conventional biochemical studies are based on
100 averaged and equilibrium measurements, making it challenging to elucidate the
101 molecular events responsible for these kinetic events. Here, we used single-molecule
102 tethered particle motion (TPM) and fluorescence resonance energy transfer (smFRET)

103 experiments to characterize individual Rad51 filament assembly and disassembly
104 kinetics as well as the nucleation process in real-time. Our single-molecule results
105 support a model in which Swi5-Sfr1 stabilizes Rad51 on DNA by preventing its
106 dissociation. This effect leads to both stable nucleus formation and longer lasting
107 filament. Specifically, this stabilization decreases the nucleation size from 3 to 2
108 Rad51 in mouse and reduces filament disassembly nearly 3-fold in fission yeast. In
109 spite of different kinetic properties of the mouse and fission yeast Rad51, Swi5-Sfr1
110 complex stimulates Rad51 process through a similar and conserved mechanism.

111

112 RESULTS

113 **Mouse SWI5-SFR1 (mS5S1) stimulates mRAD51 nucleoprotein filament**
114 **assembly.** Among many accessory proteins regulating homologous recombination,
115 the Swi5-Sfr1 complex stimulates various stages of the process, including filament
116 assembly and strand exchange(25, 26, 28-35). Here, we took advantage of previously
117 developed single-molecule tethered particle motion (TPM) experiments(36-38) to
118 monitor Rad51 nucleoprotein filament assembly in real-time (Figure 1A). We
119 designed a gapped DNA substrate containing a 135 nt secondary structure-free, poly
120 dT ssDNA region ((dT)₁₃₅ gapped DNA, Figure 1A) immobilized on the surface of
121 glass slide via a 5'-digoxigenin-anti-digoxigenin linkage. The substrate was annealed
122 to a short oligo labeled with biotin at its 5' end, which was, in turn, attached to a
123 streptavidin-coated polystyrene bead for visualization purposes. The 151 bp
124 double-stranded handle in the gapped DNA was used to prevent potential
125 Rad51-surface interaction during TPM experiments. Bead Brownian motion (BM) of
126 DNA tether is constrained to a small region near the glass surface. The bead BM of
127 bare (dT)₁₃₅ gapped DNA for assembly experiments and 301 bp duplex DNA used for
128 control experiments are measured to be 21.3 ± 5.78 nm and 35.2 ± 3.77 nm (Figure
129 S1A-S1B). In the presence of either ATP or AMPPNP, mRAD51 preferentially
130 assembles onto the ssDNA region of the gapped substrate at 150 mM KCl(39) (Figure
131 S1A & S1C-S1G). Assembly experiments were initiated by introducing a
132 mRAD51-ATP mixture into the reaction chamber containing the surface-anchored
133 gapped substrates. Increases in bead Brownian motion reveals nucleoprotein filament
134 formation as mRAD51 assembling onto DNA increases ssDNA length and stiffness of
135 the DNA tether. This results in a change in the spatial extent of bead BM(32, 40, 41).
136 Analysis of individual single-molecule TPM time-courses reveals several kinetic
137 parameters, including (i) the dwell time prior to bead BM increase (nucleation time,
138 the time needed for RAD51 to form stable nuclei on ssDNA, Figure 1B-C), (ii)
139 extension time (Figure 1D, the time required to add RAD51 monomers to ssDNA)
140 and (iii) amount of BM increase (Figure 1E, reflecting the length of nucleoprotein

141 filament). Our results show that mRAD51 alone (0.8 μ M) exhibits a nucleation time
142 of 97.6 ± 2.89 sec (Figure 1C). Interestingly, a shorter nucleation time (67.5 ± 1.32 sec)
143 was observed when mRAD51 was pre-incubated with more than 2-fold excess mS5S1
144 (Figure 1C). This observation demonstrates that mS5S1 stimulates the nucleation step
145 of mRAD51 filament formation, which is rate-limiting. mS5S1 has neither dsDNA
146 nor ssDNA affinity(25), so adding mS5S1 in the absence of mRAD51 did not change
147 BM values (Figure S1H). Control experiments using a mS5S1 mutant that is defective
148 for mRAD51 interaction, mSWI5^{FL/AA}-SFR1 (mS5^{FL}S1)(31), showed no stimulation
149 of nucleation times (Figure 1C). Collectively, these findings suggest that the
150 interaction of mRAD51-mS5S1 in solution stimulates mRAD51 nucleation. Within
151 our experimental resolution, we did not observe any change in mRAD51 extension
152 times in the presence of mS5S1 (Figure 1D & S2A). On the other hand, the mean BM
153 increment increases in the presence of mS5S1 (Figure 1E), indicating that the
154 mS5S1-RAD51 complex forms longer filaments than mRAD51 alone.

155 **Stimulation of the mRAD51 nucleation depends on mS5S1 concentration.** We
156 next asked how much mS5S1 is required for maximum stimulation. We incubated
157 various concentrations of mS5S1 (0-2.0 μ M) with 0.8 μ M mRAD51 in solution and
158 observed filament assembly kinetics as in Figure 1A. Interestingly, a sigmoidal
159 dependence of mS5S1/mRAD51 ratios is shown for nucleation rates (Figure 1F), with
160 nucleation rates starting to increase at a ratio larger than 1.5 and reaching a constant
161 maximum nucleation rate of ~ 0.015 s⁻¹ when the ratio was larger than 2. This finding
162 implies that two mS5S1 per one mRAD51 are required for the maximum nucleation
163 stimulation. For the comparison purposes, we measured nucleation rates in the
164 presence of the non-hydrolysable ATP analog, AMPPNP (black open square in Figure
165 1F). Under these conditions, the nucleation rate for mRAD51 alone is fast (~ 0.017 s⁻¹),
166 suggesting that mRAD51 nucleating clusters are more stable in the absence of ATP
167 hydrolysis, consistent with previous reports on bacterial RecA proteins(12, 42). It is
168 possible that mS5S1 stimulates mRAD51 nucleation by stabilizing mRAD51
169 nucleating clusters.

170 Bead BM increment, indicative of the length of mRAD51 filament, on (dT)₁₃₅
171 gapped DNA without mS5S1 is 20.0 ± 0.92 nm (Figure 1E and 1G), likely reflecting
172 the equilibrium filament length of disassembly and assembly dynamics of the
173 filament(14). The longer filament of 27.3 ± 1.51 nm is seen in the presence of
174 AMPPNP (black open square in Figure 1G), consistent with that mRAD51
175 disassembly requires ATP hydrolysis. Notably, in the presence of just 0.5-fold of
176 mS5S1, mRAD51 forms longer, more stable filaments, which is consistent with
177 previous biochemical studies (25, 31, 32). Control experiments confirm that longer
178 filaments in the presence of either S5S1-ATP or AMPPNP do not result from

179 mRAD51 binding to the duplex handle of gapped DNA substrates (Figure S1A &
180 S1C-S1G).

181 **Molecular determinants of mSWI5-SFR1 stimulation on mRAD51 nucleation.** In
182 the rate-limiting nucleation step of the filament assembly, recombinases first form a
183 stable nucleating cluster before extending into a longer functional filament. We used
184 TPM experiments to measure how filament nucleation rates change with mRAD51
185 concentrations. The results are fitted to a power-law dependence, providing
186 information about the mRAD51 nucleation unit of this rate-limited step. In the case of
187 mRAD51 only, the fit returns $n=2.43\pm 0.46$ (Figure 2A). As the fit renders the lower
188 limit, our result suggests that three mRAD51 monomers are required for stable
189 nucleating cluster formation. This is consistent with earlier work showing that human
190 RAD51 (hRAD51) has a nucleation unit of three monomers(14). Adding a two-fold
191 molar excess of mS5^{FL}S1 to mRAD51(green solid circle, Figure 2A) does not change
192 the mRAD51 nucleation unit. However, adding more than a two-fold molar excess of
193 mS5S1 to mRAD51 returned a power-law dependence of $n=1.67\pm 0.16$ (Figure 2B).
194 Thus, mS5S1-mRAD51 complex only needs two mRAD51 molecules to form a stable
195 nucleation cluster. This reduction in the number of mRAD51 molecules required to
196 form a stable nucleation cluster in the presence of mS5S1 provides a clear mechanism
197 to increase the rate of the mRAD51 nucleoprotein assembly process.

198 During DNA double-stranded break (DSB) repair, the ends of the DNA breaks are
199 resected to produce 3' ssDNA overhangs. Thus, the repair substrate possesses a
200 double-strand/single-strand junction (ds/ss junction) and a 3' protruding ssDNA tail.
201 Rad51 nucleation clusters could initiate filament assembly on ssDNA either near the
202 ds/ssDNA junction or onto the free ssDNA sites along the tail. We compared the
203 nucleation rates of mRAD51 in four gapped substrates containing one ds/ssDNA
204 junction but different lengths of ssDNA tail (90, 135, 165 & 200 dT). Nucleation rates
205 can be fitted linearly to ssDNA tail lengths, with the slope corresponding to the
206 apparent nucleation rate on free ssDNA site (Figure 2C). For mRAD51 only, the
207 dependence on ssDNA length was small, suggesting that mRAD51 alone prefers to
208 nucleate near the junction. On the other hand, in the presence of a two-fold excess
209 mS5S1, nucleation rates of mRAD51 showed a much stronger dependence on ssDNA
210 lengths (filled squares, Figure 2C), with a ~6.5-fold increase in the slope
211 $((8.95\pm 1.93)\times 10^{-5} \text{ s}^{-1}\text{nt}^{-1}$ for mS5S1-mRAD51 and $(1.40\pm 0.52)\times 10^{-5} \text{ s}^{-1}\text{nt}^{-1}$ for
212 mRAD51 alone, Figure 2C and Table S1). These data indicate that mS5S1 stimulates
213 mRAD51 binding by increasing its ssDNA affinity. Previous studies showed that DSB
214 ends are resected to lengths of up to several kilobases in cells(4, 5), therefore, by
215 dramatically increasing the ssDNA affinity of mRAD51, mS5S1 can effectively
216 stimulate mRAD51 filament assembly.

217 **smFRET experiments reveal Rad51 binding and dissociation dynamics during**
218 **nucleating events.** In TPM assembly experiments, we monitored the filament
219 assembly kinetics that led to the successful assembly of recombinase nucleoprotein
220 filaments. Due to their limited spatiotemporal resolution, TPM experiments cannot
221 detect dynamics during non-productive assembly events. For example, transient
222 recombinase binding events are likely taking place but would be difficult to detect by
223 TPM. To monitor transient binding events, we used single-molecule fluorescence
224 resonance energy transfer (smFRET) to characterize nucleation dynamics of mRAD51
225 at high spatiotemporal resolution. The DNA substrates used in the smFRET
226 experiments were short and composed of an 18 bp dsDNA handle and a short 3'
227 terminating dT overhangs (13 or 18 nt, Figure 3A & S3A-S3D). The fluorophore
228 donor (Cy3) and acceptor (Cy5) dyes were positioned so that mRAD51 monomer
229 binding and dissociation on the ssDNA region could be monitored. In the absence of
230 mRAD51, ssDNA is flexible, and separation between the dye pairs is short, resulting
231 in a high FRET efficiency (~ 0.85 for (dT)₁₃ and ~ 0.8 for (dT)₁₈, Figure S3A-S3D).
232 When mRAD51 assembles onto ssDNA, the distance between the dye pair increased
233 resulting in reduced FRET efficiency (Figure 3B-3C; S3C-S3D). Therefore, each
234 high-to-low FRET transition represents one or more mRAD51 binding events. In the
235 case of mRAD51 alone, using a shorter (dT)₁₃ substrate, the percentage of DNA
236 molecules with FRET alternation observed within 3 minutes (binding fraction) was
237 $18.5 \pm 3.62\%$ (Figure S3E), with the time traces dominated by the protein-free,
238 high-FRET state (Figure 3B, S3C & S4A). The low binding fraction and the
239 transience of the low FRET states indicate that the (dT)₁₃ substrate is too short to form
240 stable nucleating clusters of mRAD51. On the other hand, in the presence of mS5S1,
241 the binding fraction of mRAD51 dramatically increases to $66.6 \pm 14.0\%$ (Figure S3E)
242 and the time traces are dominated by low-FRET states (Figure 3C, S3C & S4B),
243 reflecting more RAD51 binding. This observation is consistent with our previous
244 finding that mS5S1 reduces the nucleating unit from three mRAD51 molecules to two
245 (Figure 2B-2C) and mS5S1 increases the ssDNA affinity of mRAD51 and stabilizes
246 mRAD51 nucleating clusters on ssDNA (Figure 2C). Adding mS5^{FL}S1 leads to the
247 similar consequences as mRAD51 alone case (Figure S3C, S3E, S4C & S5A),
248 consistent with the inability of mS5^{FL}S1 to stimulate mRAD51 assembly. For the
249 longer (dT)₁₈ ssDNA, mRAD51 alone results in stable binding with many more bound
250 ssDNA molecules ($58.0 \pm 7.51\%$) and the middle-to-low FRET signal is dominant
251 (Figure S3D & S4C). We identified seven FRET states (Figure S5) and corresponding
252 binding/dissociation rate constants (Figure S6) using the longer (dT)₁₈ substrates,
253 reflecting the binding of up to six mRAD51 monomers.

254 The (dT)₁₃ substrates allowed at most four mRAD51 to bind the ssDNA but
255 these binding events were not long enough to form stable filaments. We observed
256 multiple FRET states, as well as alternations among these states, reflecting dynamics
257 among multiple mRAD51 bound states. These intermediate FRET states are identified
258 by the FRET histograms (Figure S3C-S3D). Previous work on budding yeast *S.*
259 *cerevisiae* Rad51 (ScRad51) on the same (dT)₁₃ substrates resulted in five different
260 FRET states, corresponding to between zero and four ScRad51 molecules bound(17).
261 We used Bayesian analysis(43) to globally fit all of the FRET time-courses, and a
262 total of four FRET states was best found in mRAD51-only experiments (Figure 3B).
263 The four identified FRET states in mRAD51-only experiments match to zero, one,
264 two and three Rad51-bound states seen in ScRad51 experiments(17), confirming the
265 validity of our analysis. We did not observe the lowest FRET state seen in the
266 ScRad51 studies (~0.1, the four Rad51-bound state, Figure 3B), reflecting that four
267 mRAD51 oligomers in (dT)₁₃ substrates are not stable enough to be seen. On the other
268 hand, in the mixture of mRAD51/mS5S1 complex, we identified five FRET states,
269 even though the highest FRET state (protein-free state, state 0, Figure 3C) is less
270 populated. To confirm these FRET state assignments, we analyzed the FRET
271 time-courses to generate the transition density plots(18, 44) (TDP) (Figure 3D-3E) in
272 both cases. The TDP analysis identifies the FRET states before and after each
273 transition, and the heat maps allow the identifications of the distribution of multiple
274 FRET states. For example, for the mRAD51-only case, a transition from FRET value
275 of ~0.85 (state 0) to ~0.75 (state 1) will score in the “binding” section in the TDP, as
276 it reflects the binding of the first mRAD51 onto the ssDNA. The mirror symmetry
277 along the diagonal of TDP indicates the reversible changes between these FRET
278 states.

279 The transitions seen in time-courses and TDP suggest that up to five FRET states
280 observed represent the zero to four mRAD51 bound states in the (dT)₁₃ substrates.
281 The intermediate FRET values identified for the mRAD51/S5S1 complex are
282 different from the ones seen in ScRad51 and mRAD51-only cases. This difference
283 likely reflects the steric effect of the large mRAD51-S5S1 complex (~ 80 kDa),
284 driving separation between the donor and acceptor dye. The large mRAD51-S5S1
285 complex could also account for wider FRET values corresponding to zero, one and
286 two mRAD51-bound states (Figure 3E). We also noted that total fluorescence signal
287 increases upon mRAD51 binding (Figure 3B-C), suggesting a protein-induced
288 fluorescence enhancement (PIFE) effect, consistent with the previous observation in
289 ScRad51(16, 17, 45). This PIFE effect is more apparent in the presence of mS5S1
290 (Figure 3C & S7) or on the (dT)₁₈ substrates, potentially because mRAD51 is able to

291 fully extend towards the Cy3-tagged 3' terminating end with mS5S1 or on the longer
292 ssDNA.

293 Identification of these FRET states in time-courses allows us to determine the
294 evolution of these FRET states and the dwell time associated with individual states.
295 The FRET time-courses are best described by a consecutive and reversible kinetic
296 model, where individual mRAD51 monomer can bind and dissociate during the
297 nucleating cluster formation and the extension also occurs in monomer, with or
298 without mS5S1 (Figure 3B-C). The kinetics of each binding ($k_{i \rightarrow i+1}$, i is a number of
299 mRAD51 bound to ssDNA) and dissociation ($k_{i \rightarrow i-1}$) can be determined in both
300 mRAD51-only and mRAD51-S5S1 mixtures (Figure 3F). Surprisingly, when
301 comparing mRAD51-only (open bars, Figure 3F) and mRAD51-S5S1 mixture (filled
302 bars, Figure 3F), mS5S1 significantly reduces the mRAD51 dissociation rates during
303 the nucleating cluster formation. Although mS5S1 could possibly increase mRAD51
304 binding rates, the change is not significant in our experimental resolution. Therefore,
305 the major stabilization effort of mS5S1 in mRAD51 nucleating cluster formation
306 comes from the reduction in dissociation rates.

307 **Fission yeast Rad51 filament assembly is fast, with no apparent stimulation from**
308 **S5S1.** Mouse mS5S1 stimulates mRAD51 activity by accelerating the nucleation step
309 during the nucleoprotein filament assembly. Fission yeast Swi5-Sfr1 (SpS5S1) is also
310 known to stimulate SpRad51 activity(26, 29, 30, 33, 35). To examine whether the
311 activation mechanism by S5S1 is evolutionally conserved, we used the same TPM
312 approach towards SpS5S1. Under the same reaction condition (150 mM KCl, pH=7.5),
313 SpRad51 does not assemble on dsDNA in either ATP or AMPPNP (Figure S1I-S1J &
314 S1L-S1M). At the same recombinase concentration (0.8 μ M), SpRad51 displayed
315 much faster assembly kinetics than mouse mRAD51 (Figure 4A-4B, Figure 1B-1C).
316 In the absence of S5S1, SpRad51 nucleation time is 23.2 ± 0.70 s (Figure 4B), 4-fold
317 faster than that observed for mRAD51 (97.6 ± 2.89 s) (Figure 1C). To see if SpS5S1
318 complex further stimulates SpRad51 assembly, we used a reduced recombinase
319 concentration (0.3 μ M) to allow nucleation rates to be determined accurately (Figure
320 4E & S8). Interestingly, SpS5S1 did not stimulate SpRad51 nucleation at low
321 concentration and even inhibited SpRad51 nucleation at higher concentrations (solid
322 circles, Figure 4E & S8B). It is possible that SpRad51 nucleation is sufficiently fast
323 that no additional stimulation is necessary, unlike the slow nucleation observed for
324 mRAD51. As to the inhibition effect seen at higher SpS5S1 concentrations, it likely
325 results from the ssDNA binding property of SpS5S1(26, 30). Even though SpS5S1
326 has DNA affinity, its binding to DNA substrates does not alter bead BM (Figure
327 S1K-S1N). The control experiments verify that a decrease in bead BM increment with
328 increasing SpS5S1 concentration derives from reduced amounts of SpRad51 binding

329 to the gapped ssDNA substrate (Gray solid circles in Figure 4F). To test whether or
330 not ssDNA binding property of SpS5S1 inhibits SpRad51 filament assembly, we used
331 a N-terminus truncation mutant of SpSfr1 in a complex with Swi5 (SpS5S1C). The
332 N-terminal region of SpSfr1 possesses an initial interaction site with Rad51 to serve
333 as an anchor and DNA binding site, both of which are overlapped with each other.
334 Thus SpS5S1C is deficient in DNA binding but retaining SpRad51 filament
335 stabilization(30). This DNA binding-deficient mutant showed neither inhibition nor
336 stimulation of nucleoprotein filament formation even when two-fold excess amounts
337 were included (open diamonds, Figure 4E). Therefore, SpS5S1 and SpRad51 compete
338 for ssDNA binding and we conclude that SpS5S1 has no stimulatory effects on
339 SpRad51 nucleation. In addition, the magnitude of BM increment (Figure 4F & S8D)
340 drops with increasing amounts of wild-type SpS5S1, while the SpS5S1C mutant
341 protein induced no apparent change. Thus, we confirmed that higher SpS5S1
342 concentrations can compete with SpRad51 for substrates.

343 With the fast nucleation rates observed, SpRad51 displays more apparent
344 dependence on ssDNA length than mRAD51 (Figure S9A). A ~40-fold difference in
345 slope observed and similar y-intercepts here suggest that SpRad51 has higher ssDNA
346 binding affinity than mRAD51, and likely contributes to the faster nucleation rates.
347 SpRad51 concentration-dependence of nucleation rates returns a power law fitting
348 of 2.70 ± 0.29 , suggesting that three SpRad51 monomers are required for stable
349 nucleation events (Figure S9B), similar to that of mRAD51 (Figure 2A).

350 **S5S1 prevents Rad51 filament disassembly.** In addition to accelerating the binding
351 event, nucleoprotein filament stability can also be achieved by the prevention of
352 filament dissociation. In the TPM-based disassembly experiments (Figure 5),
353 surface-bound (dT)₁₃₅ gapped DNA substrates were first incubated with Rad51/ATP
354 mixture, and then another mixture of Rad51, ATP and S5S1 was added to the
355 microscope slide. This set of disassembly experiments was done for mouse (Figure
356 5B) and fission yeast (Figure 5F) proteins, respectively. The two-stage incubation
357 avoids potential ssDNA substrate competition between SpS5S1 and SpRad51.
358 Extensive buffer wash containing no Rad51 but all other components removed free
359 Rad51 from the reaction chamber. This was defined as time zero of the disassembly
360 reaction. The bead Brownian motions are measured in real-time to monitor the
361 filament length. Several kinetic parameters were determined, including (i) lifetime of
362 the stable filament (dwell time prior to BM decrease), (ii) dissociation time, time for
363 individual RAD51 monomer dissociation continuously and (iii) net BM decrease, a
364 decrease in filament coverage. Our results showed that the mRAD51 filament is quite
365 stable in ATP even without mS5S1, with minimum mean lifetime around 350 ± 39.3
366 sec (Figure 5C). In the presence of $1.0 \mu\text{M}$ mS5S1, the lifetime of the mRAD51

367 filament was further stabilized to 535 ± 49.9 sec (~ 1.53 -fold). Using low
368 concentrations of mS5S1 (0.05 or 0.3 μM) also resulted in longer lifetimes (441 ± 51.1
369 and 436 ± 45.1 sec respectively, ~ 1.27 -fold). This suggests that mS5S1 prevents
370 mRAD51 filament disassembly. Control experiments using mS5^{FL}S1 mutant return no
371 additional stabilization, confirming that mRAD51-S5S1 interaction is essential for
372 mRAD51 nucleoprotein filament stabilization. We also noticed that the fraction of
373 full-length mRAD51 filaments retained at the end of the 15-minute reaction,
374 un-disassembled filament (Figure 5D), increases in the presence of mS5S1,
375 correlating with the increased filament lifetime with mS5S1 (Figure 5C). However,
376 once dissociation was initiated (as BM starts to decrease), the dissociation rate is
377 similar either with or without mS5S1, within the resolution of our TPM measurements
378 (Figure 5E). Compared to mRAD51, the SpRad51-alone filament is less stable
379 (lifetime of 140 ± 17.9 sec, Figure 5F-5G). Essentially all SpRad51 filaments were
380 disassembled within 15 mins (Figure 5H). In the presence of SpS5S1, the lifetime of
381 the SpRad51 filament is significantly increased, as was the fraction of filaments
382 retained at the end of 15-minute observations. For example, 0.01 μM of SpS5S1
383 increases the lifetime to 382 ± 32.6 sec (~ 2.73 -fold). SpS5S1 increases the dissociation
384 time as well, making the disassembly events slower (Figure 5I). SpS5S1C mutant also
385 protects SpRad51 filament (empty bars in Figure 5G), but less effective than
386 wild-type SpS5S1 (gray solid bars) especially at lower concentrations. This may be
387 due to the lower affinity to SpRad51(35) because higher amount of SpS5S1C shows a
388 similar ability to protect the filament disassembly. Therefore, we conclude that both
389 S5S1 heterodimers act a stabilizer of Rad51 filament via direct interaction with the
390 recombinase.

391 Comparing S5S1 from these two species, we found that 1.0 μM of mS5S1 only
392 achieves ~ 1.53 -fold increase in filament lifetime while SpS5S1 increases to
393 ~ 2.73 -fold. Considering the fast disassembly kinetics of SpRad51, SpS5S1
394 predominantly acts on this filament k_{off} step. In addition, comparing bead BM changes
395 between the assembly and disassembly experiments (Figure S10), we found that not
396 all mRAD51 dissociated from the gapped DNA substrates, reflecting the incomplete
397 disassembly of mRAD51 filaments, as seen in human RAD51(14). On the contrary,
398 SpRad51 was almost entirely released from DNA as filaments initiate disassembly
399 even in the presence of SpS5S1, confirming that SpRad51 filament is more
400 susceptible to disassembly. The reason why the apparent function of S5S1 seems to be
401 different is due to the different stabilities of Rad51 filaments between yeast and
402 mouse proteins. Thus, we conclude that the primary conserved function of S5S1 is to
403 stabilize Rad51 on DNA, allowing both the formation of the stable nucleus and the
404 maintenance of filament length.

405

406 **DISCUSSIONS**

407 Nucleoprotein filament assembly is the first committed step in homologous
408 recombination and is targeted for regulation(1, 2, 23, 26, 30, 32, 46, 47). A
409 nucleoprotein filament with sufficient length is advantageous for initial homology
410 search. The filament is also expected to be dynamic during the directional exchange
411 of different parts of duplex homologous DNA. Accessory proteins have been found to
412 stimulate the recombination process by maintaining a stabilized and yet dynamic
413 recombinase nucleoprotein filament. Stabilization of the nucleoprotein filament can
414 be achieved by speeding up the filament assembly, reducing filament disassembly or
415 both. However, these kinetic parameters are typically obscured in ensemble
416 biochemical experiments. In this study, we used two different single-molecule tools to
417 determine these kinetics parameters that allow us to characterize the mechanism of
418 S5S1 regulation in mouse and fission yeast proteins. Several kinetic steps are
419 involved in filament assembly: initial Rad51 binding and dissociation events leading
420 to a stable nucleus, fast extension steps and dissociation events within growing
421 filaments. S5S1 of both species stabilized Rad51 nucleoprotein filaments by
422 preventing Rad51 dissociation from nucleation clusters and from the assembled
423 filaments. Although the S5S1 complex of these species alters the kinetic steps
424 differentially due to intrinsic characteristics of Rad51 recombinases in different
425 species, they both prevent Rad51 dissociation to facilitate efficient recombination
426 progression. Here, we used two complementary single-molecule tools to characterize
427 the assembly. TPM experiments allow to characterize the formation and disassembly
428 of individual stable filaments, and FRET experiments capture the dynamics of
429 individual Rad51 binding and dissociation before a stable nucleus is formed. An
430 apparent stimulation of the Rad51 filament nucleation by S5S1 seen in TPM
431 experiments is attributed to the reduction of the dissociation rate in nucleus formation
432 observed in FRET. A nearly 4-fold reduction of dissociation rate ($k_{l \rightarrow 0}$) of mRAD51
433 is seen in the presence of mS5S1, but no apparent change in binding rates is seen
434 (Figure 3F). This then leads to a reduction in nucleation size of three mRAD51
435 monomers to two mRAD51 monomers in the presence of mS5S1. Fission yeast
436 Rad51 is fast in filament assembly, but is prone to disassembly.. SpS5S1 stabilizes the
437 SpRad51 filaments by specifically preventing SpRad51 dissociation. Therefore, S5S1
438 of two species stabilize Rad51 filaments by using the same strategy of preventing
439 Rad51 dissociation. Our single-molecule experiments speak specifically to the Rad51
440 state when it nucleates and extends on the DNA substrates, and our data are consistent
441 with previously shown in the literature(14, 17). Previous works have suggested that
442 recombinases from various species can exist in oligomers in solution(48-52). It is

443 possible that a structural transition is made in solution before or during the DNA
444 binding, so smaller units of Rad51 oligomers are responsible for nucleation and
445 individual Rad51 molecule is added during filament growth.

446 S5S1 association with Rad51 could either expose DNA binding domain of Rad51
447 or stabilize the oligomeric interface of Rad51. SpS5S1 has two Rad51 binding sites: a
448 high-affinity one in N-terminus of Sfr1 and a low-affinity one in C-terminus(30).
449 Mouse S5S1 has only one mRAD51 binding site, residing in the C-terminus(31). The
450 difference in Rad51 binding affinity between mouse and fission yeast S5S1 is
451 responsible for the observation that more S5S1 is required for the Rad51 stability in
452 the cases of mS5S1 and SpS5S1C mutants (Figure 5C and 5G). Considering its large
453 effect on both dissociation rates (FRET experiments) and disassembly rates (TPM
454 disassembly experiments), we suggest that S5S1 acts by holding adjacent Rad51
455 molecules together, reducing dissociation. The interaction between S5S1 and RAD51
456 is thus essential for stimulation, confirmed by the abolished stimulation seen in
457 mS5^{FL}S1 mutants (Figure 1C, 2A, 5C, and S3-S5).

458 Different amounts of S5S1 required to stimulate nucleation and reduce filament
459 disassembly provides hints how S5S1 interacts with Rad51 molecules to achieve
460 filament stabilization. For the mouse proteins, a two-fold excess of mS5S1 maximally
461 stimulates mRAD51 nucleation (Figure 1F). However, stabilization in the disassembly
462 experiments can be seen with the low coverage of mS5S1 complex (~17%, Figure 5C,
463 0.05 μ M vs 0.3 μ M mRAD51 added). Previous structural studies suggested that S5S1
464 is accommodated within the groove of the Rad51 filament(30). The different
465 concentration requirements of S5S1 point to a model that S5S1 binding stabilizes
466 adjacent Rad51 molecules through binding within the filament groove to prevent
467 Rad51 dissociation (Figure 6 & S11). During the nucleus formation, more mS5S1 are
468 required so most of Rad51 are stabilized by S5S1. As Rad51 dissociation is inhibited
469 by S5S1, stable Rad51 nucleus can be formed more easily. On the other hand, as
470 filament disassembly could take place at the filament end more frequently, filament
471 stabilization can be achieved by those S5S1 binding to terminal Rad51. Therefore,
472 low coverage S5S1 is sufficient. As S5S1 has also been shown to activate Rad51
473 filaments(30, 32), S5S1 binding within Rad51 filament also contributes to the overall
474 Rad51 activity stimulation. During the dynamic progression of strand exchange, low
475 S5S1 coverage allows efficient budgeting of S5S1, so S5S1 can be available for
476 stimulation at later stages of recombination progression.

477 There exist several heterodimeric complexes regulating recombinase
478 nucleoprotein filament stability(2-4, 53, 54). The elongated crescent-like structure of
479 Hop2-Mnd1 shares a similar structural motif with S5S1. In both cases, the
480 heterodimeric complex interacts with the groove of the Dmc1 and/or Rad51 filament

481 to stabilize the nucleoprotein filaments(1, 55-58). A Rad51 paralog complex in *C.*
482 *elegans*, RFS-1/RIP-1 complex, also has been proposed to act similarly on Rad51
483 filament remodeling(54). *S. cerevisiae* Psy3-Csm2 dimer has been suggested to bind
484 to the end of Rad51 filaments to achieve filament stabilization(53). Together with the
485 structural evidence, it is possible that the mechanism proposed here likely serves as a
486 general principle for these heterodimeric complexes involved in filament stabilization.
487 For example, whether these accessory factors, such as BRCA2, PCSS complex and
488 RAD51 paralogs(24, 53, 54), work synergistically on the filament stabilization. It is
489 possible that these accessory proteins allow better modulation on filament dynamics
490 for efficient strand exchange progression.

491 Differences in kinetics are seen between mouse RAD51 and SpRad51
492 recombinases. Mouse RAD51 is slower in nucleation, but SpRad51 is more prone to
493 disassembly. We have found that mS5S1 acts effectively on the nucleation step while
494 SpS5S1 acts primarily on the disassembly step to achieve nucleoprotein filament
495 stabilization. However, DNA binding of SpS5S1 is shown to inhibit SpRad51 filament
496 assembly (Figure 4E-4F) and strand-exchange(26, 33). It is likely that accessory
497 proteins evolve to accommodate different kinetics characteristics of recombinases
498 during speciation and play the different roles of in the progression of homologous
499 recombination process. For example, SAXS and X-ray crystallographic studies
500 showed that SpS5S1 fits into the helical groove of the SpRad51 filament and also
501 extends onto ssDNA(29, 30, 35, 59). In addition to stabilizing SpRad51, SpS5S1
502 interacts with ssDNA provides addition safe latch on SpRad51. Budding yeast
503 Mei5-Sae3 complex (ScM5S3), orthologs of Sfr1 and Swi5, has been shown to
504 stabilize ScDmc1 filament and to stimulate ScDmc1-mediated strand exchange during
505 meiosis (19, 60, 61). ScM5S3 possesses both ssDNA and dsDNA affinities, and it is
506 possible that budding yeast M5S3 stabilizes ScDmc1 filament in a similar, general
507 mechanism found in mouse and fission yeast.

508 ssDNA is likely bound by single-stranded DNA binding proteins, for example,
509 replication protein A (RPA) to prevent nucleolytic cleavage. RPA binding to ssDNA is
510 a physical barrier for Rad51 assembly. Previous findings demonstrate that fission
511 yeast S5S1 works synergistically with Rad52 to stimulate the Rad51 assembly on
512 RPA-coated ssDNA(28, 35). It would be interesting to see whether SpS5S1 also
513 primarily acts on preventing SpRad51 disassembly in the presence of RPA.

514 Both mouse and fission yeast S5S1 have been shown to activate Rad51 filament
515 by stimulating ssDNA-dependent ATPase activity of Rad51(30, 32). Moreover, mouse
516 S5S1 enhances ATPase activities of mRAD51 by stimulating the release of ADP to
517 maintain the filament in an active form(30, 32). *E. coli* RecA recombinases have also
518 been shown to continuously hydrolyze ATP and bind new ATP molecules without

519 dissociating from DNA(62). It's possible that mS5S1 stabilizes interfaces between
520 adjacent mRAD51 molecules within the filament during ATPase turnover events, and
521 thus maintains active nucleoprotein filaments. It is important to note that co-factors
522 like AMPPNP and Ca^{2+} increase the stability of Rad51 filaments by inhibiting ATP
523 hydrolysis and maintaining the ATP-bound form of Rad51, and then these co-factors
524 promote strand exchange activity(25, 33, 35, 63, 64). Therefore, in contrast to
525 AMPPNP and Ca^{2+} effects, S5S1 stimulates Rad51 progression in a unique
526 mechanism. Maintaining a dynamic nucleoprotein filament homeostasis requires
527 Rad51 dissociation at appropriate rates. Swi5-Sfr1 and other accessory proteins serve
528 the purpose to modulate dissociation rates of Rad51 to fine tune recombinase
529 progression.

530

531 **MATERIALS AND METHODS**

532 **Supporting Information.** A detailed description of the DNA substrates preparations,
533 proteins & buffer conditions and detailed experimental procedures of single-molecule
534 tethered particle motion (TPM) assembly experiment are provided in Supporting
535 Information.

536 **Single-molecule TPM assembly experiment and data analysis.**
537 Streptavidin-labeled beads were prepared as previously described(65). In filament
538 assembly experiments, glass slide was coated with 5 $\mu\text{g}/\text{mL}$ anti-digoxigenin and
539 blocked with 2 mg/mL bovine serum albumin (BSA) sequentially. 4 nM DNA
540 substrates were incubated on the anti-digoxigenin-coated slide for 30 min followed by
541 buffer washing to remove unbound DNA. 220 nm streptavidin-decorated polystyrene
542 beads were then attached to the DNA substrates for microscopic visualization. All
543 TPM reactions were performed in either mouse or fission yeast buffers supplemented
544 with 1 mM DTT and 2 mM ATP. TPM assembly experiments were initiated by
545 introducing a Rad51-ATP (or with S5S1) mixture into the reaction chamber
546 containing the surface-anchored gapped substrates.

547 We used an inverted optical microscope (IX-71, Olympus) with a differential
548 interference contrast (DIC) imaging mode to visualize tethers and measure bead
549 Brownian motion (BM). Images of assembly experiments were acquired at 30 Hz
550 using a Newvicon camera (Dage-MTI) and were analyzed using software written in
551 Labview. The amplitude of tether Brownian motion is defined by the standard
552 deviation of the bead centroid positions of 20 images using sliding windows. In
553 addition to the DNA contour length change, polymer stiffness and camera exposure
554 time alter the Brownian motion amplitudes in practice(42). For each independent
555 TPM assembly experiments, images were first recorded for around 30 seconds (~
556 1000 image frames) before the addition of Rad51 or Rad51-S5S1 mixture and then for

557 about 15 minutes (~ 30000 image frames) after the addition of the mixtures. For
558 snapshot control experiments, 1000 image frames were recorded at 5-6 different
559 field-of-views on coverslip after 5 min reaction (Figure S1).

560 **Single-molecule fluorescence resonance energy transfer (smFRET) experiment**
561 **and data analysis.** In smFRET experiments, PEGylated glass slides and coverslips
562 were prepared as previously described(66). To perform smFRET experiments,
563 reaction chambers were incubated with 20 µg/mL streptavidin for 5 min. Excess
564 streptavidin was washed away with the buffer containing 20 mM Tris and 50 mM
565 NaCl. 15 pM of 3'-biotinylated fluorophore-labeled hybrid DNA was then
566 immobilized on the surface for 5 min. After 5 min incubation, free DNA was removed
567 by flowing in mRAD51 imaging buffer containing 1 mM Trolox (Sigma-Aldrich), 2.6
568 mM protocatechuic acid (PCA, Sigma-Aldrich), 0.21 units/mL protocatechuate
569 3,4-dioxygenase (PCD, OYC Americas Inc.), 30 mM Tris, 2.5 mM magnesium
570 chloride and 150 mM potassium chloride at pH 7.5. The reaction includes a mixture
571 of 1 µM mRAD51 and 2 mM ATP in mRAD51 imaging buffer into reaction chambers.
572 mS5S1 (or mS5FLS1)-containing experiments includes 1 µM mRAD51, 2 µM mS5S1
573 (or mS5FLS1) and 2 mM ATP in mRAD51 imaging buffer. Under our imaging
574 conditions, ~78 % of fluorophores in hybrid DNA survives for more than 200 sec.

575 We utilized objective-type total internal reflection fluorescence microscope
576 (TIRFM, Olympus IX2) and 532 nm laser as excitation light source in smFRET
577 experiments. Fluorescence intensity signals of both Cy3 and Cy5 were acquired with
578 EMCCD (ProEM 512B, Princeton Instrument) at 20 Hz using a dual-view system.
579 Emission movies of Cy3 and Cy5 fluorescence were recorded using a software
580 program written in Labview 8.6. Colocalized Cy3 and Cy5 spots were analyzed using
581 a mapping software program written in IDL. Fluorescence intensity time-traces of
582 each individual mapped DNA molecule were analyzed using Matlab. Alternation in
583 FRET values was analyzed using variational Bayesian analysis (vbFRET) to globally
584 fit all time-courses(43).

585

586 **ACKNOWLEDGEMENTS:** This work was supported by grants from Ministry of
587 Science and Technology of Taiwan (MOST 104-2628-M-002-008-MY3 to H.W.L.;
588 MOST 105-2314-B-002-073-MY4 to P.C.), from Academia Sinica (to P.C.), the career
589 development program from National Taiwan University (to H.W.L. and to P. C.), and
590 partly by Grants-in-Aids for Scientific Research on Innovative Areas (15H05974) and
591 for Scientific Research-A (18H03985) from Japan Society for the Promotion of
592 Science (JSPS) (to H.I.). We thank Steve Bell (MIT, Biology) for helpful comments
593 and suggestions, and Kai-Chun Chang (NTU) for discussion in the smFRET data
594 analysis.

595

596 **ADDITIONAL INFORMATION:** Authors have no conflicts of interest with the
597 contents of this article.

598

599 **REFERENCES**

- 600 1. Heyer WD, Ehmsen KT, & Liu J (2010) Regulation of Homologous
601 Recombination in Eukaryotes. *Annual Review of Genetics* 44:113-139.
- 602 2. Filippo JS, Sung P, & Klein H (2008) Mechanism of eukaryotic homologous
603 recombination. *Annu Rev Biochem* 77:229-257.
- 604 3. Cox MM, *et al.* (2000) The importance of repairing stalled replication forks.
605 *Nature* 404(6773):37-41.
- 606 4. Zhou Y, Caron P, Legube G, & Paull TT (2014) Quantitation of DNA
607 double-strand break resection intermediates in human cells. *Nucleic Acids Res*
608 42(3).
- 609 5. Nimonkar AV, *et al.* (2011) BLM-DNA2-RPA-MRN and
610 EXO1-BLM-RPA-MRN constitute two DNA end resection machineries for
611 human DNA break repair. *Gene Dev* 25(4):350-362.
- 612 6. Niu HY, *et al.* (2010) Mechanism of the ATP-dependent DNA end-resection
613 machinery from *Saccharomyces cerevisiae*. *Nature* 467(7311):108-U143.
- 614 7. Cejka P, *et al.* (2010) DNA end resection by Dna2-Sgs1-RPA and its
615 stimulation by Top3-Rmi1 and Mre11-Rad50-Xrs2. *Nature*
616 467(7311):112-U149.
- 617 8. Kowalczykowski SC (2015) An Overview of the Molecular Mechanisms of
618 Recombinational DNA Repair. *Csh Perspect Biol* 7(11).
- 619 9. Krejci L, Altmannova V, Spirek M, & Zhao XL (2012) Homologous
620 recombination and its regulation. *Nucleic Acids Res* 40(13):5795-5818.
- 621 10. Morrical SW (2015) DNA-Pairing and Annealing Processes in Homologous
622 Recombination and Homology-Directed Repair. *Csh Perspect Biol* 7(2).
- 623 11. van der Heijden T, *et al.* (2007) Real-time assembly and disassembly of
624 human RAD51 filaments on individual DNA molecules. *Nucleic Acids Res*
625 35(17):5646-5657.
- 626 12. Bell JC, Plank JL, Dombrowski CC, & Kowalczykowski SC (2012) Direct
627 imaging of RecA nucleation and growth on single molecules of SSB-coated
628 ssDNA. *Nature* 491(7423):274-U144.
- 629 13. Candelli A, *et al.* (2014) Visualization and quantification of nascent RAD51
630 filament formation at single-monomer resolution. *P Natl Acad Sci USA*
631 111(42):15090-15095.
- 632 14. Hilario J, Amitani I, Baskin RJ, & Kowalczykowski SC (2009) Direct imaging

- 633 of human Rad51 nucleoprotein dynamics on individual DNA molecules. *P*
634 *Natl Acad Sci USA* 106(2):361-368.
- 635 15. Ma CJ, Gibb B, Kwon Y, Sung P, & Greene EC (2017) Protein dynamics of
636 human RPA and RAD51 on ssDNA during assembly and disassembly of the
637 RAD51 filament. *Nucleic Acids Res* 45(2):749-761.
- 638 16. Antony E, *et al.* (2009) Srs2 Disassembles Rad51 Filaments by a
639 Protein-Protein Interaction Triggering ATP Turnover and Dissociation of
640 Rad51 from DNA. *Mol Cell* 35(1):105-115.
- 641 17. Qiu YP, *et al.* (2013) Srs2 prevents Rad51 filament formation by repetitive
642 motion on DNA. *Nat Commun* 4.
- 643 18. Joo C, *et al.* (2006) Real-time observation of RecA filament dynamics with
644 single monomer resolution. *Cell* 126(3):515-527.
- 645 19. Say AF, *et al.* (2011) The budding yeast Mei5-Sae3 complex interacts with
646 Rad51 and preferentially binds a DNA fork structure. *DNA Repair*
647 10(6):586-594.
- 648 20. Chun J, Buechelmaier ES, & Powell SN (2013) Rad51 Paralog Complexes
649 BCDX2 and CX3 Act at Different Stages in the BRCA1-BRCA2-Dependent
650 Homologous Recombination Pathway. *Mol Cell Biol* 33(2):387-395.
- 651 21. Sugawara N, Wang X, & Haber JE (2003) In vivo roles of Rad52, Rad54, and
652 Rad55 proteins in Rad51-mediated recombination. *Mol Cell* 12(1):209-219.
- 653 22. Liu J, *et al.* (2011) Rad51 paralogues Rad55-Rad57 balance the
654 antirecombinase Srs2 in Rad51 filament formation. *Nature*
655 479(7372):245-U129.
- 656 23. Yang HJ, Li QB, Fan J, Holloman WK, & Pavletich NP (2005) The BRCA2
657 homologue Brh2 nucleates RAD51 filament formation at a dsDNA-ssDNA
658 junction. *Nature* 433(7026):653-657.
- 659 24. Esashi F, Galkin VE, Yu X, Egelman EH, & West SC (2007) Stabilization of
660 RAD51 nucleoprotein filaments by the C-terminal region of BRCA2. *Nat*
661 *Struct Mol Biol* 14(6):468-474.
- 662 25. Tsai SP, *et al.* (2012) Rad51 presynaptic filament stabilization function of the
663 mouse Swi5-Sfr1 heterodimeric complex. *Nucleic Acids Res*
664 40(14):6558-6569.
- 665 26. Haruta N, *et al.* (2006) The Swi5-Sfr1 complex stimulates Rhp51/Rad51- and
666 Dmcl-mediated DNA strand exchange in vitro. *Nat Struct Mol Biol*
667 13(9):823-830.
- 668 27. Akamatsu Y, Dziadkowiec D, Ikeguchi M, Shinagawa H, & Iwasaki H (2003)
669 Two different Swi5-containing protein complexes are involved in mating-type
670 switching and recombination repair in fission yeast. *P Natl Acad Sci USA*

- 671 100(26):15770-15775.
- 672 28. Argunhan B, Murayama Y, & Iwasaki H (2017) The differentiated and
673 conserved roles of Swi5-Sfr1 in homologous recombination. *Febs Lett*
674 591(14):2035-2047.
- 675 29. Kokabu Y, *et al.* (2011) Fission Yeast Swi5-Sfr1 Protein Complex, an
676 Activator of Rad51 Recombinase, Forms an Extremely Elongated
677 Dogleg-shaped Structure. *J Biol Chem* 286(50):43569-43576.
- 678 30. Kuwabara N, *et al.* (2012) Mechanistic Insights into the Activation of
679 Rad51-Mediated Strand Exchange from the Structure of a Recombination
680 Activator, the Swi5-Sfr1 Complex. *Structure* 20(3):440-449.
- 681 31. Su GC, *et al.* (2016) Role of the RAD51-SWI5-SFR1 Ensemble in
682 homologous recombination. *Nucleic Acids Res* 44(13):6242-6251.
- 683 32. Su GC, *et al.* (2014) Enhancement of ADP release from the RAD51
684 presynaptic filament by the SWI5-SFR1 complex. *Nucleic Acids Res*
685 42(1):349-358.
- 686 33. Ito K, Murayama Y, Takahashi M, & Iwasaki H (2018) Two three-strand
687 intermediates are processed during Rad51-driven DNA strand exchange. *Nat*
688 *Struct Mol Biol* 25(1):29-36.
- 689 34. Akamatsu Y & Jasin M (2010) Role for the Mammalian Swi5-Sfr1 Complex
690 in DNA Strand Break Repair through Homologous Recombination. *Plos Genet*
691 6(10).
- 692 35. Kurokawa Y, Murayama Y, Haruta-Takahashi N, Urabe I, & Iwasaki H (2008)
693 Reconstitution of DNA strand exchange mediated by Rhp51 recombinase and
694 two mediators. *Plos Biol* 6(4):836-848.
- 695 36. Lu YW, *et al.* (2013) Using Single-Molecule Approaches To Study Archaeal
696 DNA-Binding Protein Alba1. *Biochemistry* 52(44):7714-7722.
- 697 37. Piechura JR, *et al.* (2015) Biochemical characterization of RecA variants that
698 contribute to extreme resistance to ionizing radiation. *DNA Repair* 26:30-43.
- 699 38. Wu H-Y, Lu C-H, & Li H-W (2017) RecA-SSB Interaction Modulates RecA
700 Nucleoprotein Filament Formation on SSB-Wrapped DNA. *Sci Rep*
701 7(1):11876.
- 702 39. Liu YL, Stasiak AZ, Mellwraith MJ, Stasiak A, & West SC (2004)
703 Conformational changes modulate the activity of human RAD51 protein. *J*
704 *Mol Biol* 337(4):817-827.
- 705 40. Ristic D, *et al.* (2005) Human Rad51 filaments on double- and single-stranded
706 DNA: correlating regular and irregular forms with recombination function.
707 *Nucleic Acids Res* 33(10):3292-3302.
- 708 41. Towles KB, Beausang JF, Garcia HG, Phillips R, & Nelson PC (2009)

- 709 First-principles calculation of DNA looping in tethered particle experiments.
710 *Phys Biol* 6(2).
- 711 42. Hsu HF, Ngo KV, Chitteni-Pattu S, Cox MM, & Li HW (2011) Investigating
712 *Deinococcus radiodurans* RecA Protein Filament Formation on
713 Double-Stranded DNA by a Real-Time Single-Molecule Approach.
714 *Biochemistry* 50(39):8270-8280.
- 715 43. Bronson JE, Fei JY, Hofman JM, Gonzalez RL, & Wiggins CH (2009)
716 Learning Rates and States from Biophysical Time Series: A Bayesian
717 Approach to Model Selection and Single-Molecule FRET Data. *Biophys J*
718 97(12):3196-3205.
- 719 44. McKinney SA, Joo C, & Ha T (2006) Analysis of single-molecule FRET
720 trajectories using hidden Markov modeling. *Biophys J* 91(5):1941-1951.
- 721 45. Hwang H, Kim H, & Myong S (2011) Protein induced fluorescence
722 enhancement as a single molecule assay with short distance sensitivity. *P Natl*
723 *Acad Sci USA* 108(18):7414-7418.
- 724 46. Davies OR & Pellegrini L (2007) Interaction with the BRCA2 C terminus
725 protects RAD51-DNA filaments from disassembly by BRC repeats. *Nat Struct*
726 *Mol Biol* 14(6):475-483.
- 727 47. Lusetti SL, *et al.* (2006) The RecF protein antagonizes RecX function via
728 direct interaction. *Mol Cell* 21(1):41-50.
- 729 48. Passy SI, *et al.* (1999) Human Dmc1 protein binds DNA as an octameric ring.
730 *P Natl Acad Sci USA* 96(19):10684-10688.
- 731 49. Davies AA, *et al.* (2001) Role of BRCA2 in control of the RAD51
732 recombination and DNA repair protein. *Mol Cell* 7(2):273-282.
- 733 50. Pellegrini L, *et al.* (2002) Insights into DNA recombination from the structure
734 of a RAD51-BRCA2 complex. *Nature* 420(6913):287-293.
- 735 51. McIlwraith MJ, *et al.* (2001) RadA protein from *Archaeoglobus fulgidus* forms
736 rings, nucleoprotein filaments and catalyses homologous recombination.
737 *Nucleic Acids Res* 29(22):4509-4517.
- 738 52. Yang SX, Yu X, Seitz EM, Kowalczykowski SC, & Egelman EH (2001)
739 Archaeal RadA protein binds DNA as both helical filaments and octameric
740 rings. *J Mol Biol* 314(5):1077-1085.
- 741 53. Sasanuma H, *et al.* (2013) A new protein complex promoting the assembly of
742 Rad51 filaments. *Nat Commun* 4:1676.
- 743 54. Taylor MRG, *et al.* (2016) A Polar and Nucleotide-Dependent Mechanism of
744 Action for RAD51 Paralogs in RAD51 Filament Remodeling. *Mol Cell*
745 64(5):926-939.
- 746 55. Bugreev DV, *et al.* (2014) HOP2-MND1 modulates RAD51 binding to

- 747 nucleotides and DNA. *Nat Commun* 5.
- 748 56. Chi P, San Filippo J, Sehorn MG, Petukhova GV, & Sung P (2007) Bipartite
749 stimulatory action of the Hop2-Mnd1 complex on the Rad51 recombinase.
750 *Gene Dev* 21(14):1747-1757.
- 751 57. Zhao WX & Sung P (2015) Significance of ligand interactions involving
752 Hop2-Mnd1 and the RAD51 and DMC1 recombinases in homologous DNA
753 repair and XX ovarian dysgenesis. *Nucleic Acids Res* 43(8):4055-4066.
- 754 58. Kang HA, *et al.* (2015) NAR Breakthrough Article Crystal structure of
755 Hop2-Mnd1 and mechanistic insights into its role in meiotic recombination.
756 *Nucleic Acids Res* 43(7):3841-3856.
- 757 59. Saikusa K, *et al.* (2013) Characterisation of an intrinsically disordered protein
758 complex of Swi5-Sfr1 by ion mobility mass spectrometry and small-angle
759 X-ray scattering. *Analyst* 138(5):1441-1449.
- 760 60. Ferrari SR, Grubb J, & Bishop DK (2009) The Mei5-Sae3 Protein Complex
761 Mediates Dmc1 Activity in *Saccharomyces cerevisiae*. *J Biol Chem*
762 284(18):11766-11770.
- 763 61. Hayase A, *et al.* (2004) A protein complex containing Mei5 and Sae3 promotes
764 the assembly of the meiosis-specific RecA homolog Dmc1. *Cell*
765 119(7):927-940.
- 766 62. Kim SH, *et al.* (2014) Cooperative Conformational Transitions Keep RecA
767 Filament Active During ATPase Cycle. *J Am Chem Soc* 136(42):14796-14800.
- 768 63. Bugreev DV & Mazin AV (2004) Ca²⁺ activates human homologous
769 recombination protein Rad51 by modulating its ATPase activity. *P Natl Acad*
770 *Sci USA* 101(27):9988-9993.
- 771 64. Chi P, Van Komen S, Sehorn MG, Sigurdsson S, & Sung P (2006) Roles of
772 ATP binding and ATP hydrolysis in human Rad51 recombinase function. *DNA*
773 *Repair* 5(3):381-391.
- 774 65. Chung C & Li HW (2013) Direct Observation of RecBCD Helicase as
775 Single-Stranded DNA Translocases. *J Am Chem Soc* 135(24):8920-8925.
- 776 66. Lu C-H, Chang T-T, Cho C-C, Lin H-C, & Li H-W (2017) Stable Nuclei of
777 Nucleoprotein Filament and High ssDNA Binding Affinity Contribute to
778 Enhanced RecA E38K Recombinase Activity. *Sci Rep* 7(1):14964.

779

780 Figure Legends

781 **Figure 1. Mouse SWI5-SFR1 (mS5S1) stimulates mRAD51 nucleoprotein**
782 **filament assembly. (A)** Schematic illustration of the RAD51 nucleoprotein assembly
783 experiments. **(B)** Representative bead BM time-courses of mRAD51 (0.8 μ M)
784 assembly on (dT)₁₃₅ DNA substrates without mS5S1 (upper), with 1.6 μ M mS5S1

785 (middle) or with 1.6 μM mS5^{FL}S1 mutant (lower). Gray bars correspond to the
786 deadtime when recombinase mixtures with 2 mM ATP were introduced. Histograms
787 of nucleation time (C), mean extension time (second/RAD51) (D) and bead BM
788 increment (E) of mRAD51 assembling. All experiments were carried out at 2 mM
789 ATP. Error bar of nucleation rate was the standard deviation of the mean by
790 bootstrapping 5000 times, and error bar of extension time is one standard error of the
791 mean (SEM). (F) 0.8 μM mRAD51 was pre-incubated with various stoichiometric
792 ratios of mS5S1 and the mixture was introduced into a reaction chamber containing
793 surface-bound (dT)₁₃₅ gapped DNA. Nucleation rates are about constant ($\sim 0.010 \text{ s}^{-1}$)
794 when the [mS5S1]/[mRAD51] ratio is less than 1.625. The nucleation rates of
795 mRAD51 increase and achieve maximum value ($\sim 0.015 \text{ s}^{-1}$) when the ratio of
796 [mS5S1]/[mRAD51] is larger than 2, suggesting that maximum nucleation stimulation
797 occurs in the mixture of one mRAD51 and two mS5S1. Individual nucleation rates
798 were obtained based on Maximum likelihood estimation (MLE). (G) Bead BM
799 increment of mRAD51 assembly on (dT)₁₃₅ DNA substrates in the presence of
800 indicated ratios of mS5S1 to mRAD51. Bead BM increment reflects the coverage of
801 the RAD51 nucleoprotein filaments. mRAD51 forms longer and more stable
802 filaments in the presence of mS5S1. All experiments were carried out at 2 mM ATP.
803 Black open square represents the nucleation rate of mRAD51 in the presence of
804 non-hydrolyzable ATP analog, AMPPNP, in the absence of mS5S1. Dash lines are the
805 mean, and the shaded region span two standard deviations. Error bar of bead BM
806 increment is one SEM.

807

808 **Figure 2. Mouse mS5S1 reduces nucleation unit of mRAD51 and increases the**
809 **ssDNA affinity. (A-B)** RAD51 concentration dependence of filament nucleation
810 obtained by TPM experiments. Power law fitting to the observed nucleation rates
811 suggests the nucleation unit of RAD51: 2.43 ± 0.46 for mRAD51 (A) and 1.67 ± 0.16
812 for mRAD51-S5S1 complex (B). Green open circles in (A) are nucleation rates of
813 mRAD51 in the presence of excess mS5^{FL}S1 mutants, defective in stimulating
814 mRAD51. mS5S1 & mS5^{FL}S1 are in two-fold excess in (A) & (B). (C) ssDNA length
815 dependence of mRAD51 filament nucleation rate obtained by TPM experiments.
816 Gapped DNA substrates contain only one 5' ds/ss junction but various lengths of
817 ssDNA gaps (90-200 nt). As the gapped DNA substrate structure, overall nucleation
818 rates are fitted to $k_{ssDNA}^{app}(L_{ssDNA}) + k_{junction}^{app}$, where k_{ssDNA}^{app} and $k_{junction}^{app}$ are
819 apparent ssDNA-dependent nucleation rate constant and apparent ds/ss
820 junction-dependent nucleation rate constant. (Red) 0.8 μM mRAD51 only and (blue)
821 mixture of 0.8 μM mRAD51 and 1.6 μM mS5S1. All experiments were carried out at
822 2 mM ATP.

823

824 **Figure 3. Single-molecule FRET experiments demonstrate that mS5S1 stabilizes**
825 **mRAD51 nucleating clusters.** (A) Schematic illustration of single-molecule
826 fluorescence resonance energy transfer (smFRET) experimental setup. mRAD51
827 assembles onto (dT)₁₃ ssDNA results in the FRET decrease due to the increase of dye
828 pair separation. (B–F) Single-molecule FRET observation of mRAD51 nucleating
829 cluster dynamics. Exemplary FRET time trace of (B) mRAD51 and (C)
830 mRAD51-S5S1 complex assembling on (dT)₁₃ ssDNA substrate. High FRET state
831 (~0.8) corresponds to a DNA-only state, and low FRET state (0.0~0.6) corresponds to
832 the mRAD51-bound state. (D–E) Transition density plots (TDP) clearly reflect 4 states
833 (without mS5S1) and 5 states (with mS5S1) in mRAD51 nucleating cluster dynamics.
834 (F) Rate constants of mRAD51 nucleating cluster dynamics in the absence (empty bar)
835 and presence (solid bar) of mS5S1. Error bar of binding and dissociation rates were
836 the standard deviation of the mean by bootstrapping 5000 times.

837

838 **Figure 4. Fission yeast SpS5S1 does not stimulate SpRad51 filament assembly.** (A)
839 Representative bead BM time-courses of fission yeast Rad51 (0.8 μM) assembly on
840 the (dT)₁₃₅ DNA substrates without S5S1. (B) Nucleation time, (C) mean extension
841 time (second/Rad51) and (D) bead BM increment analyzed from individual assembly
842 time-courses. Nucleation time histograms are fitted by single exponential decay. (E)
843 Nucleation rates of various concentrations of SpS5S1 at constant 0.3 μM of SpRad51.
844 (F) Bead BM increments of SpRad51 assembly at various ratios of SpS5S1 and
845 SpRad51 mixtures also decreased at higher SpS5S1 concentrations. All experiments
846 were carried out at 2 mM ATP and 0.3 μM SpRad51. Gray solid circles are from
847 wild-type SpS5S1 experiments. Black diamonds are from the N-terminus truncation
848 mutant of SpS5S1 (SpS5S1C) deficient in ssDNA binding. Dash lines are the mean,
849 and the shaded region span two standard deviations.

850

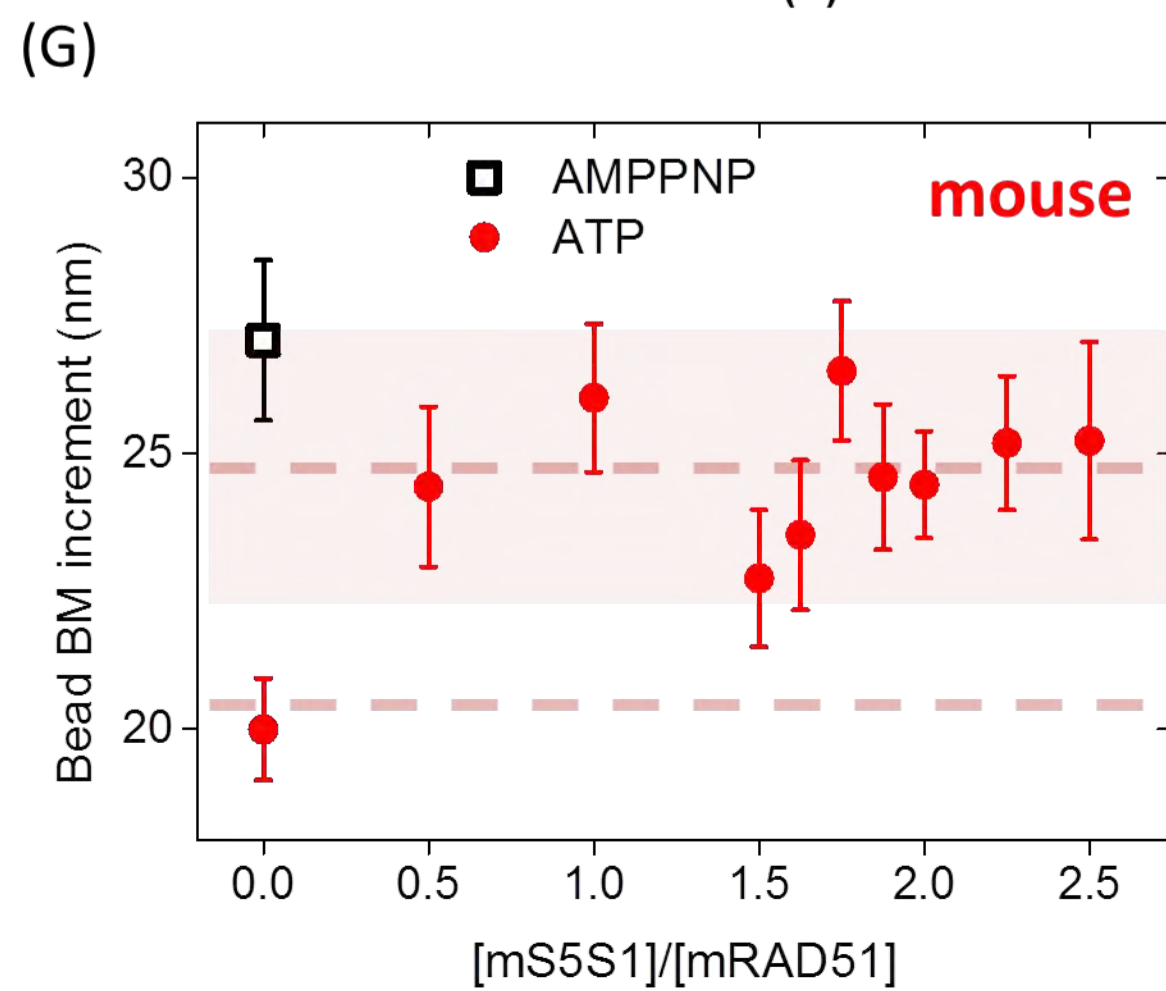
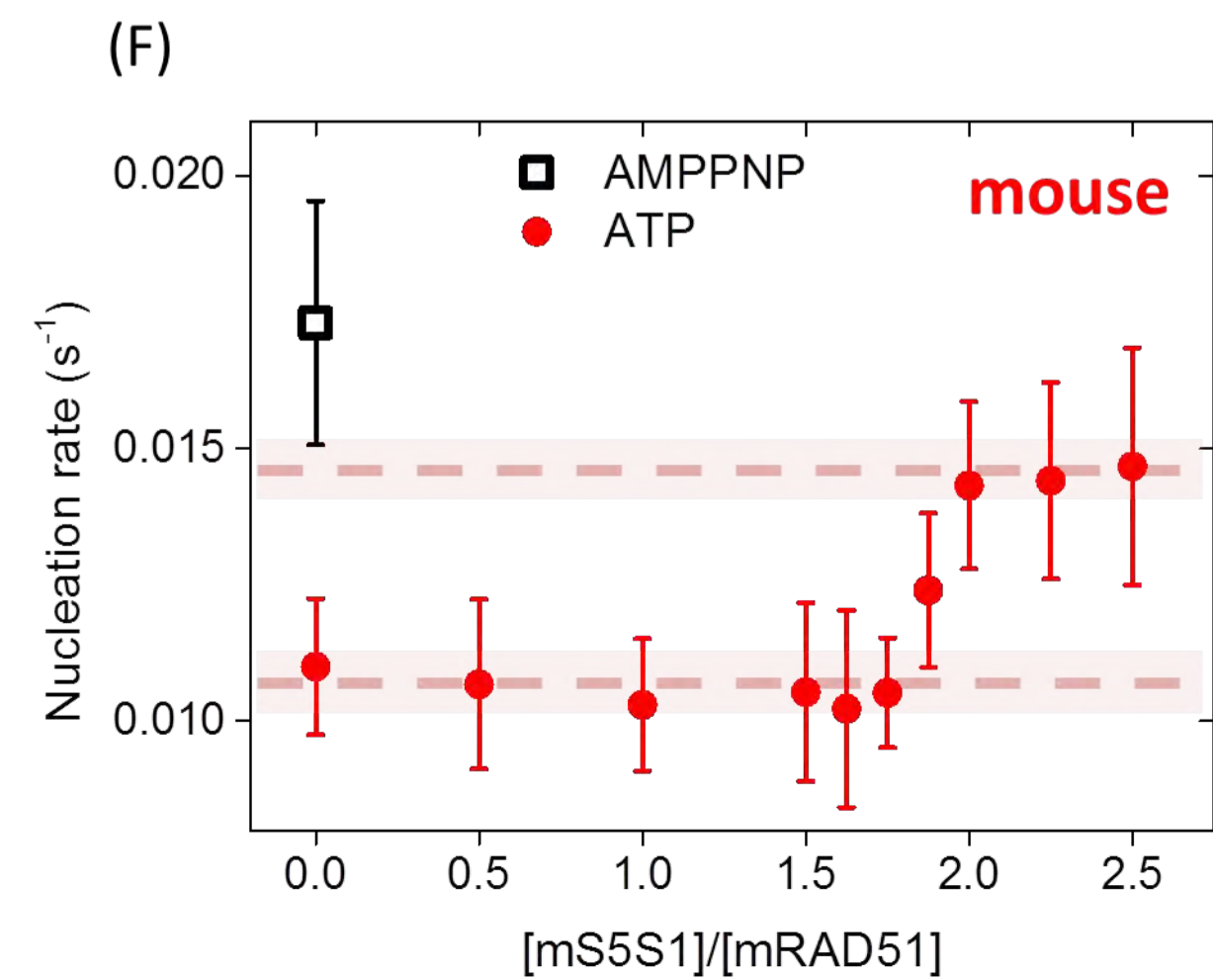
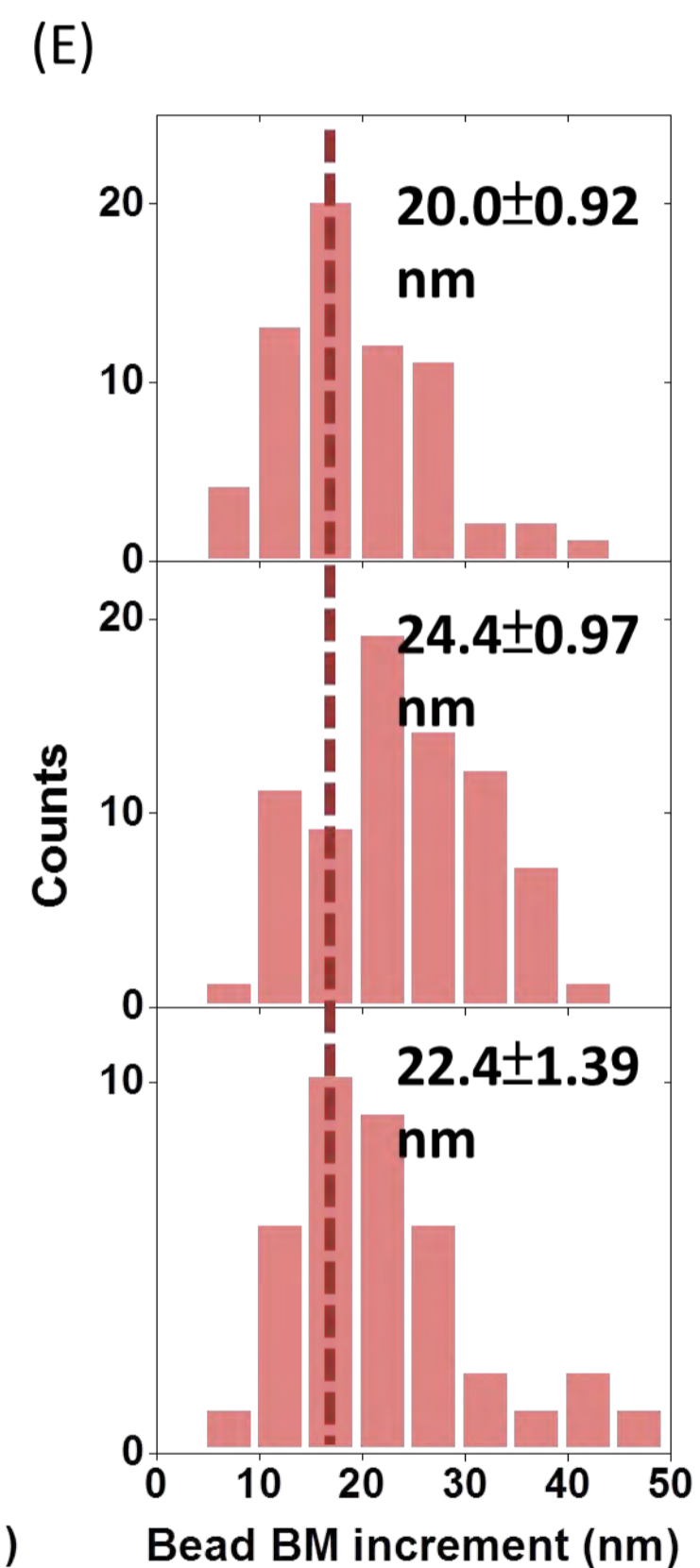
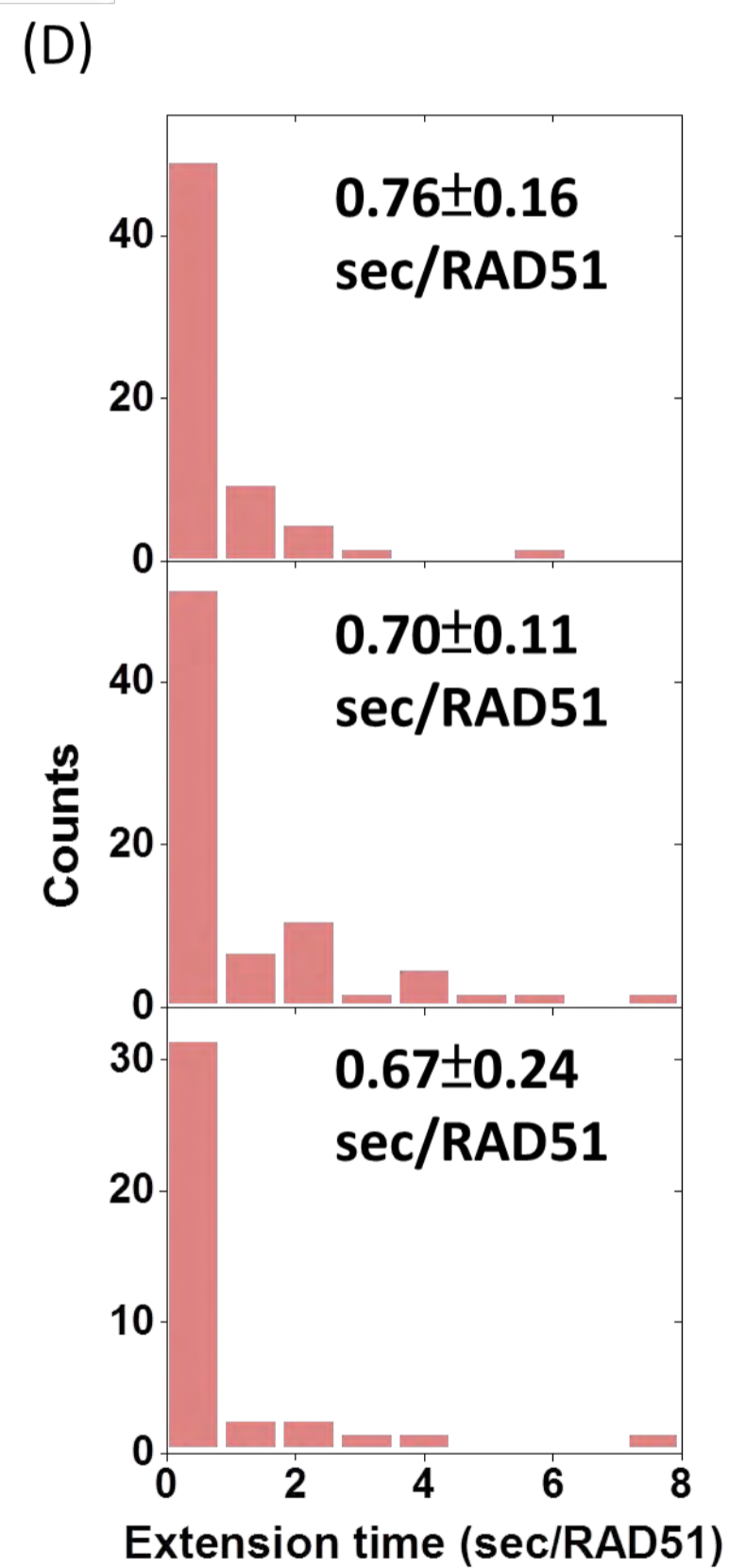
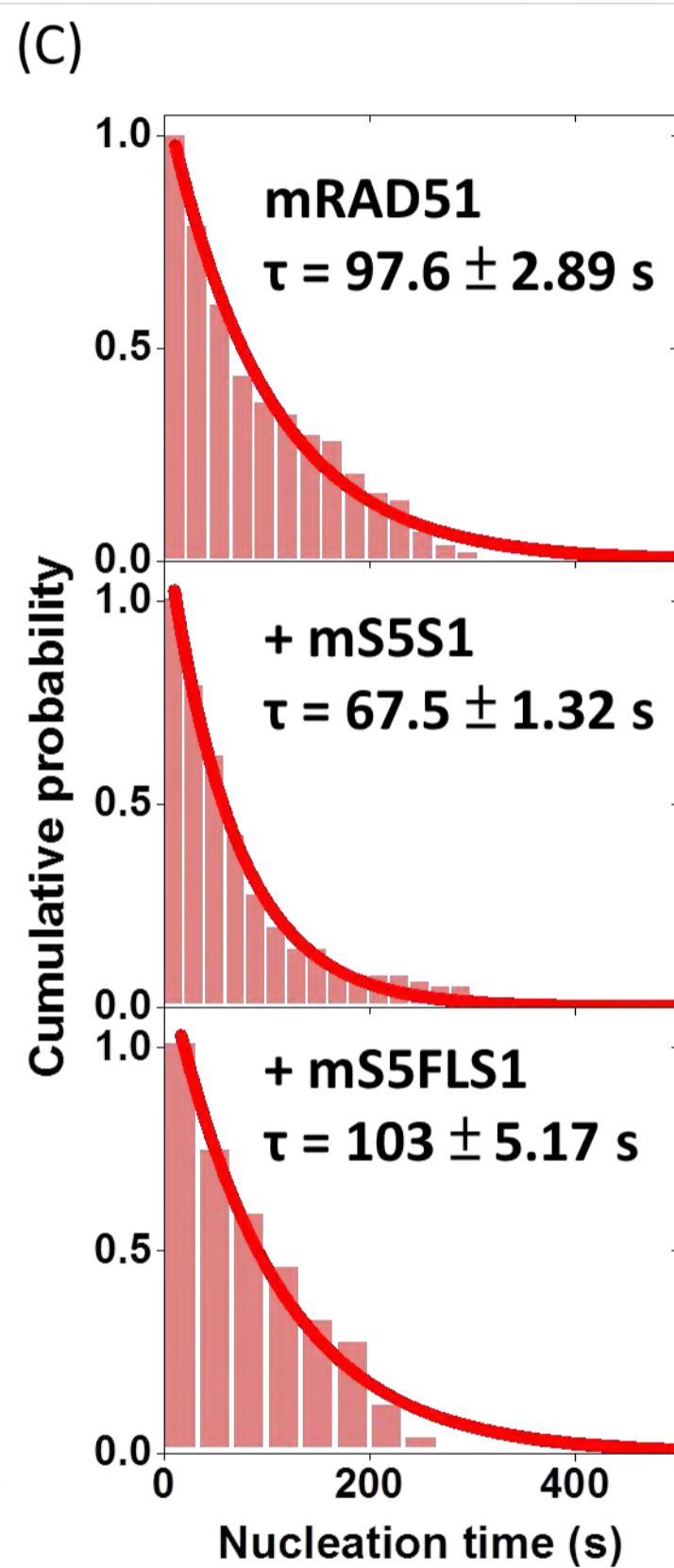
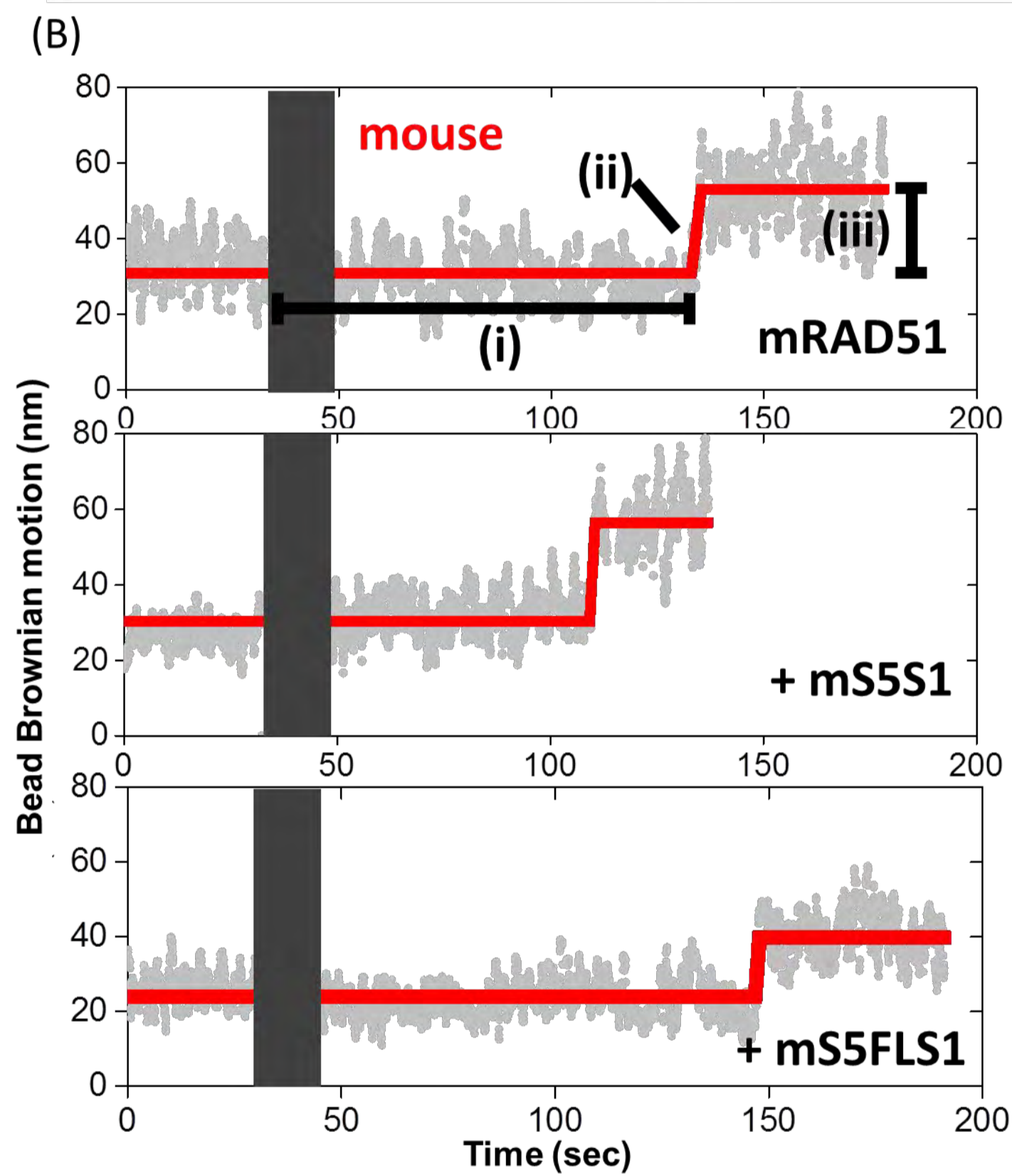
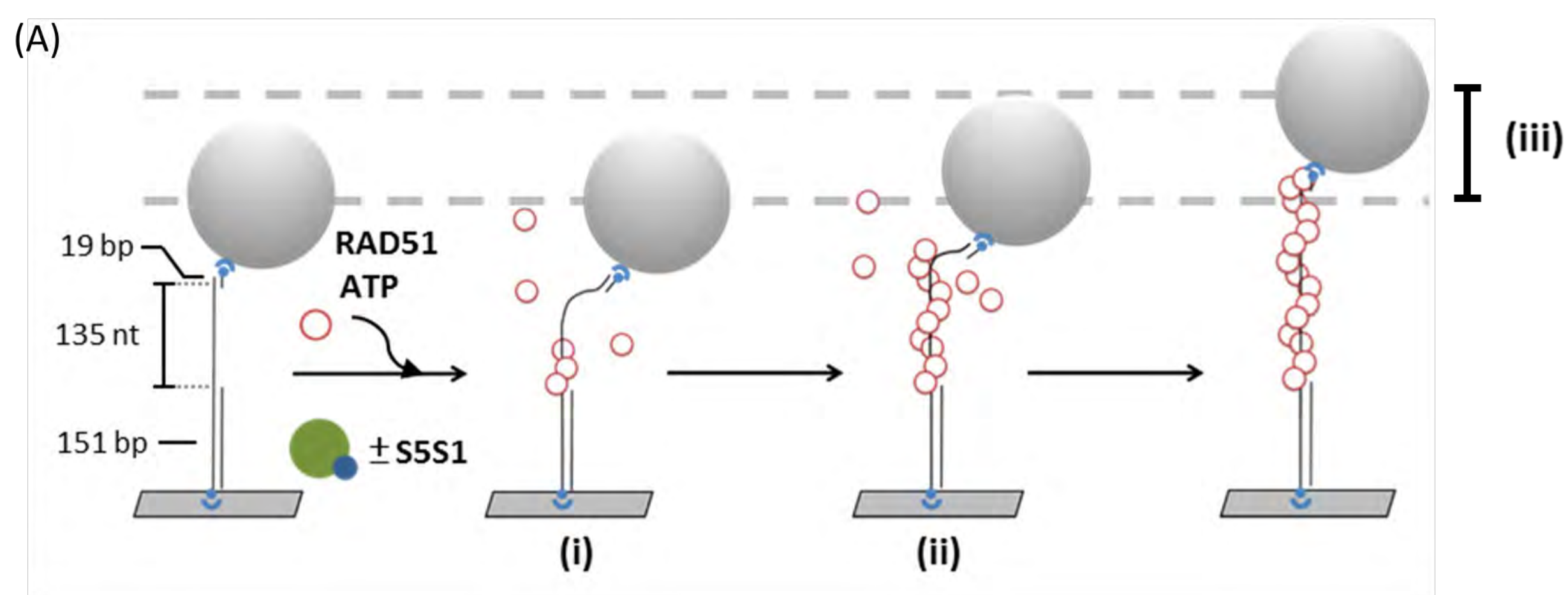
851 **Figure 5. Nucleoprotein filament disassembly experiments showed that S5S1**
852 **prevent Rad51 filament disassembly.** (A) Schematic illustration of nucleoprotein
853 filament disassembly experiments using the TPM setup. (B) Representative bead BM
854 time-courses of mouse mRAD51 disassembly on (dT)₁₃₅ DNA substrates without
855 mS5S1 (top) and in the presence of 1.0 μM mS5S1 (bottom). mRAD51 filaments
856 were pre-assembled in the presence of ATP. Dark grey bars stand for void time for
857 extensive buffer wash to remove free mRAD51. A lifetime of the pre-assembled
858 filament before the BM decrease dictates the mRAD51 disassembly kinetics. (C)
859 Mean lifetime of mouse mRAD51 nucleoprotein filament, (D) fraction of the
860 un-disassembled filament within 15 minutes and (E) mean dissociation time per

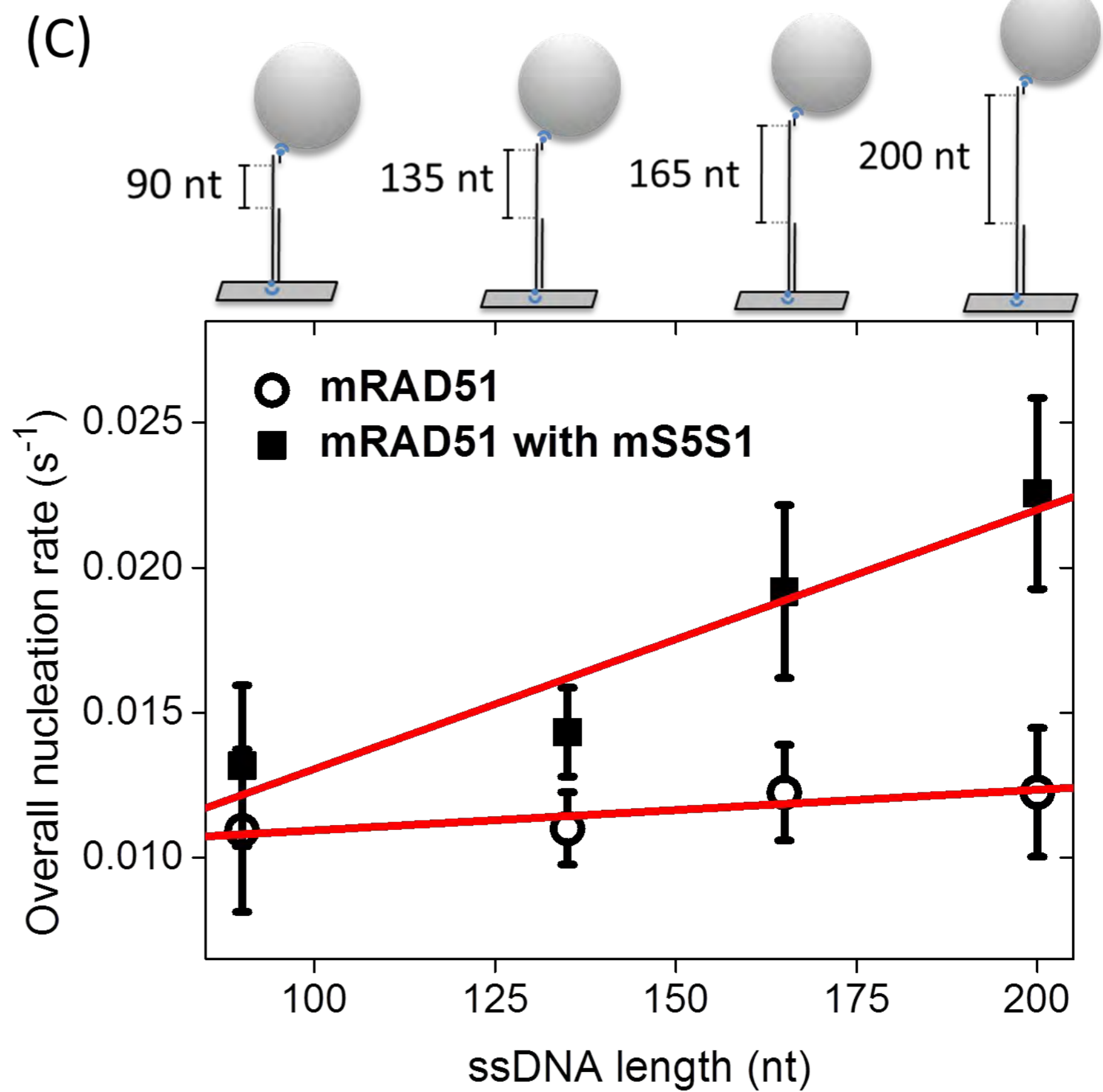
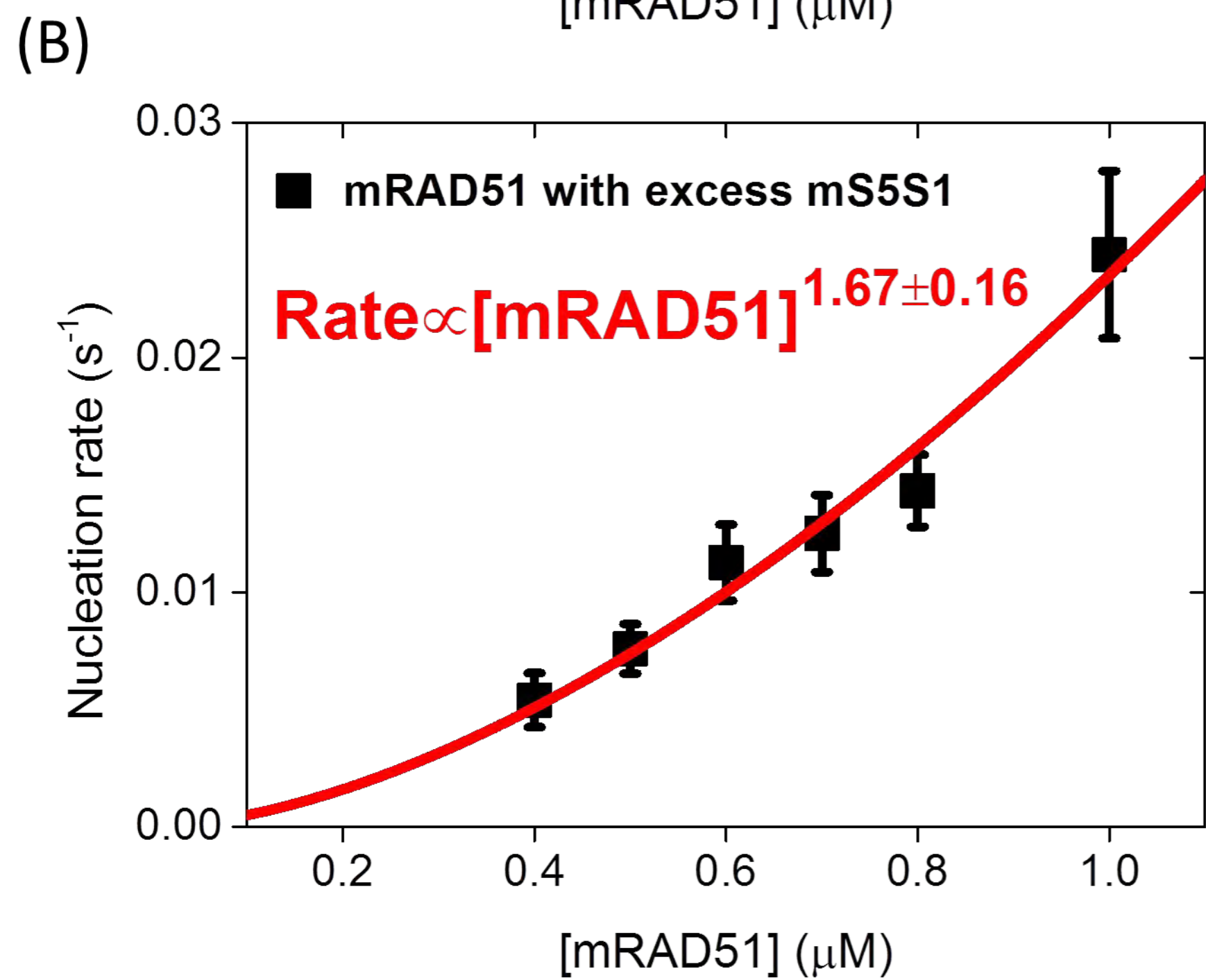
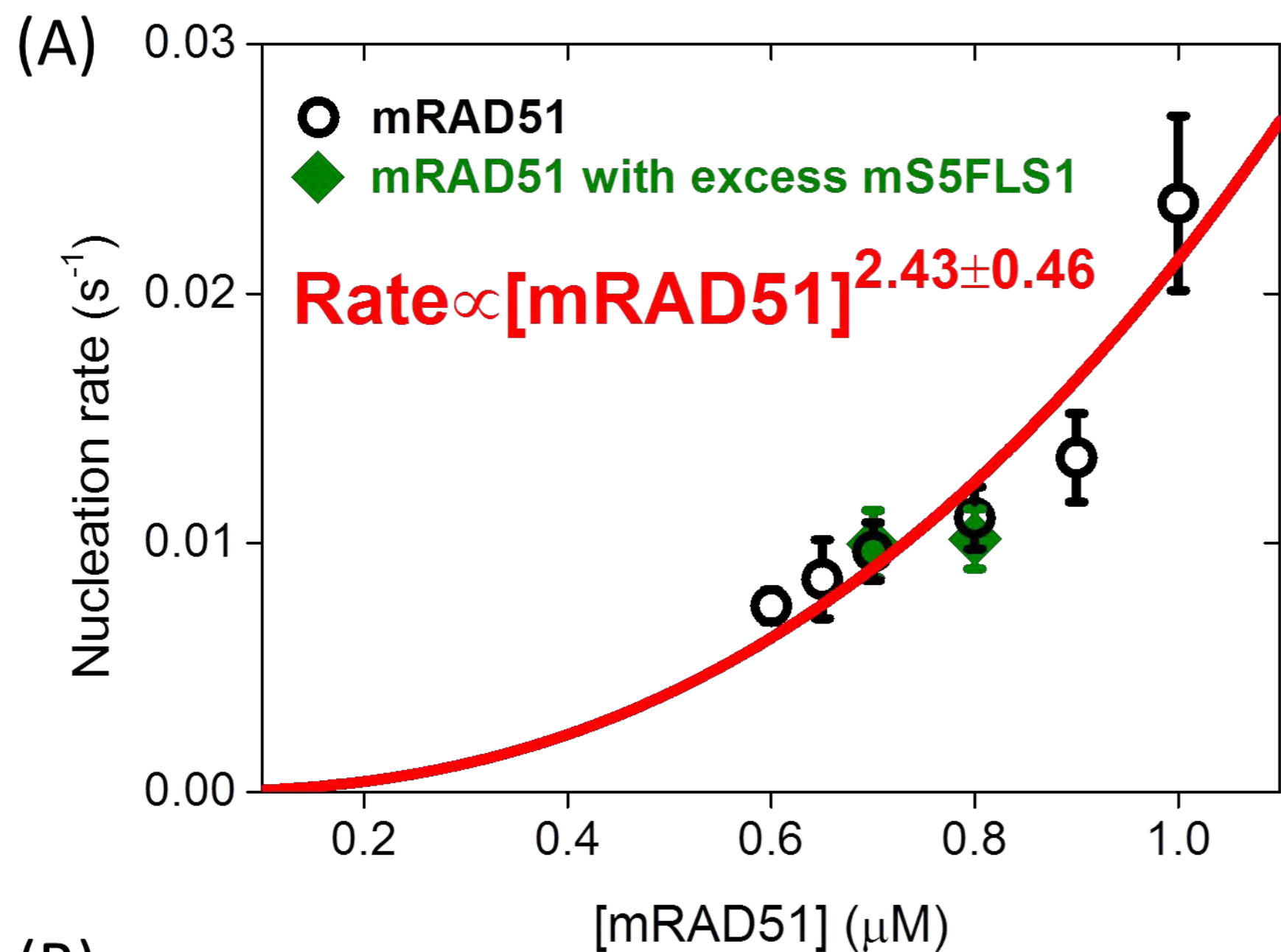
861 mRAD51 in the presence of various mS5S1 concentrations and nucleotide conditions.
862 (F) Representative bead BM time-courses of SpRad51 disassembly without SpS5S1
863 (top) and in the presence of 0.3 μ M SpS5S1 (bottom). (G-I) Kinetic parameters for
864 fission yeast. The fraction of un-disassembled tethers is correlated with the mean
865 lifetime of the SpRad51 filament in both species. In (G-I), the N-terminus truncation
866 S5S1C mutants (open bars) are deficient in DNA binding. All experiments were
867 carried out at 2 mM ATP. Error bar is one standard error of the mean.

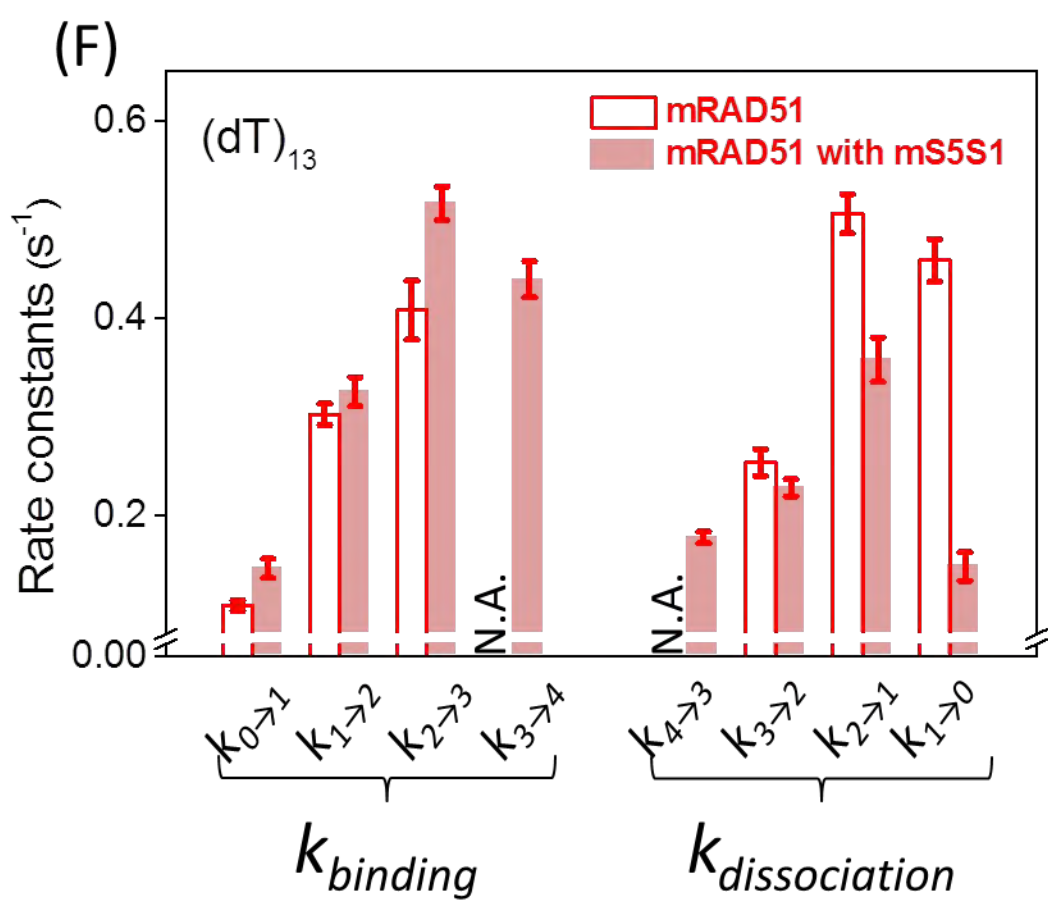
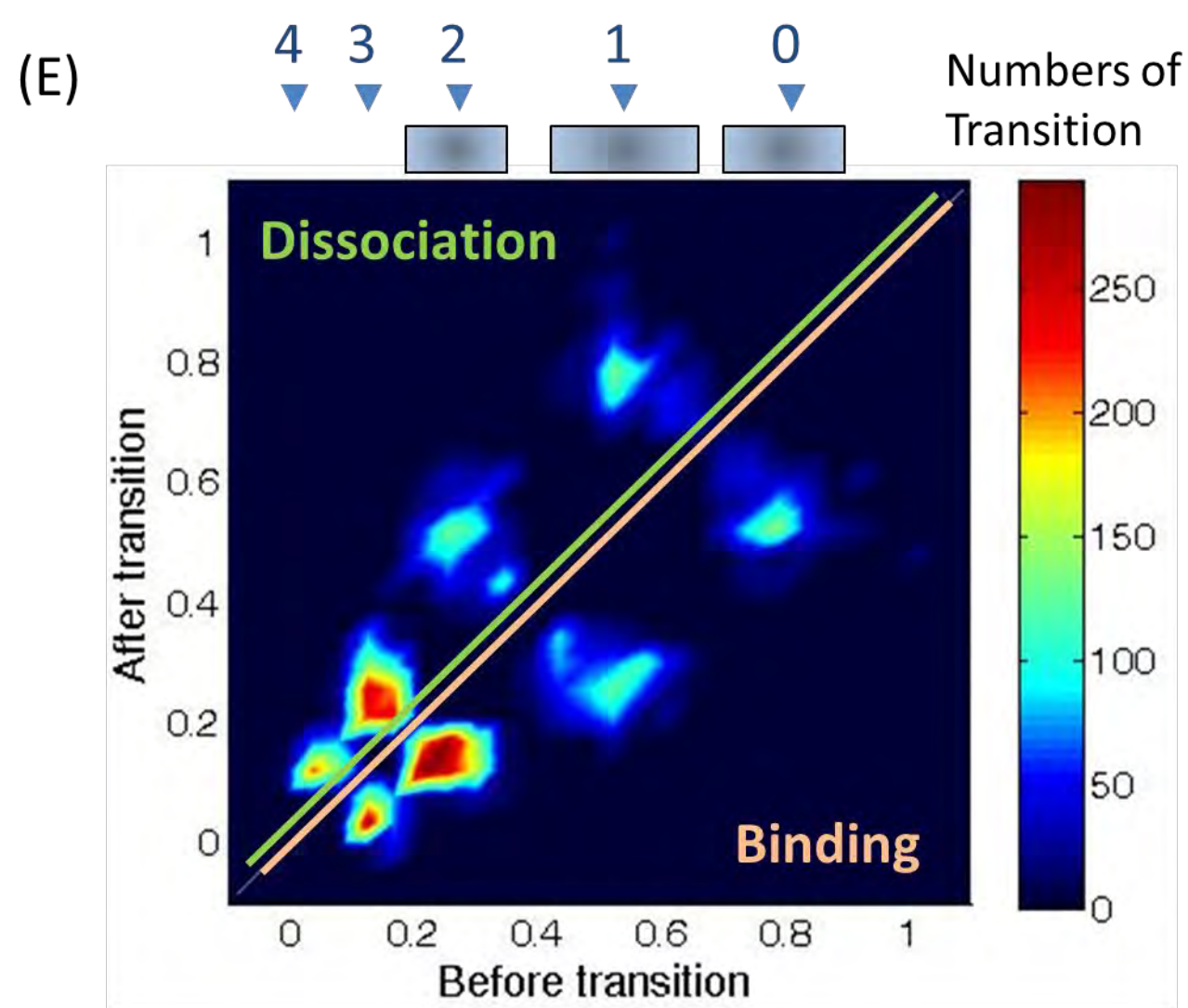
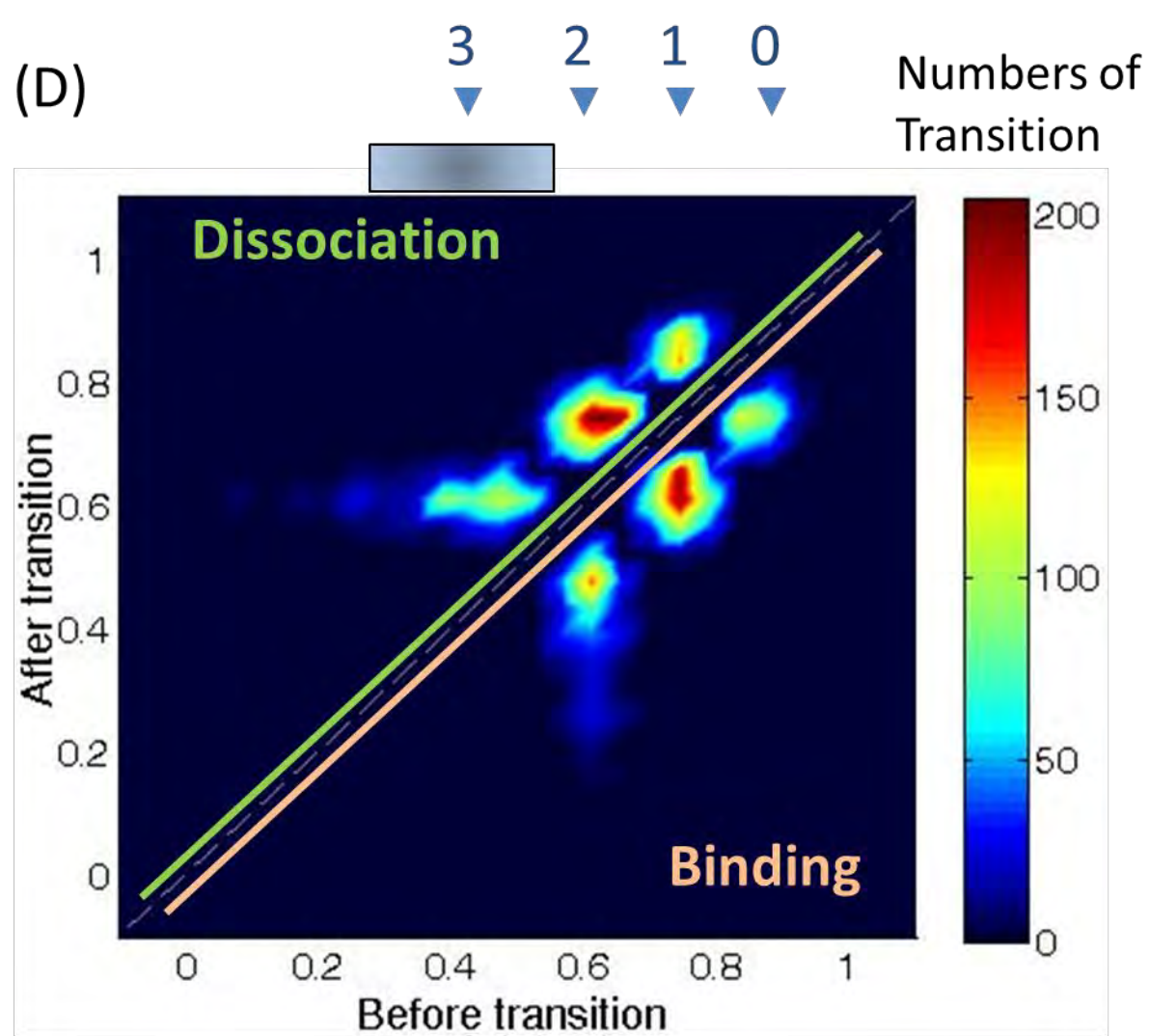
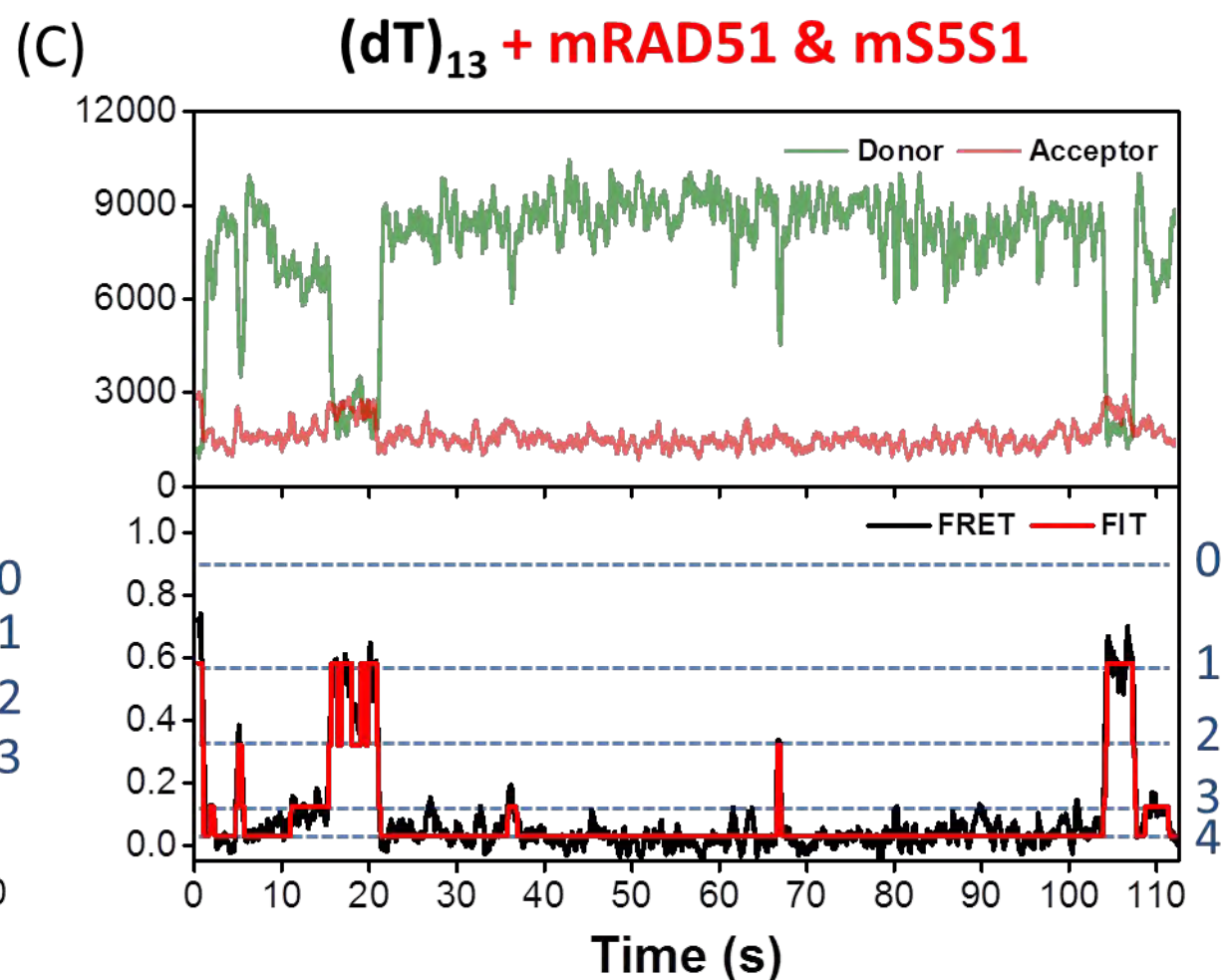
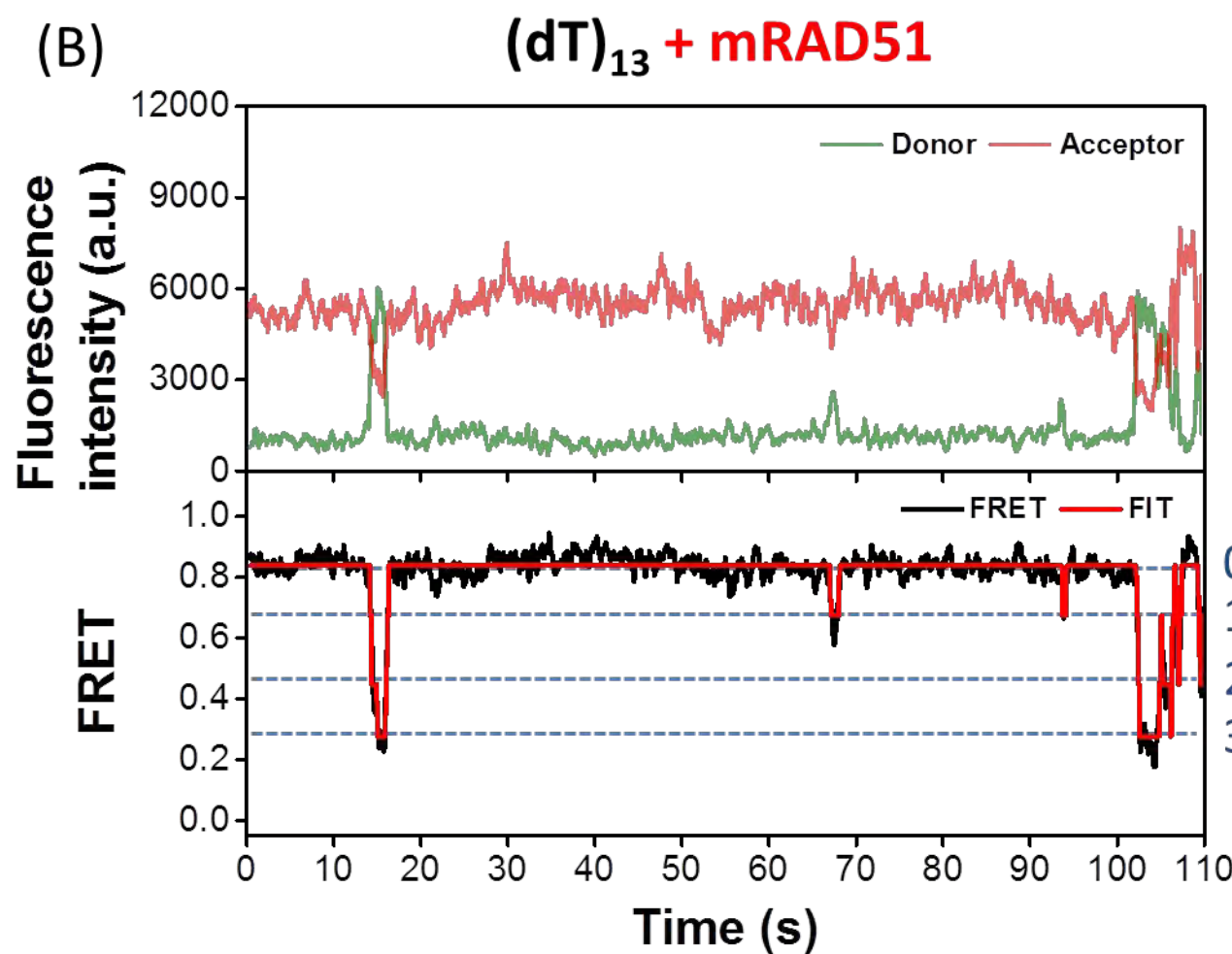
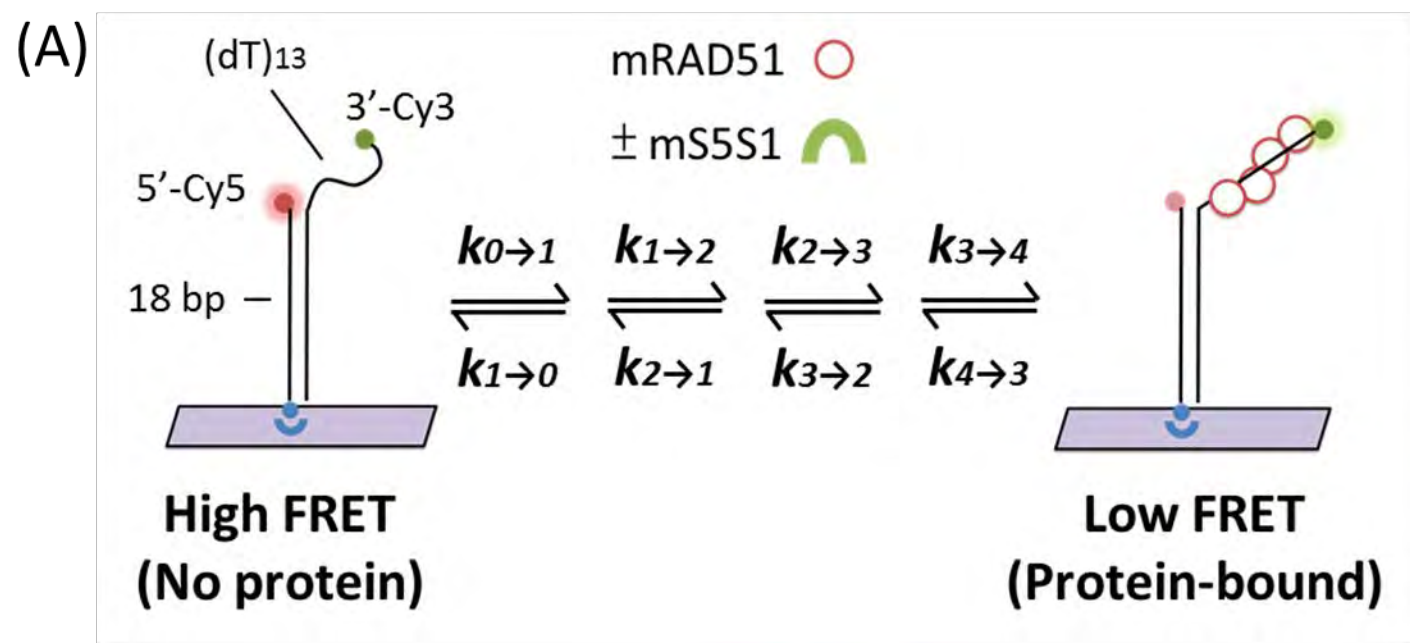
868

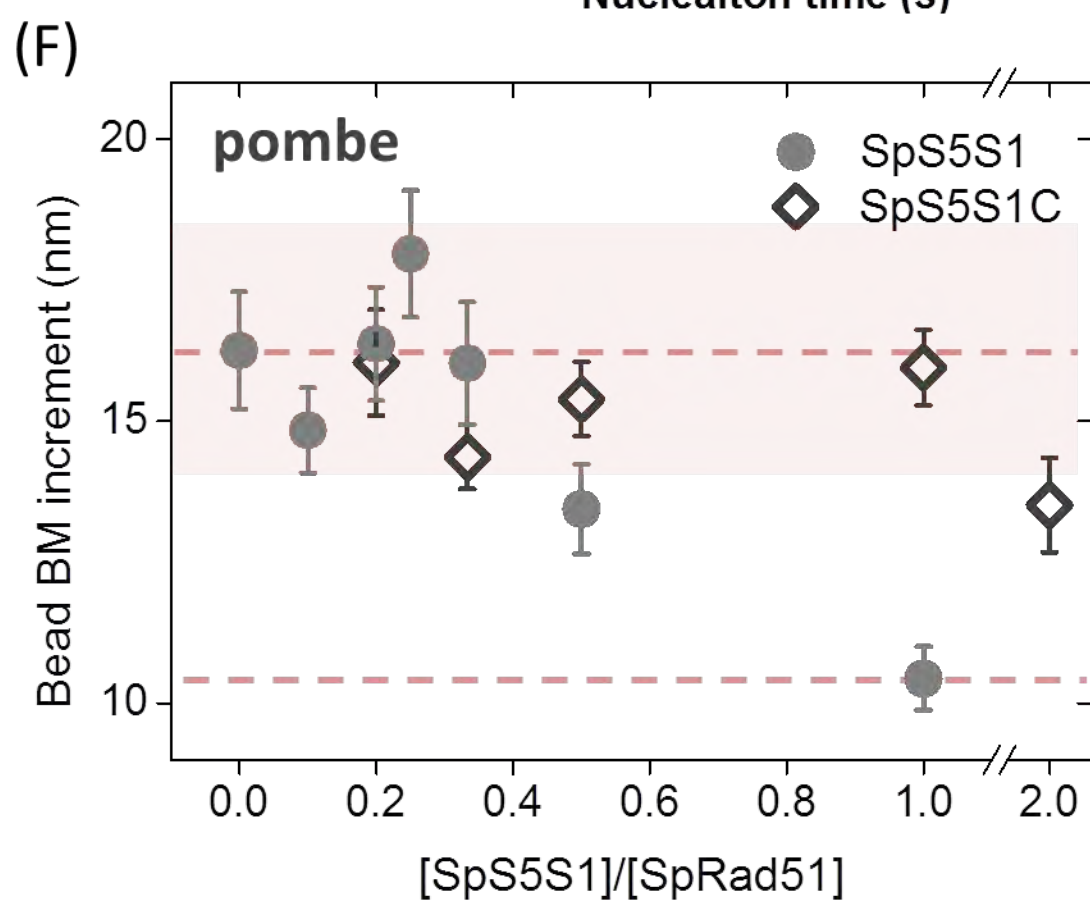
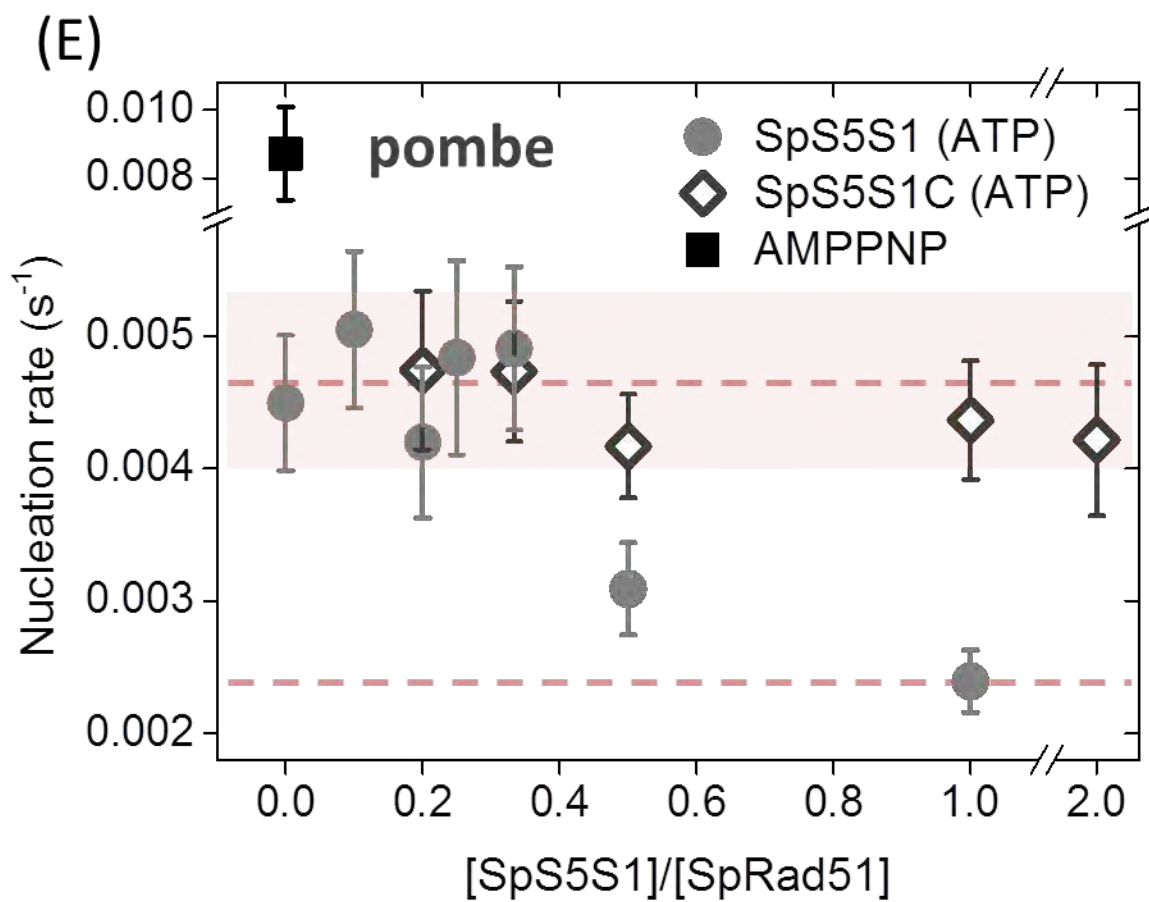
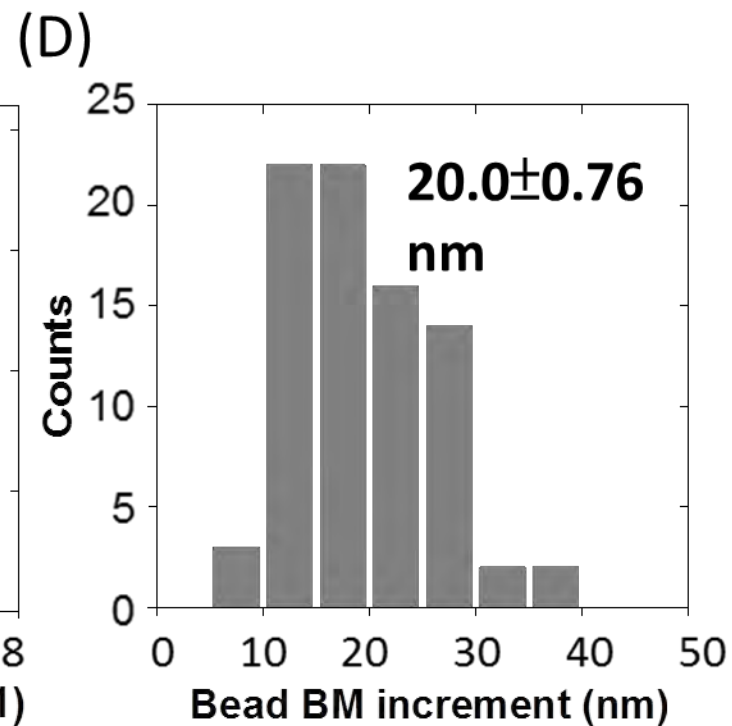
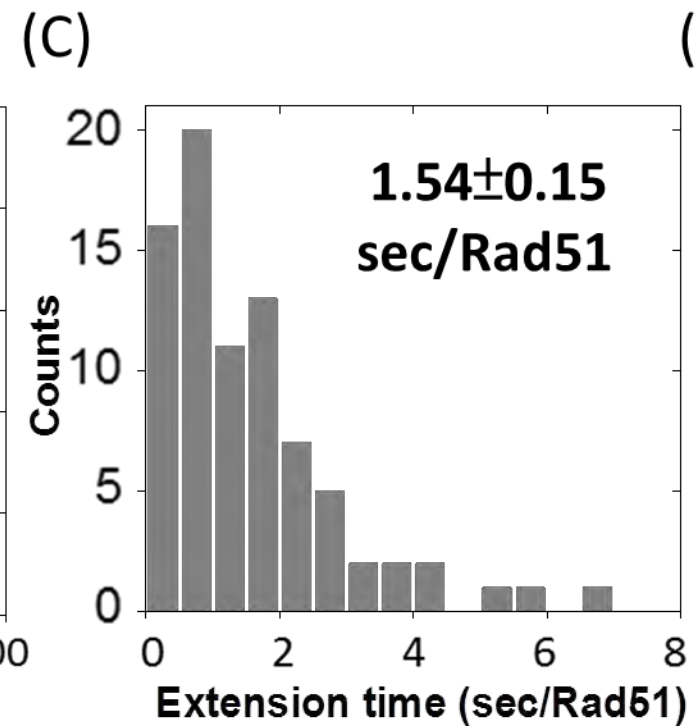
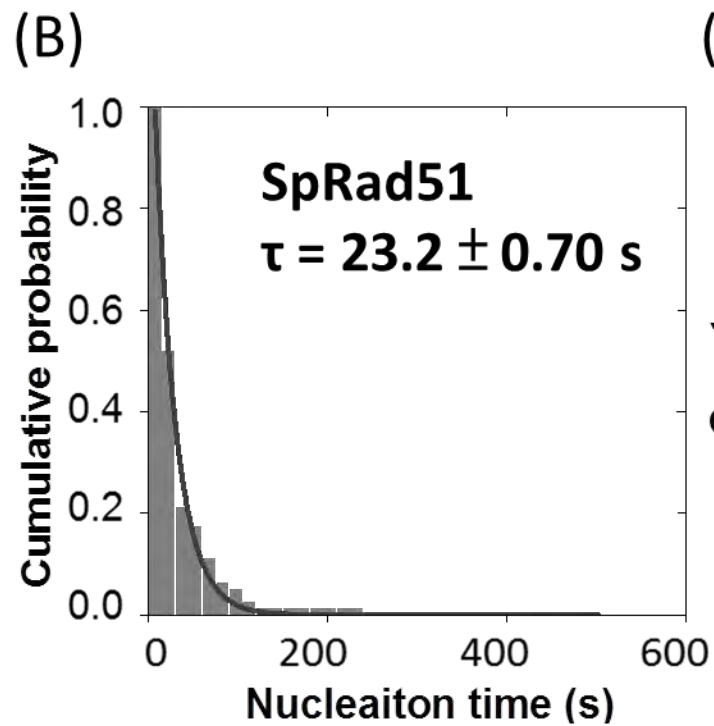
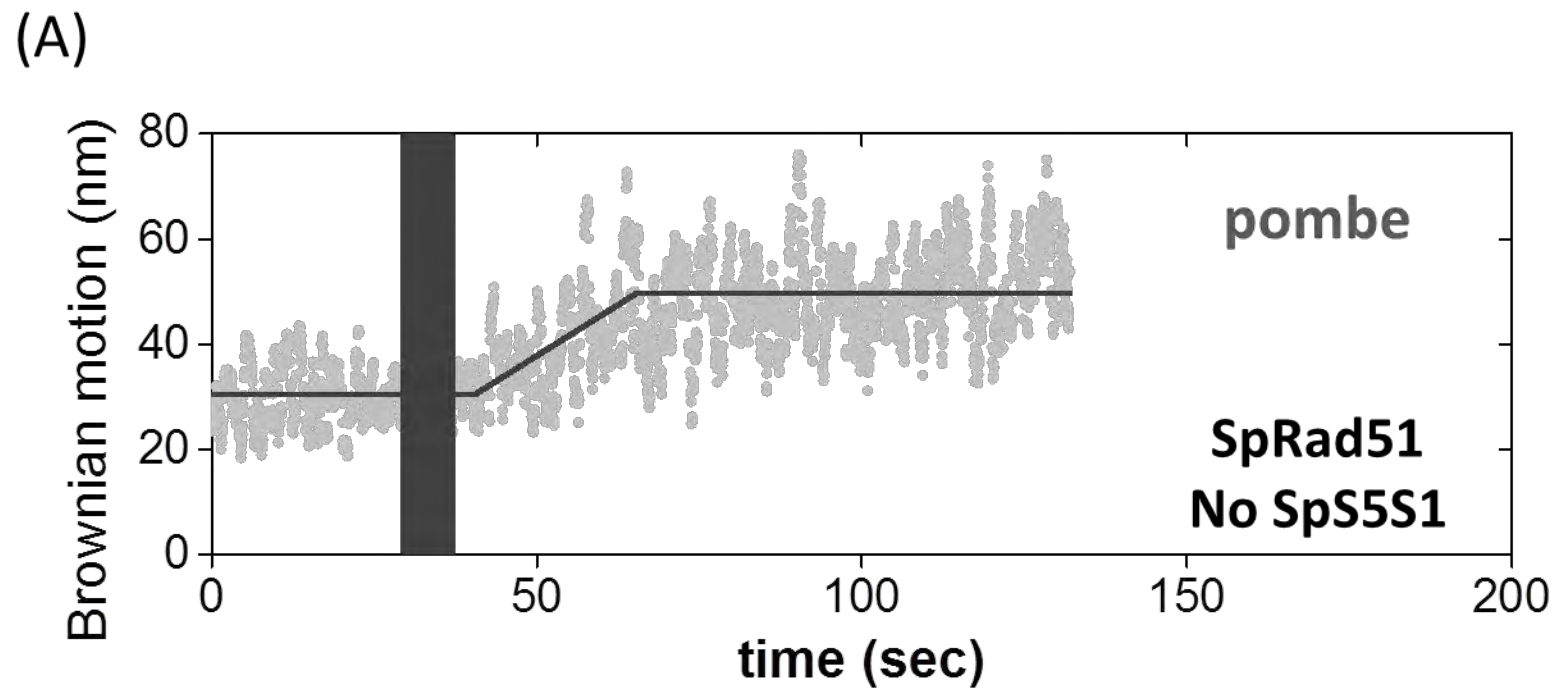
869 **Figure 6. Proposed models for regulating Rad51 nucleoprotein filament**
870 **formation by the S5S1 complex.** Swi5-Sfr1 stabilizes Rad51 on ssDNA primarily by
871 preventing its dissociation. This stabilization effect leads to a stable nucleating cluster
872 formation and a reduction in filament disassembly. In spite of different kinetic
873 properties of mouse and fission yeast Rad51, Swi5-Sfr1 complex stimulates Rad51
874 process through a general, evolutionally-conserved mechanism. Red half-arrows
875 indicate the kinetic steps affected by S5S1.

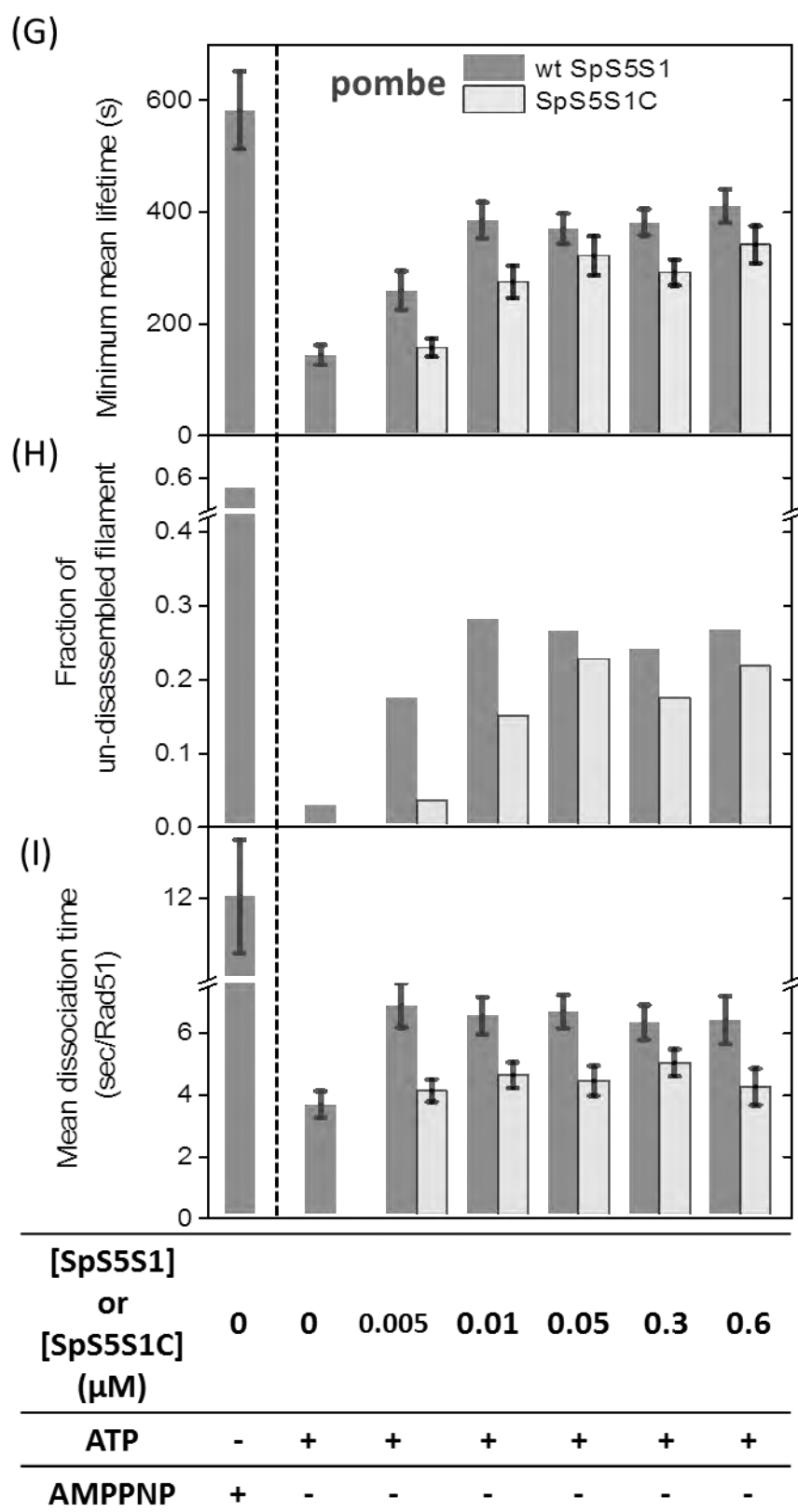
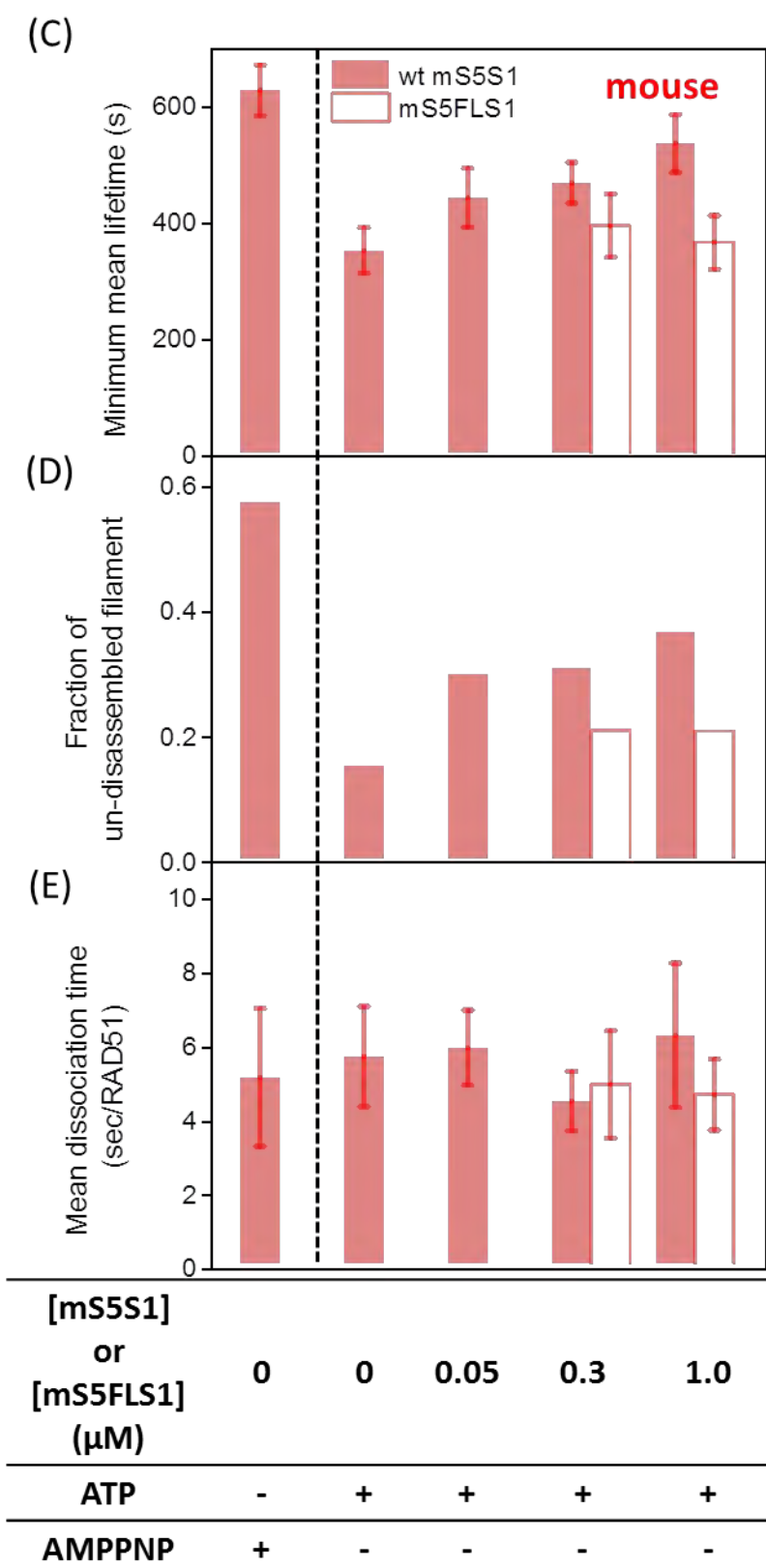
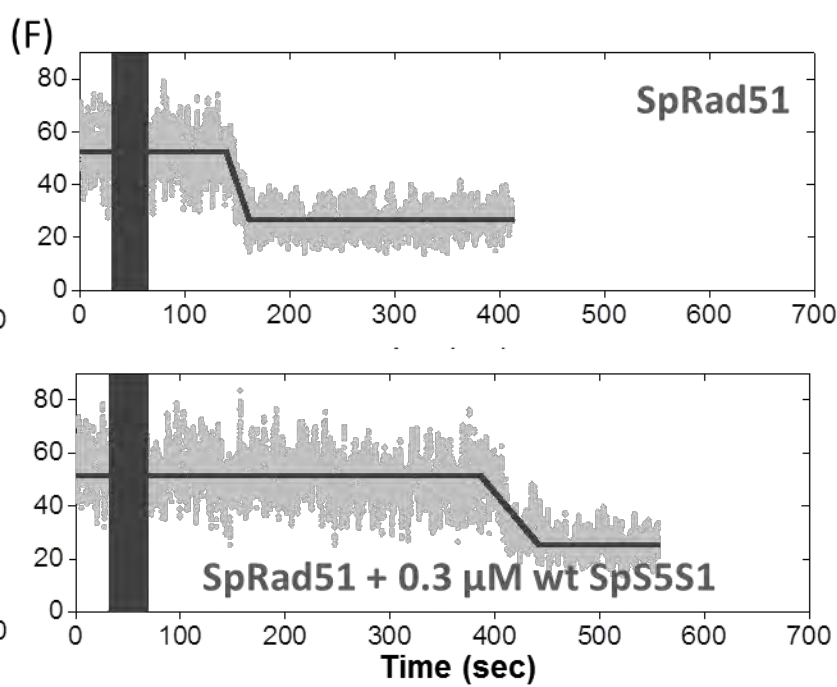
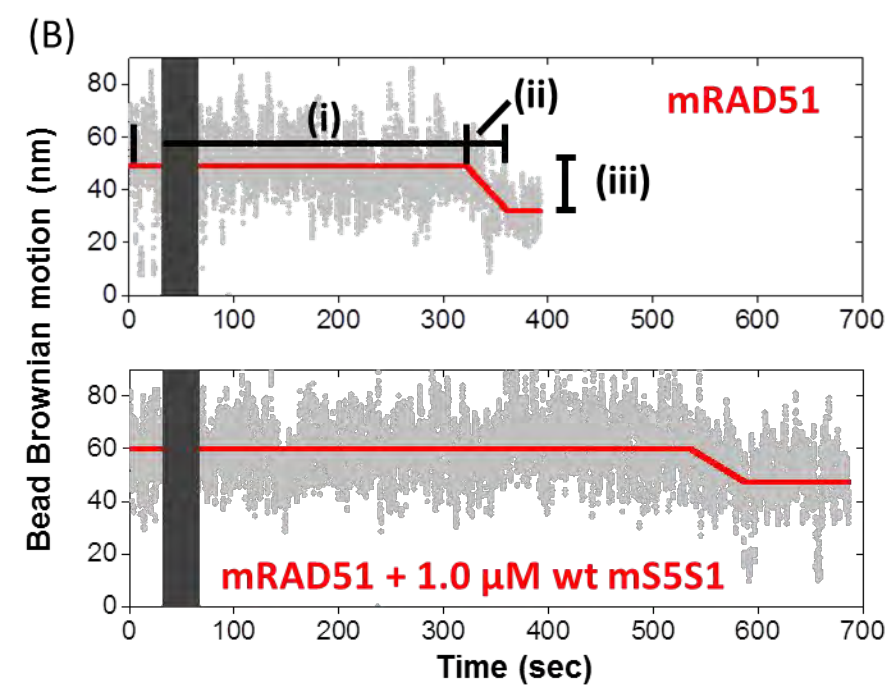
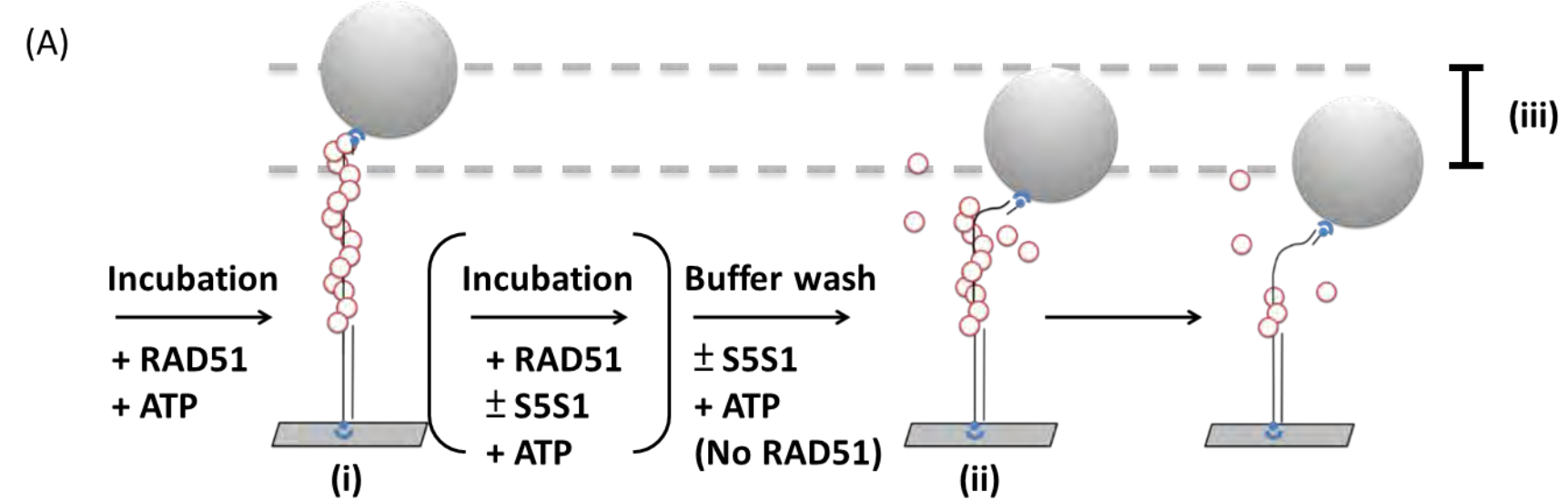
876







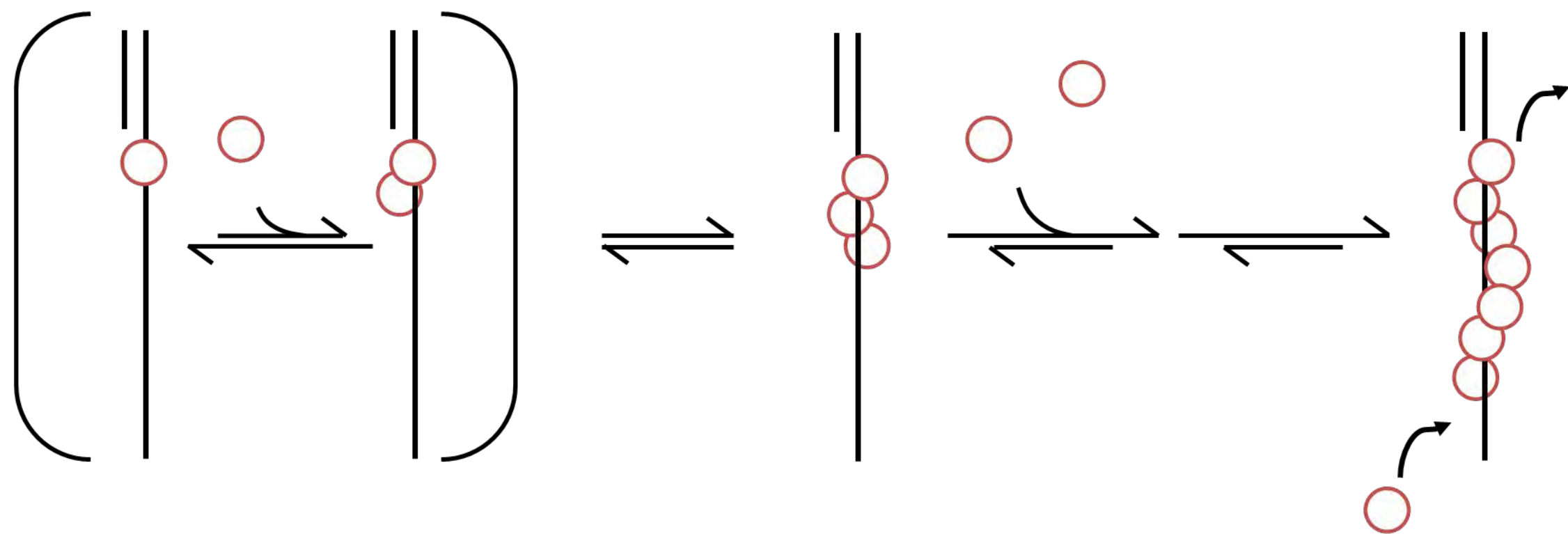




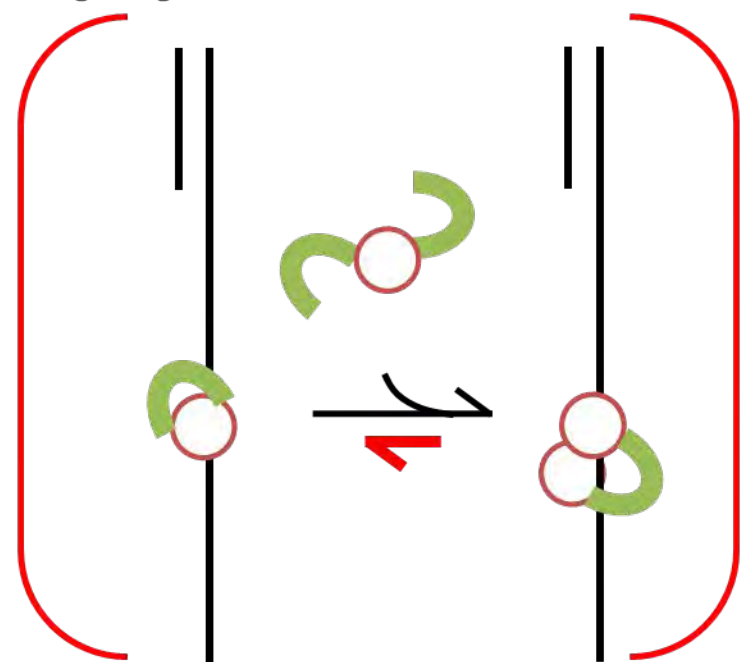
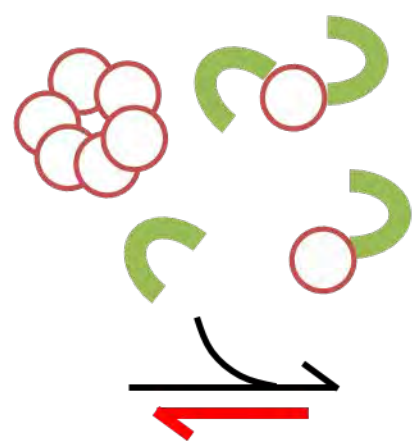
○ Rad51

⤿ Swi5-Sfr1

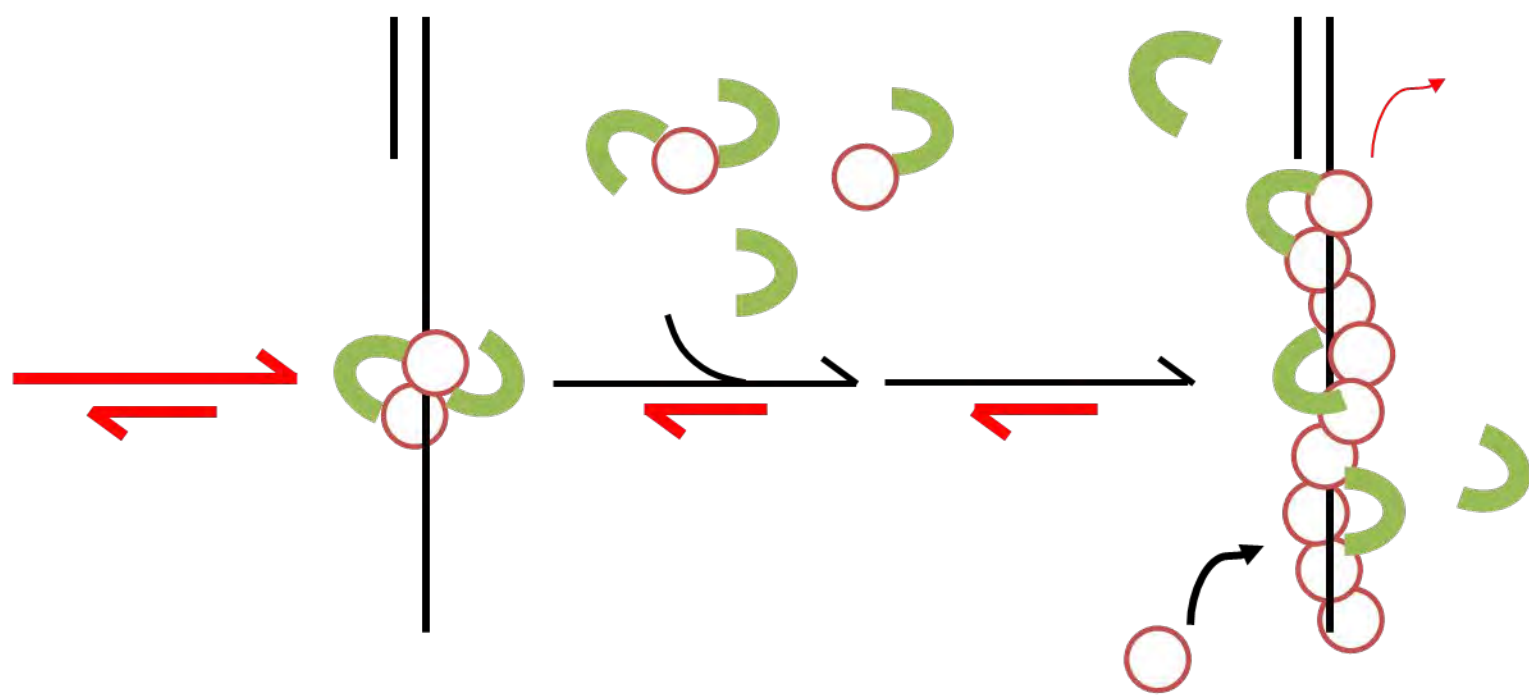
(A) - Swi5-Sfr1



(B) + Swi5-Sfr1



**Nucleating cluster
stabilization**



**Filament
stabilization**

Supplementary Information for

Swi5-Sfr1 Stimulates Rad51 Recombinase Filament Assembly by Modulating Rad51 Dissociation

Chih-Hao Lu¹, Hsin-Yi Yeh², Guan-Chin Su², Kentaro Ito³, Yumiko Kurokawa^{3,¶}, Hiroshi Iwasaki^{3,*}, Peter Chi^{2,4,*} and Hung-Wen Li^{1,*}

¹ Department of Chemistry, National Taiwan University, Taiwan

² Institute of Biochemical Sciences, National Taiwan University, Taiwan

³ Institute of Innovative Research, Tokyo Institute of Technology, Japan

⁴ Institute of Biological Chemistry, Academia Sinica, Taiwan

* To whom correspondence should be addressed:

Hiroshi Iwasaki, E-mail: hiwasaki@bio.titech.ac.jp

Peter Chi, E-mail: peterhchi@ntu.edu.tw

Hung-Wen Li, E-mail: hwli@ntu.edu.tw

¶ current address: Center for Frontier Research, National Institute of Genetics, Japan

This PDF file includes:

Supplementary text

SI Materials and Methods

Figures S1 to S11

Tables S1 to S10

References for SI reference citations

Author contributions: C.H.L., H.I., P.C. and H.W.L. designed research; C.H.L. performed all single-molecule experiments and analyzed data; H.Y.Y., G.C.S., K.I. and Y.K. purified proteins used in this article; C.H.L. H.I., P.C. and H.W.L. wrote the paper.

SI Materials and Methods

DNA substrates. The (dT)₁₃₅ gapped DNA substrate for TPM assembly and disassembly experiments contains 135 nt poly dT sandwiched by a 151 bp, 5'-digoxigenin-labeled dsDNA handle and a 5'-biotin-labeled 19 bp handle. To prepare the (dT)₁₃₅ gapped DNA, we first used auto-sticky polymerase chain reaction (PCR)(1) to prepare a 131/151 hybrid DNA with a 20 nt 5'-overhang using a digoxigenin-labeled primer (5'-dig/CGTGGGTATGGTGGCAGG), and a primer containing an abasic nucleotide at the 21th position (5'- ATCGGTTCGACGCTCTCCC TT/idSp/TGCGACTCCTGCATTAGGAA) using pBR322 as template. Oligos containing 135 thymidylates (5'-AAGGGAGAGCGTCGACCGAT(T)₁₃₅CTTACTG TCATGCCATCCG) was first phosphorylated by T4 PNK (NEB) and then ligated with the 131/151 hybrid in the presence of T4 DNA ligase (NEB) to generate a 151/305 hybrid DNA. After gel purification, the 151/305 hybrid DNA was then annealed with a biotin-tagged primer (5'-biotin-CGGATGGCATGACAGTAAG) to create the final (dT)₁₃₅ gapped DNA. (dT)₉₀, (dT)₁₀₀, (dT)₁₆₅ and (dT)₂₀₀ gapped DNA substrates were made with the same procedure as (dT)₁₃₅ DNA preparation, but using oligos with various lengths of (dT)_n (n=90, 100, 165 and 200) (Figure S9). Oligos were purchased from Gene Link (oligos containing (dT)₁₆₅ and (dT)₂₀₀), Integrated DNA Technologies (the primer with one abasic site and oligos containing (dT)₉₀, (dT)₁₀₀ and (dT)₁₃₅) and Bio Basic Inc. (digoxigenin-labeled primers). For smFRET experiments, the surface-anchored hybrid DNA substrates were prepared by annealing a 5'-Cy5 and 3'-biotin (5'-Cy5/GCCTCGCTGCCGTCGCCA/bio-3') double-labeled oligo and a 3'-Cy3-labeled oligo containing various numbers of thymidylate at 3' overhang (5'-TGGCGACGGCaGCGAGGC(dT)_n/Cy3-3') in the buffer containing 20 mM Tris and 0.5 M NaCl at pH = 8.

Proteins and buffers. mRAD51, mS5S1, mS5^{FL/AA}S1, SpRad51, SpS5S1, and SpS5S1C were purified as previously described(2-5). All mouse experiments were carried out with buffer containing 30 mM Tris, 2.5 mM magnesium chloride and 150 mM potassium chloride at pH=7.5. Fission yeast reactions were performed with buffer containing 25 mM Tris, 3 mM magnesium acetate and 150 mM potassium chloride at pH=7.5. ATP and AMPPNP were purchased from Sigma-Aldrich.

Detailed experimental procedures of single-molecule tethered particle motion (TPM) assembly experiment. For S5S1 titration experiments (Figure 1 and 4), 0.8 μM mouse RAD51 (or 0.3 μM fission yeast Rad51) was pre-incubated with the indicated concentrations of mouse S5S1 (or fission yeast S5S1) in corresponding buffers to form complexes at 37°C for 10-15 min. The RAD51-S5S1-ATP mixture

was cooled down to the room temperature and flowed into the reaction chamber containing bead-tagged DNA substrates. For nucleation unit determination, mRAD51 (or SpRad51) at different concentrations (Figure 2A & S9B) or 0.4-1.0 μM mRAD51 plus 1.6 or 2.0 μM (2-fold excess) mS5S1 (Figure 2B) were pre-incubated in corresponding buffers for 10-15 min at 37°C before experiments. For binding preference determination (Figure 2C & S9B), 0.8 μM mRAD51, 0.8 μM mRAD51 plus 1.6 μM mS5S1 or 0.5 μM SpRad51 in corresponding reaction buffers were incubated for 10-15 min at 37°C.

Single-molecule TPM disassembly experiment and data analysis. In disassembly experiments, we used silanized glass slide to avoid extensive surface-protein interaction. To prepare the silanized surface, the glass slides were sequentially sonicated in 2 M KOH for 5 min, 99 % ethanol for 15-20 min and ddH₂O for 15-20 min. After these sonication steps, slides were rinsed with ddH₂O and dried with N₂ gas. Glass slides were then functionalized in a solution containing 1,7-dichloro-octamethyltetrasiloxane (Sigma-Aldrich) in 99 % ethanol in the dark overnight at room temperature. Slides were then rinsed with 99 % ethanol and ddH₂O alternatively and dried with N₂. Surface-bound (dT)₁₃₅ gapped DNA substrates were pre-incubated with mixtures of either 0.8 μM mRAD51-2 mM ATP or 0.8 μM SpRad51-2 mM ATP to form nucleoprotein filaments. After 5-10 min incubation, free mRAD51 or SpRad51 were removed with reaction buffer containing no mRAD51/SpRad51. The extensive wash used in our experiments didn't lead to disruption of protein filaments. For disassembly experiments involving S5S1, we added pre-incubated mixtures including 0.3 μM mRAD51 (or SpRad51), indicated amounts of mS5S1 (or SpS5S1), 2 mM ATP and ATP regeneration system (1 mM phosphoenolpyruvate and 4 units/ml pyruvate kinase) into reaction chambers and incubated for 10-15 min to form S5S1-coated Rad51-ssDNA filaments. After 10-15 min incubation, free Rad51 were removed by reaction buffer containing S5S1, ATP, and ATP regeneration system but without mRAD51/SpRad51. Tethers with BM ranging from 35 to 80 nm were scored as Rad51 nucleoprotein filaments (Figure S1).

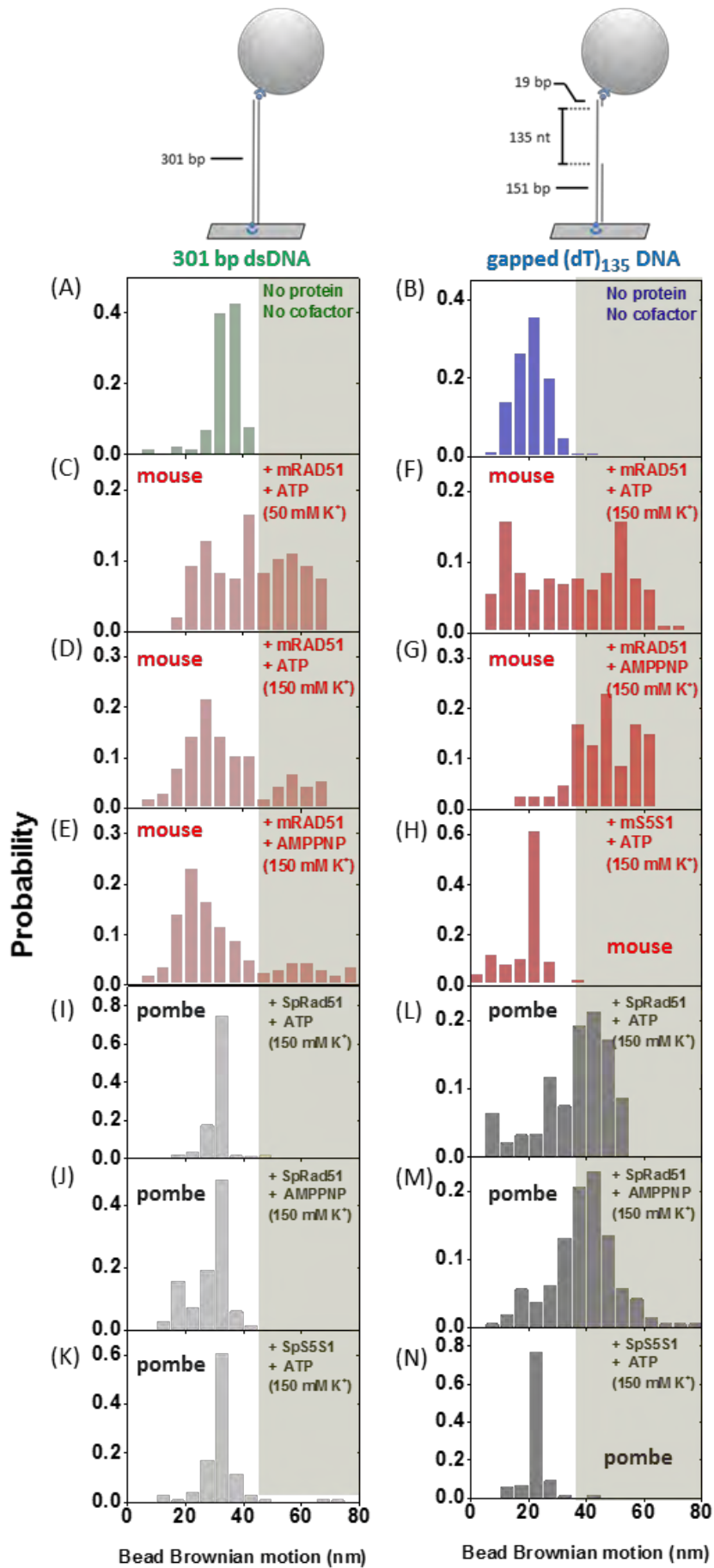


Figure S1. Bead BM histograms of RAD51/S5S1 assembly on either 301 bp dsDNA or (dT)₁₃₅ gapped DNA. Brownian motion (BM) amplitudes of **(A)** bare 301 bp dsDNA and **(B)** bare (dT)₁₃₅ gap DNA substrates are about 35.2 ± 3.77 and 21.3 ± 5.78 nm, respectively. BM higher than 35 nm (for (dT)₁₃₅ gapped DNA experiments) or 45 nm (for 301 bp dsDNA experiments) is considered to be extended by recombinases (yellow shaded region). Mouse mRAD51 binds to duplex DNA substrates at low salt **(C)**, but shows a reduced dsDNA affinity at higher (150 mM) KCl concentration in the presence of either **(D) ATP** or **(E) AMPPNP**. In contrast, mouse mRAD51 assembles efficiently on the (dT)₁₃₅ gapped DNA under ATP **(F)**, and it assembles much faster under AMPPNP **(G)**. mS5S1 didn't alter BM **(H)**, consistent with the biochemical characterization that mS5S1 has no ssDNA affinity. For pombe, SpRad51 has negligible dsDNA affinity and caused no increase in bead BM in either ATP **(I)** or AMPPNP **(J)**. **(L-M)** In contrast, SpRad51 preferentially assembled onto ssDNA region of (dT)₁₃₅ gapped DNA at higher KCl concentration in the presence of two cofactors, resulting in the increase of bead BM. Even though SpS5S1 can bind dsDNA and ssDNA, its binding does not change the BM of both substrates **(K and N)**. All assembly experiments were performed at 2 mM ATP or AMPPNP and collected after 5 minutes of protein introduction.

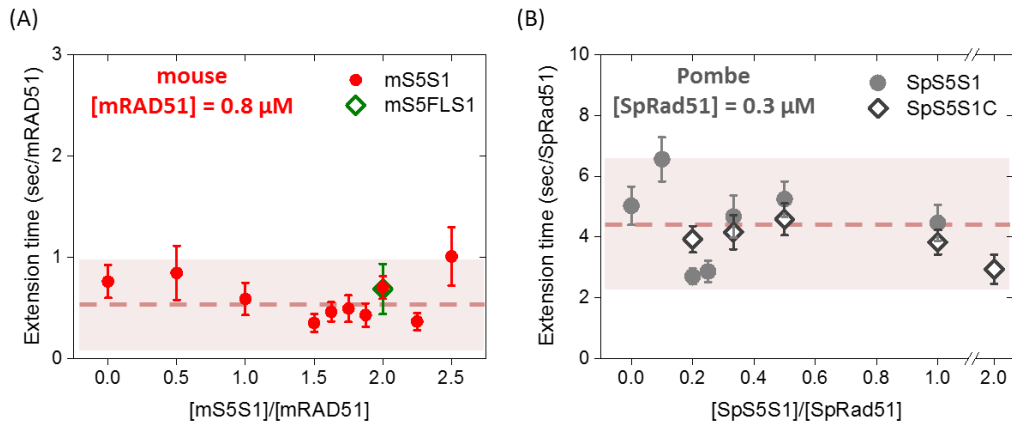


Figure S2. S5S1 shows negligible effects on Rad51 extension time in both two species. At fixed Rad51 concentrations (0.8 μM for mRAD51 and 0.3 μM for SpRad51), Rad51 extension times of both (A) mouse and (B) pombe display no apparent dependence on S5S1 concentration. Dash line is the mean of all measurements, and the shaded region span two standard deviations. Error bar is one standard error of the mean. Extension times of each concentration ratios are determined as the mean from at least 5 independent experiments.

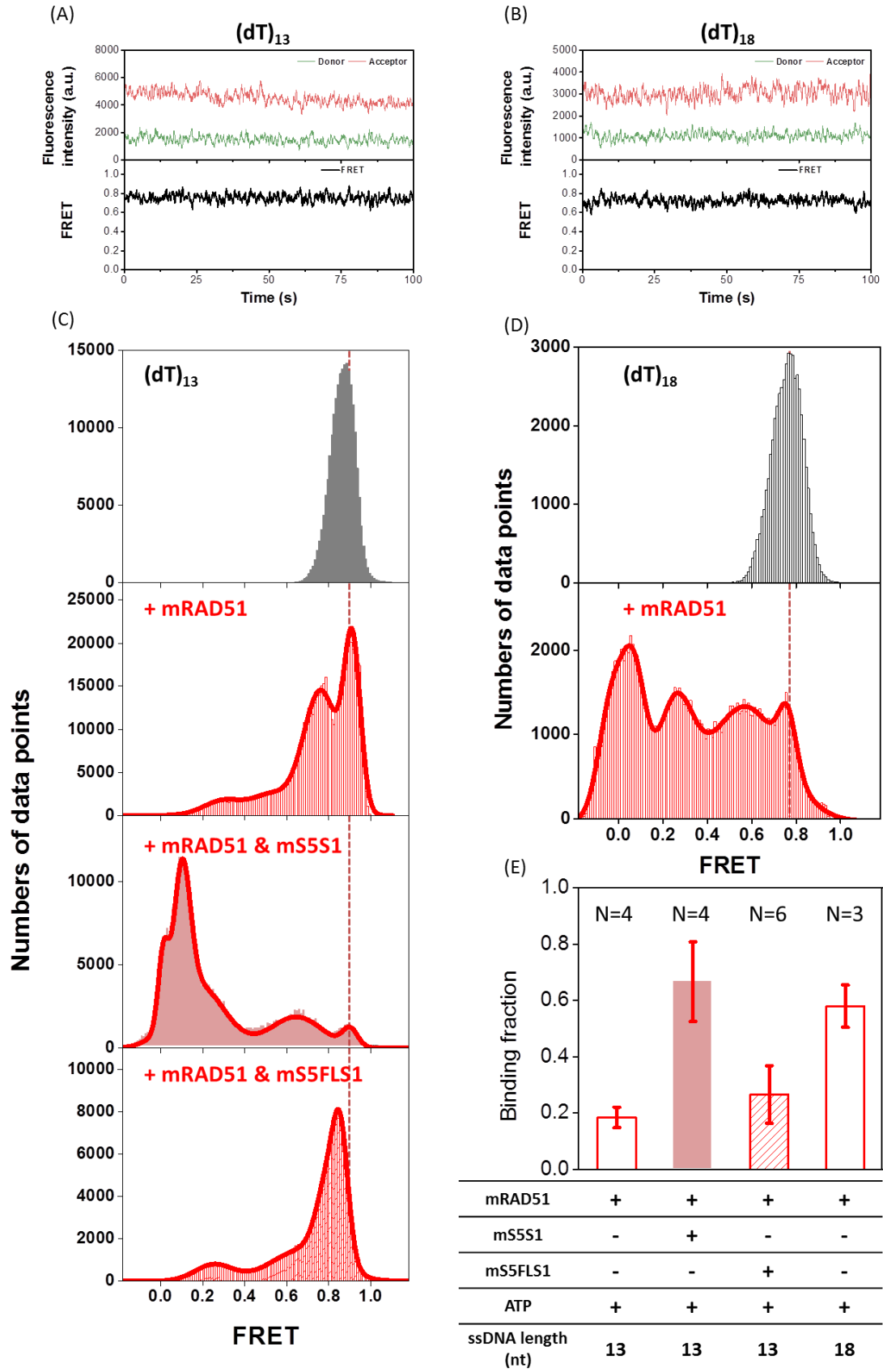


Figure S3. FRET histograms and binding fraction of mRAD51 assembling under different conditions. (A) & (B) In the absence of proteins, DNA molecules exist in

the high FRET state owing to the flexibility of ssDNA region. Both bare DNA substrates of different ssDNA lengths exhibit a high FRET state ($E \sim 0.7-0.8$). **(C)** FRET histograms of (dT)₁₃ DNA substrate in the absence of mRAD51 (top panel); in the presence of mRAD51 (second panel from top); in the presence of mRAD51 and mS5S1 mixture (third panel from top) or in the presence of mRAD51 and mS5^{FL}S1 mixture (bottom panel). **(D)** FRET histograms of (dT)₁₈ DNA substrate in the absence (upper) or in the presence (lower) of mRAD51. **(E)** Binding fraction of mRAD51 assembling on (dT)₁₃ DNA substrate increases in the presence of mS5S1. At this (dT)₁₃ substrate, binding fraction of mRAD51-only is $18.5 \pm 3.62\%$, and that of mRAD51 and mS5S1 mixture is $66.6 \pm 14.0\%$. mRAD51 and mS5^{FL}S1 mixture gives a binding fraction of $26.6 \pm 10.2\%$, which is similar to that of mRAD51-only case. mRAD51 concentration is $1.0 \mu\text{M}$, mS5S1 and mS5^{FL}S1 concentration are $2.0 \mu\text{M}$. At longer (dT)₁₈ DNA substrates, the binding fraction is $58.0 \pm 7.51\%$. *N* indicates the number of independent experiments. Dash lines were drawn for guidance purpose.

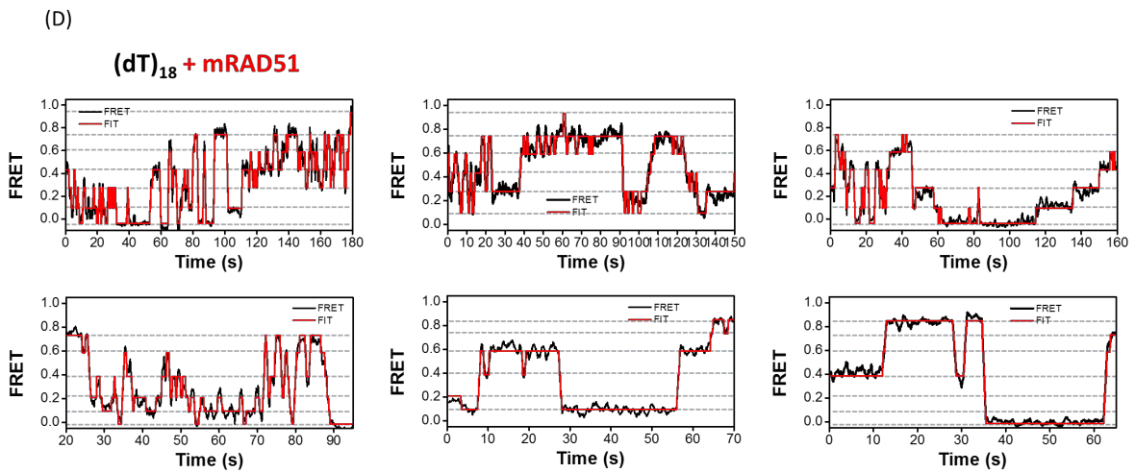
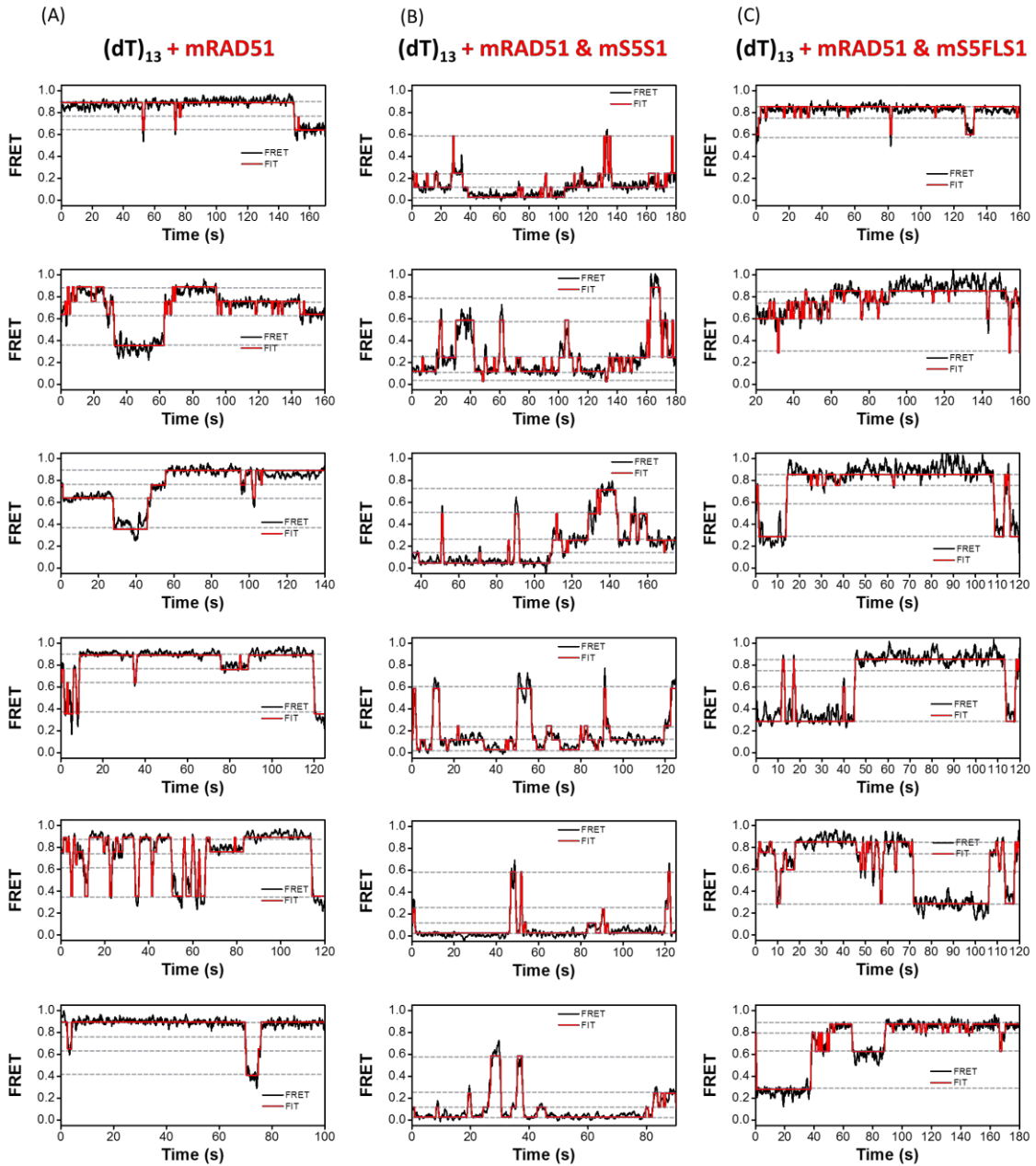


Figure S4. Representative FRET time traces of mRAD51 assembling under three different conditions: (A) on (dT)₁₃ substrate; **(B)** on (dT)₁₃ substrate in the presence of 2 μM mS5S1; **(C)** on (dT)₁₃ substrate in the presence of 2 μM mS5^{FL}S1; **(D)** on (dT)₁₈ substrate.

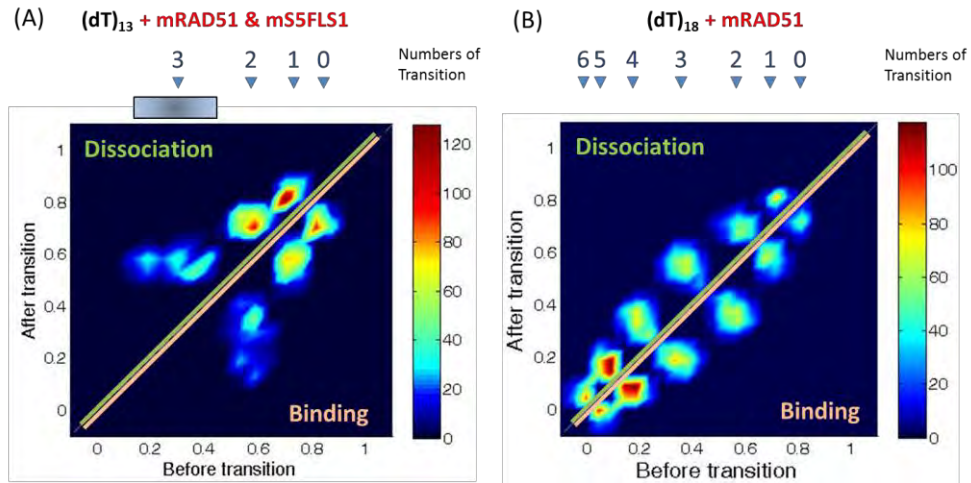


Figure S5. Transition density plot of mRAD51 assembly on $(dT)_{13}$ substrate in the presence of $mS5^{FL}S1$ and $(dT)_{18}$ substrate in the absence of $mS5S1$. (A) Adding $mS5^{FL}S1$ mutant gave similar transition with RAD51-only case. (B) TDP of mRAD51 assembly on $(dT)_{18}$ substrate clearly identifies 7 states, corresponding to zero, one to six mRAD51 monomer(s) binding.

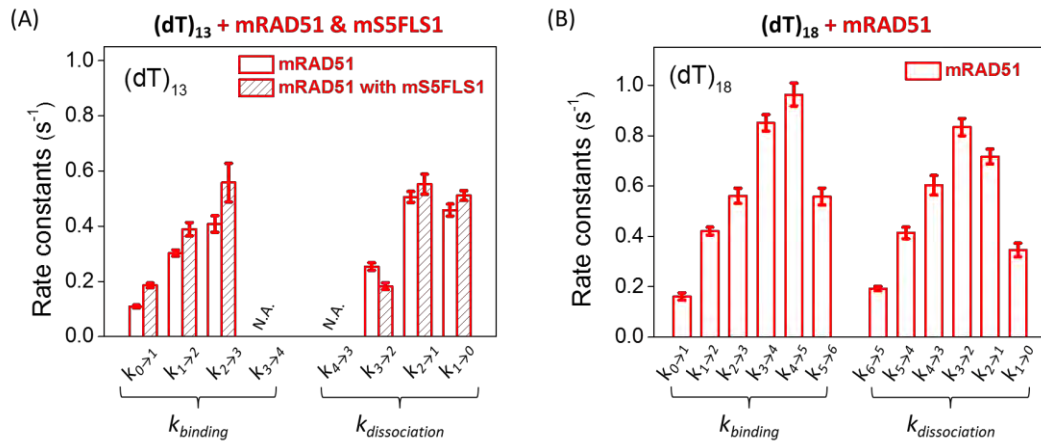


Figure S6. Rate constants of mRAD51 assembling on (A) on (dT)₁₃ substrate in the presence of mS5^{FL}S1 and (B) (dT)₁₈ DNA substrate in the absence of mS5S1.

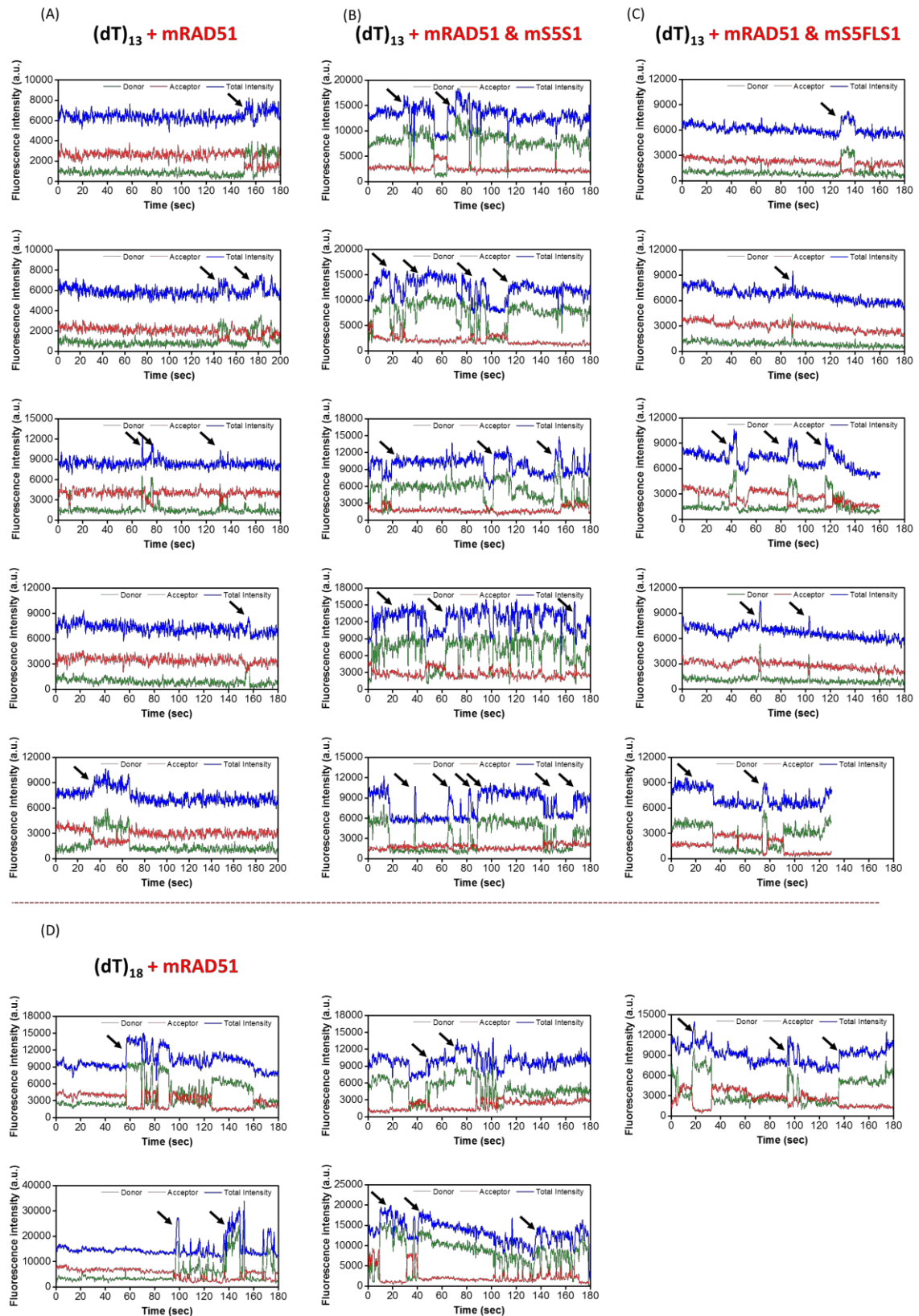


Figure S7. Protein-induced fluorescence enhancement (PIFE) effects are more apparent as mRAD51 assembles on (dT)₁₃ substrate in the presence of mS5S1 or on longer (dT)₁₈ substrate. Representative fluorescence intensity time traces of

mRAD51 assembling under three different conditions: **(A)** on (dT)₁₃ substrate; **(B)** on (dT)₁₃ substrate in the presence of 2 μM mS5S1; **(C)** on (dT)₁₃ substrate in the presence of 2 μM mS^{FL}S1; **(D)** on (dT)₁₈ substrate. Black arrows indicate the increase in total fluorescence intensity owing to the Cy3 PIFE effect.

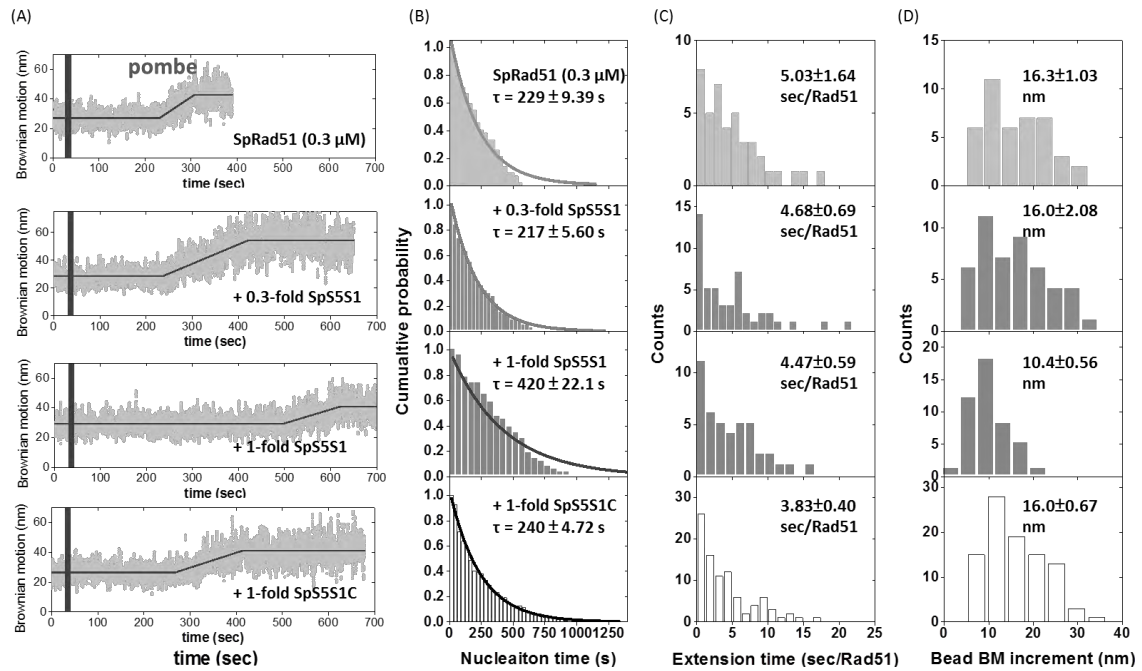


Figure S8. SpRad51 nucleoprotein filament assembly experiments. (A) Representative bead BM time-courses of SpRad51 (0.3 μM) assembly on (dT)₁₃₅ DNA substrates without SpS5S1 (top), with 0.3-fold (0.1 μM) SpS5S1 (middle top), with 0.3 μM SpS5S1 (middle bottom) or with 0.3 μM SpS5S1C mutant (bottom). Gray bars correspond to the deadtime when recombinase mixtures with 2 mM ATP were introduced. Histograms of nucleation time (B), mean extension time (second/Rad51) (C) and bead BM increment (D) of SpRad51 assembling. All experiments were carried out at 2 mM ATP. Error bar of nucleation rate was the standard deviation of the mean by bootstrapping 5000 times, and error bar of extension time and bead BM increment is one SEM.

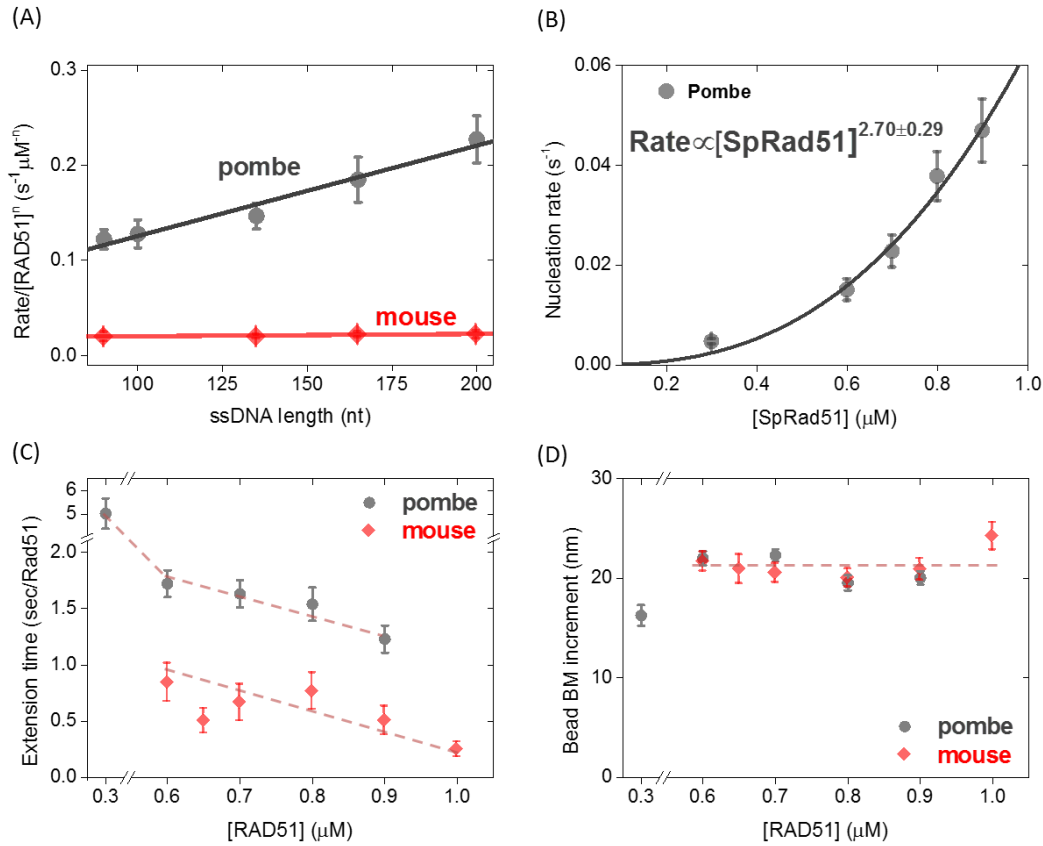


Figure S9. Kinetic parameters of SpRad51 nucleoprotein filament assembly and comparison with mRAD51. (A) ssDNA length dependence of pombe and mouse Rad51 obtained from TPM experiments. Nucleation rates are fitted by a $Rate/[RAD51]^n = k_{ssDNA} * L_{ssDNA} + k_{junction}$. Compared to mRAD51, SpRad51 shows a strong tendency to form nuclei on the ssDNA tail of the resected DNA. (B) SpRad51 concentration dependence of filament nucleation obtained by TPM experiments. Power-law fitting returns the nucleation unit of $n=2.70\pm0.29$ for SpRad51. (C) Extension time obtained from the slope of the BM time-courses and was expressed by the time required to add one Rad51 onto the filament. SpRad51 extends slower than mRAD51. (D) Similar bead BM increments between mRAD51 and SpRad51 assembly indicate the similar nucleoprotein filament structure of these two recombinases. At low SpRad51 concentration (0.3 μM), the equilibrium filament length is shorter. Dashed lines are drawn for guidance purpose. Error bar is one standard error of the mean.

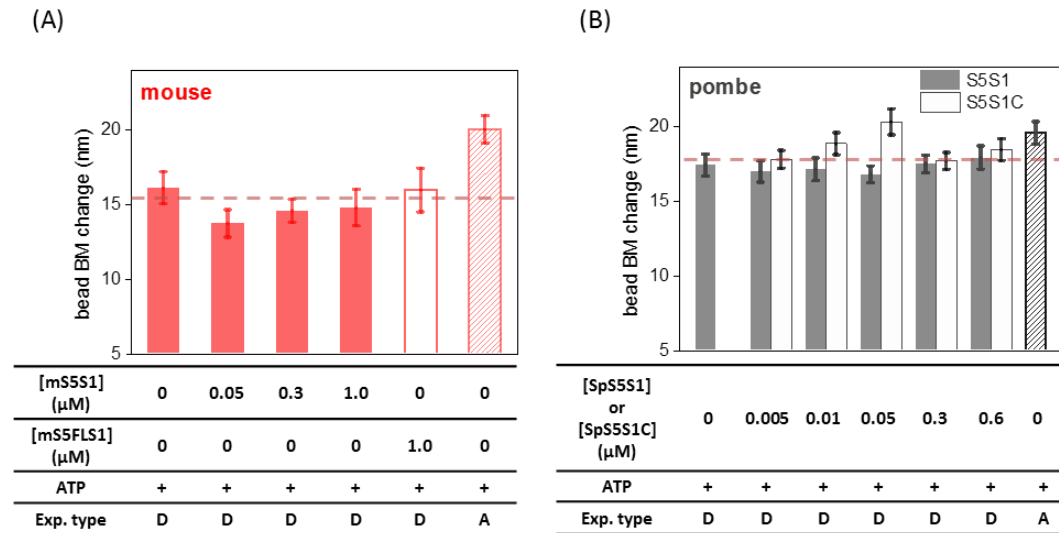


Figure S10. Filament disassembly of mRAD51 and SpRad51 filaments. (A) Bead BM decreases in TPM disassembly experiments of mRAD51 with either S5S1 or S5^{FL}S1 are all smaller than BM increment in mRAD51 assembly experiment (the last column in dashed bar) as (dT)₁₃₅ gapped DNA substrate was used in both assembly and disassembly experiments, implicating that not all mRAD51 dissociated from the gapped DNA substrates. **(B)** Compared to mRAD51 disassembly, SpRad51 most entirely dissociated from DNA. Both wild-type SpS5S1 (gray bars) and SpS5S1C mutants (light bars) showed a similar pattern. 0.8 μM of mRAD51 and SpRad51, a specified amount of S5S1 and ATP were used in the preparation of the filament before the disassembly was initiated. Dashed lines are drawn for guidance purpose (A: assembly experiment; D: disassembly experiment). Error bar is one standard error of the mean.

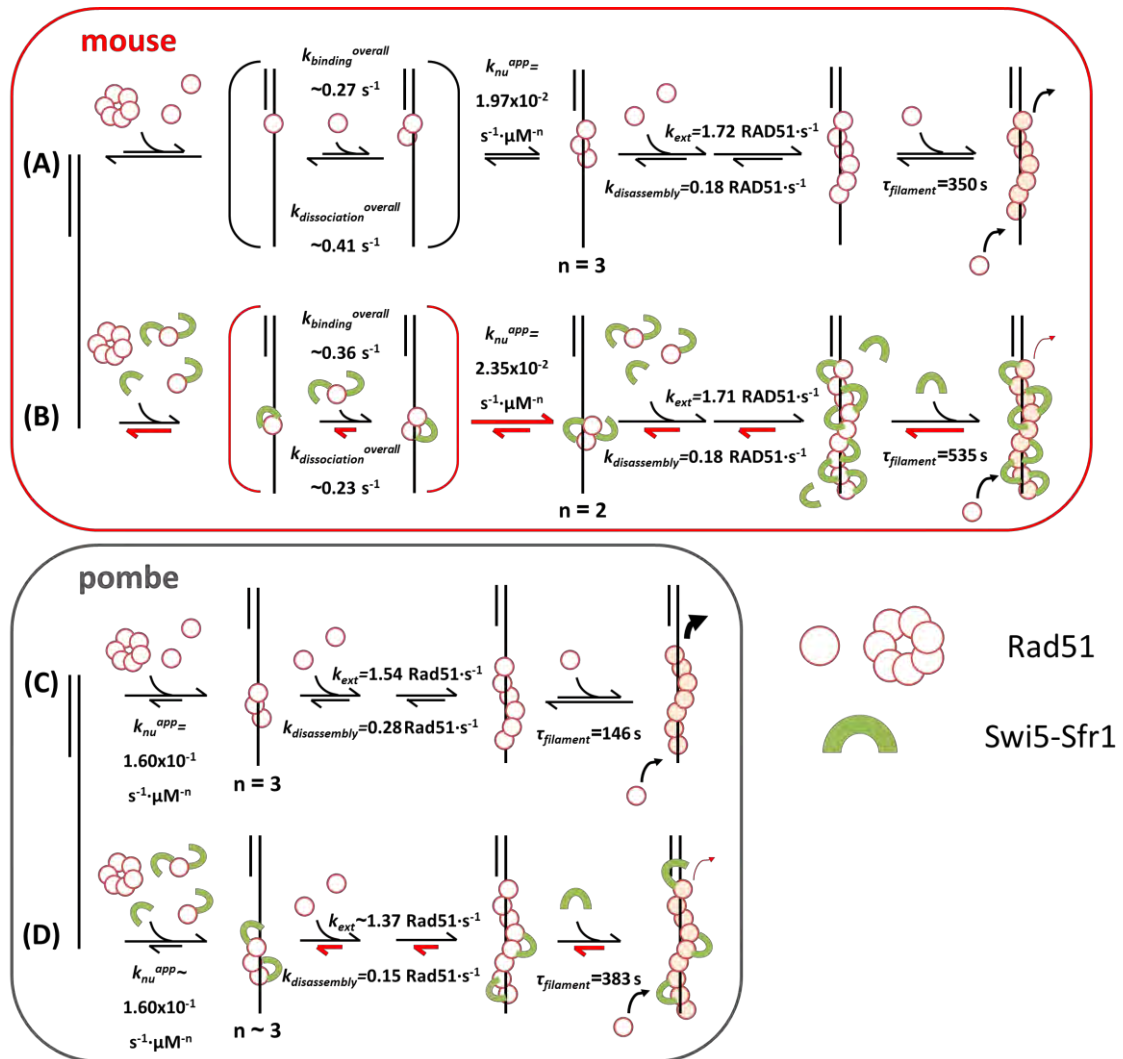


Figure S11. Kinetic parameters for S5S1-regulated Rad51 presynaptic filament formation obtained collectively from smFRET and TPM experiments. (A) Mouse RAD51 forms a stable nucleating cluster made of 3 monomers and extends on ssDNA as a monomer. **(B)** In the presence of mS5S1, mRAD51 interacts with S5S1 to form complex in solution. mS5S1 stimulates mRAD51 nucleation step by reducing mRAD51 nucleation unit from 3 to 2 monomers, stabilizing mRAD51 nucleating clusters and increasing mRAD51 ssDNA affinity. Also, mS5S1 prevents mRAD51 nucleoprotein filament disassembly. **(C & D)** Fission yeast SpS5S1 showed no stimulation on SpRad51 nucleation. Compared to mRAD51, SpRad51 displays a much higher nucleation rate owing to greater k_{ssDNA} . 3 SpRad51 monomers are required for stable nucleating cluster formation. SpRad51 filament is prone to disassembly compared to mRAD51. SpS5S1 efficiently prevents the disassembly of SpRad51 filament, and only small amounts of SpS5S1 is sufficient for stabilization. Different regulation strategies among species allow S5S1 to stabilize Rad51 filament efficiently. Red half-arrows indicate the kinetic steps affected by the S5S1.

Table S1. Summary of *apparent* nucleation rate constants of mRAD51 and mRAD51-S5S1 assembly on various gapped DNA substrates from Figure 2C. Error bar is the standard error of the fits.

	mRAD51	mRAD51-S5S1
k_{ssDNA}^{app} ($s^{-1} \cdot nt^{-1}$)	$(1.40 \pm 0.52) \times 10^{-5}$	$(8.95 \pm 1.93) \times 10^{-5}$
$k_{junction}^{app}$ (s^{-1})	$(9.54 \pm 0.70) \times 10^{-3}$	$(4.11 \pm 2.96) \times 10^{-3}$

Table S2. Summary of nucleation rate constants of mRAD51 and SpRad51 assembly on various gapped DNA substrates in Figure S9A. Error bar is the standard error of the fits.

	mRAD51	SpRad51
k_{ssDNA} ($s^{-1} \cdot nt^{-1} \cdot \mu M^{-n}$)	$(2.41 \pm 0.90) \times 10^{-5}$	$(9.50 \pm 0.99) \times 10^{-4}$
$k_{junction}$ ($s^{-1} \cdot \mu M^{-n}$)	$(1.64 \pm 0.14) \times 10^{-2}$	$(3.07 \pm 1.43) \times 10^{-2}$

Table S3. Summary of data in Figure 1 & S2A.

Initial [mRAD51] (μM)	[mS5S1]/ [mRAD51]	SWI5-SFR1 type	Cofactor type	Nucleation rate (s^{-1})	Extension time (sec/RAD51)	Bead BM increment (nm)	<i>n</i> (Numbers of molecules)
0.8	0	--	ATP	$(1.10 \pm 0.12) \times 10^{-2}$	0.76 ± 0.16	20.0 ± 0.92	67
	0.5	Wild-type mS5S1		$(1.07 \pm 0.16) \times 10^{-2}$	0.85 ± 0.27	24.4 ± 1.45	43
	1			$(1.03 \pm 0.12) \times 10^{-2}$	0.59 ± 0.16	26.0 ± 1.35	52
	1.5			$(1.05 \pm 0.16) \times 10^{-2}$	0.35 ± 0.09	22.7 ± 1.24	44
	1.625			$(1.02 \pm 0.18) \times 10^{-2}$	0.46 ± 0.09	23.5 ± 1.36	48
	1.75			$(1.05 \pm 0.10) \times 10^{-2}$	0.49 ± 0.13	26.5 ± 2.26	51
	1.875			$(1.24 \pm 0.14) \times 10^{-2}$	0.43 ± 0.11	24.6 ± 1.32	59
	2			$(1.43 \pm 0.15) \times 10^{-2}$	0.70 ± 0.11	24.4 ± 0.97	76
	2.25			$(1.44 \pm 0.18) \times 10^{-2}$	0.37 ± 0.08	25.2 ± 1.21	54
	2.5			$(1.49 \pm 0.24) \times 10^{-2}$	1.01 ± 0.29	25.2 ± 1.79	30
	2			mS5 ^{FL/AA} S1 mutant	$(1.02 \pm 0.12) \times 10^{-2}$	0.67 ± 0.24	22.5 ± 1.39
	0	--	AMPPNP	$(1.73 \pm 0.22) \times 10^{-2}$	0.37 ± 0.07	27.1 ± 1.46	45

Table S4. Summary of data in Figure 2A, 2B, S9C & S9D.

Initial [mRAD51] (μM)	Initial [mS5S1] (μM)	SWI5-SFR1 type	Cofactor type	Nucleation rate (s^{-1})	Extension time (sec/RAD51)	Bead BM increment (nm)	<i>n</i> (Numbers of molecules)
No mS5S1							
0.6	0	--	ATP	$(7.47 \pm 0.70) \cdot 10^{-3}$	0.80 ± 0.20	21.7 ± 0.97	92
0.65				$(8.54 \pm 1.56) \cdot 10^{-3}$	0.50 ± 0.11	20.9 ± 1.45	44
0.7				$(9.65 \pm 1.16) \cdot 10^{-3}$	0.66 ± 0.16	20.5 ± 0.97	60
0.8				$(1.10 \pm 0.12) \cdot 10^{-2}$	0.76 ± 0.16	20.0 ± 0.92	67
0.9				$(1.34 \pm 0.19) \cdot 10^{-2}$	0.50 ± 0.13	20.9 ± 1.08	41
1.0				$(2.36 \pm 0.35) \cdot 10^{-2}$	0.24 ± 0.07	24.2 ± 1.38	39
With mS5S1							
0.4	1.6	Wild-type mS5S1	ATP	$(5.34 \pm 1.15) \cdot 10^{-3}$	0.80 ± 0.20	21.1 ± 1.57	29
0.5				$(7.59 \pm 1.05) \cdot 10^{-3}$	0.49 ± 0.12	25.7 ± 1.79	37
0.6				$(1.13 \pm 0.15) \cdot 10^{-2}$	0.62 ± 0.17	24.7 ± 1.63	33
0.7				$(1.25 \pm 0.16) \cdot 10^{-2}$	0.34 ± 0.11	27.6 ± 1.92	31
0.8				$(1.43 \pm 0.15) \cdot 10^{-2}$	0.70 ± 0.11	24.4 ± 0.97	76
1.0	2.0			$(2.44 \pm 0.36) \cdot 10^{-2}$	0.69 ± 0.15	25.7 ± 1.74	37
0.7	1.6	mS5 ^{FL/AA} S1 mutant	ATP	$(9.95 \pm 1.35) \cdot 10^{-3}$	0.82 ± 0.20	21.0 ± 1.17	52
0.8				$(1.02 \pm 0.12) \cdot 10^{-2}$	0.67 ± 0.24	22.5 ± 1.39	39

Table S5. Summary of data in Figure 2C.

Initial [mRAD51] (μM)	Initial [mS5S1] (μM)	SWI5-SFR1 type	Cofactor type	ssDNA length (nt)	Nucleation rate (s^{-1})	<i>n</i> (Numbers of molecules)
No mS5S1						
0.8	0	--	ATP	90	$(1.09 \pm 0.28) \cdot 10^{-2}$	31
				135	$(1.10 \pm 0.12) \cdot 10^{-2}$	67
				165	$(1.22 \pm 0.17) \cdot 10^{-2}$	33
				200	$(1.23 \pm 0.22) \cdot 10^{-2}$	42
With mS5S1						
0.8	1.6	Wild-type mS5S1	ATP	90	$(1.32 \pm 0.28) \cdot 10^{-2}$	32
				135	$(1.43 \pm 0.15) \cdot 10^{-2}$	76
				165	$(1.94 \pm 0.42) \cdot 10^{-2}$	35
				200	$(2.26 \pm 0.22) \cdot 10^{-2}$	36

Table S6. Summary of data in Figure 3F, S3E & S6.

Initial [mRAD51] (μM)	Initial [mS5S1] (μM)	SWI5-SFR1 type	Cofactor type	Binding rate (s^{-1})		Dissociation rate (s^{-1})		Binding fraction (%)	n (Numbers of molecules)
(dT)₁₃									
1.0	0	--	ATP	$k_{0 \rightarrow 1}$	0.11 ± 0.01	$k_{1 \rightarrow 0}$	0.46 ± 0.02	18.5 \pm 3.62	315
				$k_{1 \rightarrow 2}$	0.30 ± 0.01	$k_{2 \rightarrow 1}$	0.51 ± 0.02		
				$k_{2 \rightarrow 3}$	0.41 ± 0.03	$k_{3 \rightarrow 2}$	0.25 ± 0.01		
				$k_{3 \rightarrow 4}$	--	$k_{4 \rightarrow 3}$	--		
	2.0	Wild-type mS5S1		$k_{0 \rightarrow 1}$	0.15 ± 0.01	$k_{1 \rightarrow 0}$	0.15 ± 0.01	66.6 \pm 14.0	472
				$k_{1 \rightarrow 2}$	0.33 ± 0.01	$k_{2 \rightarrow 1}$	0.36 ± 0.02		
				$k_{2 \rightarrow 3}$	0.52 ± 0.02	$k_{3 \rightarrow 2}$	0.23 ± 0.01		
				$k_{3 \rightarrow 4}$	0.44 ± 0.02	$k_{4 \rightarrow 3}$	0.18 ± 0.01		
	2.0	mS5 ^{FL/AA} S1 mutant		$k_{0 \rightarrow 1}$	0.17 ± 0.01	$k_{1 \rightarrow 0}$	0.48 ± 0.02	25.0 \pm 8.51	120
				$k_{1 \rightarrow 2}$	0.38 ± 0.02	$k_{2 \rightarrow 1}$	0.50 ± 0.03		
				$k_{2 \rightarrow 3}$	0.45 ± 0.06	$k_{3 \rightarrow 2}$	0.17 ± 0.01		
				$k_{3 \rightarrow 4}$	--	$k_{4 \rightarrow 3}$	--		

(dT)₁₈									
1.0	0	--	ATP	$k_{0 \rightarrow 1}$	0.16±0.01	$k_{1 \rightarrow 0}$	0.35±0.03	58.0±7.51	467
				$k_{1 \rightarrow 2}$	0.42±0.02	$k_{2 \rightarrow 1}$	0.72±0.03		
				$k_{2 \rightarrow 3}$	0.56±0.03	$k_{3 \rightarrow 2}$	0.83±0.03		
				$k_{3 \rightarrow 4}$	0.85±0.03	$k_{4 \rightarrow 3}$	0.60±0.04		
				$k_{4 \rightarrow 5}$	0.96±0.06	$k_{5 \rightarrow 4}$	0.41±0.02		
				$k_{5 \rightarrow 6}$	0.56±0.03	$k_{6 \rightarrow 5}$	0.19±0.01		

Table S7. Summary of data in Figure 4E, 4F, S2B & S8.

Initial [SpRad51] (μM)	[SpS5S1]/[SpRad51]	Swi5-Sfr1 type	Cofactor type	Nucleation rate (s^{-1})	Extension time (sec/Rad51)	Bead BM increment (nm)	<i>n</i> (Numbers of molecules)
0.3	0	--	ATP	$(4.50 \pm 0.51) * 10^{-3}$	5.03 ± 0.64	16.3 ± 1.04	42
	0.1	Wild-type SpS5S1		$(5.05 \pm 0.59) * 10^{-3}$	6.56 ± 0.73	14.8 ± 0.76	68
	0.2			$(4.20 \pm 0.57) * 10^{-3}$	2.70 ± 0.26	16.4 ± 1.01	38
	0.25			$(4.84 \pm 0.73) * 10^{-3}$	2.87 ± 0.34	18.0 ± 1.12	41
	0.33			$(4.91 \pm 0.62) * 10^{-3}$	4.68 ± 0.69	16.0 ± 1.08	48
	0.5			$(3.09 \pm 0.35) * 10^{-3}$	5.25 ± 0.58	13.4 ± 0.80	52
	1			$(2.39 \pm 0.24) * 10^{-3}$	4.47 ± 0.59	10.4 ± 0.56	45
	0.2			SpS5S1C mutant	$(4.74 \pm 0.60) * 10^{-3}$	3.93 ± 0.44	16.0 ± 0.94
	0.33	$(4.73 \pm 0.53) * 10^{-3}$			4.16 ± 0.56	14.4 ± 0.57	73
	0.5	$(4.17 \pm 0.39) * 10^{-3}$			4.58 ± 0.52	15.4 ± 0.66	82
	1	$(4.37 \pm 0.45) * 10^{-3}$			3.83 ± 0.40	15.9 ± 0.67	94
	2	$(4.21 \pm 0.57) * 10^{-3}$			2.94 ± 0.48	13.5 ± 0.83	35
	0	--			AMPPNP	$(8.72 \pm 1.36) * 10^{-3}$	2.89 ± 0.70

Table S8. Summary of data in Figure 5 & S10.

Species	Final [S5S1] (μ M)	Swi5-Sfr1 type	Cofactor type	Minimum mean lifetime (sec)	Fraction of un-disassembled filament (%)	Disassembly time (sec/Rad51)	Bead BM decrease (nm)	<i>n</i> (Numbers of molecules)
Mouse	0	--	ATP	350 \pm 39.3	17.0	5.62 \pm 1.35	16.1 \pm 1.08	47
	0.05	Wild-type mS5S1		441 \pm 51.1	29.5	5.86 \pm 1.02	13.7 \pm 0.93	44
	0.3			467 \pm 35.2	30.5	4.41 \pm 0.80	14.5 \pm 0.79	83
	1.0			535 \pm 49.9	34.1	6.20 \pm 1.96	14.7 \pm 1.22	44
	0.3	mS5 ^{FL/AA} S1		393 \pm 54.9	20.5	4.86 \pm 1.46	18.0 \pm 1.51	39
	1.0	mutant		364 \pm 46.4	22.7	4.59 \pm 0.97	15.9 \pm 1.48	44
	0	--	AMPPNP	627 \pm 43.9	57.9	5.06 \pm 1.88	15.6 \pm 1.61	56
Fission yeast	0	--	ATP	140 \pm 17.9	2.47	3.55 \pm 0.44	17.4 \pm 0.74	81
	0.005	Wild-type SpS5S1		256 \pm 34.6	17.1	6.77 \pm 0.72	16.9 \pm 0.71	82
	0.01			382 \pm 32.6	27.9	6.43 \pm 0.61	17.1 \pm 0.68	122
	0.05			367 \pm 27.1	26.2	6.57 \pm 0.54	16.8 \pm 0.56	162
	0.3			378 \pm 23.4	23.8	6.21 \pm 0.57	17.5 \pm 0.59	210
	0.6			407 \pm 30.1	25.4	6.29 \pm 0.78	17.9 \pm 0.78	118
	0.005	SpS5S1C mutant		153 \pm 16.4	2.91	4.00 \pm 0.37	17.8 \pm 0.60	95
	0.01			271 \pm 28.8	14.7	4.51 \pm 0.41	18.8 \pm 0.74	75
	0.05			318 \pm 35.1	19.8	4.32 \pm 0.49	20.3 \pm 0.88	75
	0.3			288 \pm 23.0	17.1	4.91 \pm 0.44	17.7 \pm 0.56	123
	0.6			338 \pm 33.8	20.0	4.12 \pm 0.59	18.4 \pm 0.73	70
	0	--	AMPPNP	579 \pm 69.8	48.1	11.9 \pm 2.79	11.8 \pm 1.12	27

Table S9. Summary of data in Figure S9A.

Species	Initial [Rad51] (μM)	Initial [S5S1] (μM)	Swi5-Sfr1 type	Cofactor type	ssDNA length (nt)	Nucleation rate constant ($\text{s}^{-1}\cdot\mu\text{M}^{-n}$)	<i>n</i> (Numbers of molecules)
Mouse	0.8	0	--	ATP	90	$(1.88\pm 0.48)\cdot 10^{-2}$	31
					135	$(1.89\pm 0.21)\cdot 10^{-2}$	67
					165	$(2.10\pm 0.28)\cdot 10^{-2}$	33
					200	$(2.11\pm 0.38)\cdot 10^{-2}$	42
fission yeast	0.8	0	--	ATP	90	$(1.22\pm 0.10)\cdot 10^{-1}$	145
					100	$(1.28\pm 0.15)\cdot 10^{-1}$	49
					135	$(1.47\pm 0.14)\cdot 10^{-1}$	131
					165	$(1.85\pm 0.24)\cdot 10^{-1}$	77
					200	$(2.27\pm 0.25)\cdot 10^{-1}$	81

Table S10. Summary of data in Figure S9B-S9D.

Initial [SpRad51] (μM)	Initial [SpS5S1] (μM)	Swi5-Sfr1 type	Cofactor type	Nucleation rate (s^{-1})	Extension time (sec/Rad51)	Bead BM increment (nm)	<i>n</i> (Numbers of molecules)
0.3	0	--	ATP	$(4.50\pm 0.51)\cdot 10^{-3}$	5.03 ± 0.64	16.3 ± 1.04	42
0.6				$(1.49\pm 0.22)\cdot 10^{-2}$	1.72 ± 0.12	22.0 ± 0.70	81
0.7				$(2.26\pm 0.32)\cdot 10^{-2}$	1.63 ± 0.12	22.3 ± 0.61	104
0.8				$(3.77\pm 0.49)\cdot 10^{-2}$	1.54 ± 0.15	19.5 ± 0.76	81
0.9				$(4.68\pm 0.63)\cdot 10^{-2}$	1.22 ± 0.12	20.0 ± 0.68	104

SI References

1. Gal J, Schnell R, Szekeres S, & Kalman M (1999) Directional cloning of native PCR products with preformed sticky ends (Autosticky PCR). *Mol Gen Genet* 260(6):569-573.
2. Kuwabara N, *et al.* (2012) Mechanistic Insights into the Activation of Rad51-Mediated Strand Exchange from the Structure of a Recombination Activator, the Swi5-Sfr1 Complex. *Structure* 20(3):440-449.
3. Tsai SP, *et al.* (2012) Rad51 presynaptic filament stabilization function of the mouse Swi5-Sfr1 heterodimeric complex. *Nucleic Acids Res* 40(14):6558-6569.
4. Su GC, *et al.* (2016) Role of the RAD51-SWI5-SFR1 Ensemble in homologous recombination. *Nucleic Acids Res* 44(13):6242-6251.
5. Kuwabara N, *et al.* (2010) Expression, purification and crystallization of Swi5 and the Swi5-Sfr1 complex from fission yeast. *Acta Crystallogr F* 66:1124-1126.